ON THE SENSITIVITY OF OCEAN CIRCULATION TO ARCTIC FRESHWATER INPUT DURING THE PALEOCENE/EOCENE THERMAL MAXIMUM

by

JESSE TINER COPE IV

Presented to the Faculty of the Graduate School of
The University of Texas at Arlington in Partial Fulfillment
of the Requirements
for the Degree of

MASTER OF SCIENCE IN GEOLOGY

THE UNIVERSITY OF TEXAS AT ARLINGTON

December 2009

ACKNOWLEDGEMENTS

First, I would like to thank Dr. Arne Winguth, my advisor and mentor throughout this process. Without his knowledge and patience I would still be staring at a blank screen. His guiding hand has continually nudged me in the right direction and kept me making forward progress. This thesis would not have been possible in any form without him.

Second I would like to mention the members of my committee. From the first lunch meetings with Dr. Christopher Scotese on topography and land/sea distribution to the final corrections, which were desperately needed, by Dr. Merlynd Nestell, these two men have been instrumental in the completion of my thesis and the later even more so in the completion of coursework over the years.

I would like to thank some members of our climate model working group. Dr. Cornelia Winguth, Vinit Asher, and Chandrik Byrappa Nagaraj all provided substantial assistance with the modeling requirements. Vinit Asher specifically showed unending patience with my lack of programming knowledge, helping me to untangle scripts and refine plots. Also, I am grateful to Teresa Sykes for taking the time to read over my thesis and provide constructive criticism.

I have had multiple friends provide encouragement and a listening ear, discussing crucial portions of my thesis and asking thought provoking questions. I would like to thank specifically my cousin, James Hedrick, who went before me and remained a staunch supporter, and my great friend, Todd Killen, who continues to stand beside me in the breach no mater the cost.

I would be remiss not to mention my gratitude to my parents for their unending support, encouragement, and strength. Even late night calls and months of complaining did not dampen their love and compassion. Their wisdom and insight has helped illuminate my path to this point over the last few years and indeed over the course of my life.

I am grateful to the many national recourses that aided in the completion of this work. Without the availability of computer resources and the support of the staff at the National Center for Atmospheric Research, which is funded by the National Science Foundation (NSF), none of the simulations would have been possible. I am also grateful to Dr. Christine Shields from the University Cooperation of Atmospheric Research and Dr. Cindy Shellito from the University of Northern Colorado who provided invaluable advice on topics ranging from problems with archive scripts to model parameters. This research was funded and made possible by NSF Grant 37261006, and I am very appreciative for the opportunity.

Next, I must thank my wife, Katie Cope. Her steadfast support and endless understanding of long hours and strange schedules have been a huge boon to my attitude and my spirit. From her listening ear to her enthusiastic support of my achievements, she has managed to keep all the pieces together and catch any balls that slipped through my hands. Her loyalty and compassion are irreplaceable.

Finally I must thank the man who has stood behind the scenes and tweaked and prodded me when needed. He has focused my energy and attention when needed and consoled and comforted me on days when I felt overwhelmed. He accepts me despite my mistakes and leads me along paths I never knew were possible. My Lord, my Lord, thank You.

August 21, 2009

ABSTRACT

ON THE SENSITIVITY OF OCEAN CIRCULATION TO ARCTIC FRESHWATER PULSES DURING THE PALEOCENE/EOCENE THERMAL MAXIMUM

Jesse Tiner Cope IV, M.S.

The University of Texas at Arlington, 2009

Supervising Professor: Arne Winguth

The Paleocene/Eocene Thermal Maximum (PETM) corresponds to a period characterized by extreme global warming caused by a massive carbon input into the ocean and atmosphere. Approximately 55 Ma in the early Cenozoic, evidence suggests an ice-free Arctic exchanged relatively fresh water with the remainder of the global ocean. In this study we use the Community Climate Systems Model version 3 (CCSM-3), including a carbon cycle model, to examine the sensitivity of deep-water formation and circulation within the global ocean to freshwater exchange from the Arctic Ocean during the PETM. Past modeling experiments show how alterations to seaway exchanges can have dramatic effects upon sedimentation, global climate, and ocean circulation. Two experiments, one with freshwater exchange between the PETM Arctic and Atlantic Oceans and another between the Arctic and Pacific Oceans, are compared against a reference experiment with exchange between the Arctic and Indian Oceans. Model results are evaluated against core data recovered from Ocean Drilling Program (ODP) samples to examine if the model matched proxies observed for the PETM. As freshwater is transported into the North Pacific the model simulates a significant reduction in

salinity increasing stratification and shifting deep-water formation from there to the midlatitude West Pacific and increasing southward circulation at intermediate depths by ~2.5 Sv. Freshwater flux into the North Pacific also simulates a strong deep-water formation in the North Atlantic and north-south flow in the Atlantic basin in agreement with paleoproxies and past models. Freshwater flux into the Atlantic Ocean produces weaker deep-water formation in the North Atlantic basin as well as stronger deep-water formation in the Southern Ocean. Freshwater input into the Pacific Ocean produces the highest temperatures (~12°C) in the global ocean in intermediate and deep waters, whereas, freshwater flux into the North Tethys produces the highest surface temperatures. These results suggest that Arctic freshwater flux into the North Pacific through the Bering Strait may induce circulation patterns similar to those inferred from stable isotope reconstructions during the PETM as well as increase intermediate and deep ocean temperatures and that flow through the Turgay Strait into the North Tethys Ocean would increase surface ocean and atmosphere temperatures. Based upon circulation patterns and temperature increases due to freshwater flux through the Bering Strait, Arctic freshwater input into the North Pacific could serve as a catalyst for methane hydrate destabilization, an event suggested as a precursor to the onset of the PETM.

TABLE OF CONTENTS

LIST OF ILLUSTRATIONS

Figure Page

LIST OF TABLES

CHAPTER 1

INTRODUCTION

1.1 The Paleocene Eocene Thermal Maximum (PETM)

The PETM was a transient global warming event that occurred approximately 55 Ma in the early Cenozoic. Termed a hyperthermal it consisted of extreme warmth, large carbon additions, and lasted for a relative brief duration, around 120-220 kyr [*Kelly et al.*, 2005]. Significant global climate changes occurred during this period. Changes in the global ocean involved sea surface temperature (SST), deep-sea temperature, calcite compensation depth (CCD), and patterns of global ocean circulation. Sea surface temperatures during this time rose by varying amounts around the globe. The tropics were about 5ºC warmer than background temperatures while the high latitudes were as much as 9ºC warmer [*Kelly et al.*, 2005; *Zachos et al.*, 2005; *Sluijs et al.*, 2007] (Figure A.1). The deep-sea temperatures also altered; global deep-sea oxygen and carbon isotope records from ODP sites indicate deep-sea temperatures 4-5ºC warmer than background [*Zachos et al.*, 2001; *Tripati and Elderfield*, 2005; *Zachos et al.*, 2005]. The CCD, though varying on local levels, shoaled during this time [*Kelly et al.*, 2005; *Zachos et al.*, 2005]. Isotope records from ODP sites indicate a reversal in deep ocean circulation from Southern Hemispere overturning to Northern Hemisphere overturning at the onset of the PETM [*Nunes and Norris*, 2006].

Other variations including changes in sea level and atmospheric CO_2 concentration also took place during the PETM. Sea levels are affected by tectonic activity [e.g. *Watts and Thorne*, 1984; *Long and Shennan*, 1994; *Schmitz and Pujalte*, 2003; *Larson et al.*, 2004] as well as climatic variability [e.g. *Miller et al.*, 1998, 2005; *Gale et al.*, 2002; *Antonov et al.*, 2005] and are thus difficult to precisely resolve. Ostracode records suggest that sea levels during the PETM

rose approximately 20m from previous levels [*Speijer and Morsi*, 2002]. The plausibility of a connection between the Arctic Ocean and the Tethyan water masses via the Turgay Strait during this time of increased sea level has been shown based upon dinoflagellate cysts [*Iakovleva et al.*, 2001]. Atmospheric CO_2 levels increased and were in the range of 2000-4000 ppm during the PETM [*Yapp*, 2004; *Zachos et al.*, 2008] as opposed to present levels of 385 ppm. Salinity of the oceans during the PETM reduced due to increased runoff and ice melt [*Sluijs et al.*, 2006]. Topography and bathymetry during the PETM differed significantly compared to the modern, with changes in size of ocean basins and more or less restricted thru flow in certain seaways.

Significant ecological changes occurred during the PETM, vegetation and animal distributions changed, global latitudinal temperature gradients decreased, and shorelines transgressed. Climate change on both regional and global scales forced animals and plants to move and adjust. Examples range from crocodilian vertebrates found in higher latitudes such as on Ellesmere Island [*Estes and Hutchison*, 1980; *Markwick*, 1998] to forests in Antarctica [*Case*, 1988]. Proxy data in the form of distribution of membrane lipids of bacteria indicates a strongly reduced latitudinal temperature gradient [*Weijers et al.*, 2007]. Lastly, orography and shorelines varied greatly from the modern during the PETM as can be seen by past reconstructions such as in the PALEOMAP Project [*Scotese*, 2008] (Figure A.1).

The likely cause of a climate change was more than 2000 gigatons of carbon (GtC) entering the atmosphere and ocean over a period of 10000 years [*Bowen et al.*, 2004; *Zachos et al.*, 2008]. Multiple hypotheses have been put forward as to the cause, from intrusive volcanism liberating methane [Svensen et al., 2004; *Dickens*, 2004; *Storey et al.*, 2007], to the Earth's surface producing it as a positive feedback to initial warming [*Dickens*, 2003]. Bottom water warming indicated by isotope ratios [*Dickens et al.*, 1995] and the increased occurrence of the dinoflagellate cyst *Apectodinium* [*Sluijs et al.*, 2007] is suggested as a possible cause for the injection of carbon into the ocean and atmosphere through the dissociation of methane

hydrates. Despite these hypotheses, the source of the catalyst causing this carbon release remains uncertain [*Pagani et al.*, 2006; *Sluijs et al.*, 2007; *Zachos et al.*, 2008].

Past climate changes had significant effects on the biota and the environments in which they lived; for example, enabling tropical to sub-tropical fresh water ferns to live in the Eocene Arctic [*Brinkhuis et al.*, 2006], or members of the order Crocodylia to survive at much higher latitudes within the northern hemisphere [*Markwick*, 1998]. The amount of carbon put into the global system then, 2000 GtC, is comparable to the amount estimated to be emitted over the next few centuries due to human activities. Because of this, evaluation of modeling results under those past "hothouse" conditions could lead to improved understanding of the possible affects of anthropogenic CO_2 emissions in the future.

Specifically, this study looks at the affect of freshwater exchange between the Arctic Ocean and the rest of the global ocean. Conditions in the Arctic were similar in respects to increase in SST and sea level, but the salinity level is much lower than the remainder of the global ocean [*Sluijs et al.*, 2006]. Based upon this, fresh water pulses from the Arctic may affect deep-water formation and the strength of the deep-sea circulation. Changes in circulation, such as south to north flow in the Atlantic basin, and thereby increased northward heat transport, could affect global temperature gradients and thus the climate. Also, cooler surface temperatures overall with freshwater flow into the North Pacific or North Atlantic compared to the Indian Ocean could be seen as a cause for the PETM. If the temperatures are cooler with flow into the Pacific or Atlantic then a closing of either the North Atlantic Seaway or the Bering Strait could be a precursor, contributing to the onset of the PETM. Conversely, if freshwater flow into the North Pacific or Atlantic Oceans produces warmer temperatures, then the opening of either the Bering Strait or North Atlantic Seaway could be seen as a precursor to the onset of the PETM.

1.2 Early Cenozoic Climate Model Studies

Climate modeling provides a resource by which past and present events can be evaluated and their implications applied to future changes and variability. Modeling studies

have vastly improved knowledge of past climate periods and their effect upon the global environment. These models give the ability to run scenarios for multiple centuries or millennia and observe what long term effects of specific changes to the global system may occur. Previous models have well established the significance of seaways and past topography to Eocene climate change [e.g. *Heinze and Crowley*, 1997; *Mikolajewicz and Crowley*, 1997; *Huber and Caballero*, 2003; *Huber and Nof*, 2006].

Using a version of the Hamburg large-scale geostrophic ocean model coupled to an atmospheric energy balance model, *Mikolajewicz and Crowley* [1997] illustrated the sensitivity of deep-water circulation to changes in flow through the Central American isthmus. Their results indicate that even limited throughflow, though it reduces the strength of the circulation, still allows for it. The partial opening of the Central American isthmus also led to a cessation of the Labrador Sea convection, thus illustrating the far-reaching effects of disruption caused by exchanges of low saline water.

Heinze and Crowley [1997] demonstrated that the lysocline depth and opal deposition in the oceans is greatly affected by topography (e.g. opening and closing of the Panama and Drake Passage, *Heinze and Maier-Reimer* [1992]). Their results indicate that changes in ocean circulation due to seaway opening or closing can cause considerable changes in lysocline depth (1500-3000m) and data from multiple recent ODP legs throughout the Atlantic indicates that the CCD shoaled more than 2 km within a few thousand years [*Kelly et al.*, 2005; *Zachos et al.*, 2005] of the onset of the PETM.

Huber and Sloan [2001] use the Climate System Model (CSM) from the National Center for Atmospheric research (NCAR) to simulate an Eocene climate and investigate the effects upon vertical and meridional temperature gradients and ocean heat transport. In this experiment they use boundary conditions similar to those of *Sewall et al.* [2000] with pCO_2 of 560 ppm. They found that the temperature gradients are near modern values and that while the

ocean heat transport decreases in the Northern Hemisphere by 0.6 PW, it increases by 0.4 PW in the Southern Hemisphere.

Bice and Marotzke [2002] used the Geophysical Fluid Dynamics Laboratory's Modular Ocean Model (MOM) to run sensitivity experiments on the effects of a closed low-latitude gateway between western India and Eurasia. Their results indicate that a "Brito-Arctic bridge" preventing flow from the Arctic into the North Atlantic effects a change from dominant Southern Hemisphere thermohaline circulation to Northern Hemisphere in the Pacific Ocean. Salinity increases because of a lack of freshwater flow into the North Atlantic, thereby causing flow through the Central American Seaway and increasing the salinity of the Northern Pacific.

Huber and Caballero [2003] using the Community Climate System Model (CCSM) of NCAR, illustrated that topography also could have large effects upon the global climate and its variability. Using the model they ran simulations observing the effect of Eocene (55 to 35 million years ago) topography upon the El Nino Southern Oscillation (ENSO). Compared with modern simulations the Eocene ENSO showed approximately a 60% increase in amplitude, though with a similar frequency agreeable with findings from Eocene varved sediments from lakes in "teleconnected" [*Huber and Caballero*, 2003] regions.

Models consistently have problems reproducing the high Arctic temperatures during the Early Eocene while maintaining lower temperatures in the tropics. *Shellito et al.* [2003] examined the sensitivity of the Early Eocene to increases in CO_2 levels, using 500, 1000, and 2000 ppm in the experiments and running them on the NCAR's Climate System Model (CSM). Although *Shellito et al.* [2003] concludes that the highest (2000 ppm) CO_2 reproduces temperatures consistent in the Arctic and Antarctic, it still is ~4°C too warm in the tropics according to proxy data. *Shellito et al.* [2009] ran experiments with NCAR's fully coupled CCSM3 with pCO_2 at 560 and 2240 ppm, as well as a third experiment with 2240 ppm and a passage open to the Arctic. The results indicate that a pCO_2 of 2240 ppm reproduces Arctic warming (~8°C) and climate changes, to include an ice free Arctic, more consistent with proxy

estimates than the previous experiments. Furthermore, an opening of the Bering Strait produces an annual sea surface temperature rise of ~3°C in the Arctic Ocean, closing the gap to proxy based temperature reconstructions during the Early Eocene and even at the PETM [*Sluijs et al.*, 2006; *Weijers et al.*, 2007].

1.3 Biogeochemical Stratigraphic Data for the Late Paleocene/Early Eocene

Studies of proxy data indicate significant changes from pre to post PETM. Particularly useful are isotope ratios (Table A.1) and fossil assemblage records from the drilled cores of the ODP, now International Ocean Drilling Program (IODP). Mg/Ca, oxygen isotopes, and stable isotope date provide valuable information about paleotemperature and circulation and can be compared with results from climate simulations.

The notation $\delta^{13}C$ is defined by a comparison of carbon isotope ratios between a sample and a standard, such as Vienna Pee Dee Belemnite (V-PDB), set by the National Bureau of Standards [*Broecker and Peng*, 1982]

$$\delta^{13}C = \left[\frac{\left({}^{13}C/{}^{12}C\right)_{sample} - \left({}^{13}C/{}^{12}C\right)_{\text{standard}}}{\left({}^{13}C/{}^{12}C\right)_{\text{standard}}} \right] \quad (1)$$

Ratios from paleodata can then be compared to modern ratios indicative of specific environmental characteristics [e.g., *Kennett and Stott*, 1991; *Kelly et al.*, 2005, *Tripati and Elderfield*, 2005; *Nunes and Norris*, 2006, *Zachos et al.*, 2007]. Carbon isotope distribution within the oceans is controlled by multiple factors such as the air-sea gas exchange, ocean circulation, and productivity. Within the surface layers of the ocean wind disturbs the water causing mixing of gases between the atmosphere and ocean. This mixing can either increase of decrease the amount of carbon within the ocean. Within the photic zone microorganisms utilize carbon to produce their tests or shells. Biological production increases as nutrients become more abundant which thereby increases the intake of carbon. Since microorganisms

preferentially use Carbon-12 over Carbon-13 this increases the $\delta^{13}C$ level. In a similar way, ocean currents affect $\delta^{13}C$ ratios. In locations of upwelling nutrient rich water comes to the surface and thus stimulates the cycle described above. At depth the $\delta^{13}C$ ratio is dependent either upon the currents and the carbon rain rate from shallower ocean levels and the amount of Carbon-12 coming into a location.

Tripati and Elderfield [2005] used $\delta^{13}C$ and Mg/Ca ratios from foraminifers to investigate changes in deep-sea temperature, high latitude SSTs, and ocean circulation patterns. The Mg/Ca ratios indicate a warming of 4-5°C in SSTs and of around 4°C in bottom water temperatures. $\delta^{13}C$ data indicate a switch from convection in the Southern Ocean to the North Pacific at the PETM followed by a return during the recovery period to strong Southern Ocean circulation and a decline in the Pacific Ocean circulation.

Nunes and Norris [2006] use the carbon isotope ($\delta^{13}C$) records from 14 deep-sea ODP sites to reconstruct changes in deep-ocean circulation at the PETM boundary. $\delta^{13}C$ levels lower the longer deep-water is away from the surface due to an increase in nutrients and ^{12}C [*Nunes and Norris*, 2006]. Therefore, observing relative levels of Carbon-13 isotopes from different ODP sites indicates how close each site was to the point of deep-water formation in the past, suggesting that a switch in global circulation occurred around the PETM. Prior to the PETM event the most positive $\delta^{13}C$ values were in the Southern Hemisphere Oceans, followed by the appearance of higher values in the Northern Hemisphere coincident with the PETM event, and then a return to deep-water formation in the Southern Oceans during the recovery period.

Sluijs et al. [2006] use the palaeothermometer, TEX_{86} to measure Arctic sea surface temperatures over the course of the PETM. This technique is based upon the distribution of crenarchaeotal membrane lipids, which show a significant linear correlation between the numbers of cyclopentane rings in the lipids and the annual mean sea surface temperature [*Schouten et al.*, 2002]. Using this method, therefore, *Sluijs et al.* [2006] reconstructed Arctic

SSTs, finding that they rose from ~18°C before the PETM, to over 23°C during the event, and then back down to ~17°C in the early Eocene.

In a companion paper to *Sluijs et al.* [2006], *Pagani et al.* [2006] obtain stable hydrogen and carbon isotope records from terrestrial plant and aquatic n-alkanes to recreate changes throughout the PETM in surface water salinity and precipitation in the Arctic. N-alkyl lipids record source water hydrogen and different weight n-alkanes record different source water [*Sternberg*, 1988; *Yakir*, 1998; *Sauer et al.*, 2001; *Pagani et al.*, 2006]. Based upon this, *Pagani et al.* [2006] argues that decreased concentrations of low-molecular-weight n-alkanes ($\delta D_{n-C_{17}}$) indicate decreased salinity levels in Arctic surface waters, while decreases in high-molecular-weight ($\delta D_{n-C_{27/29}}$) n-alkanes signify increases in precipitation over the Arctic during the PETM.

Biological studies provide significant insight into oceanographic and climatic conditions; for example, different nannoplankton communities are sensitive to specific environmental conditions [*McIntyre and Bé*, 1967; *Fincham and Winter*, 1989, *Boeckel and Baumann*, 2004]. Paleobiogeography then is an important tool for interpreting changes in paleoclimate and paleoecology [*Aubry*, 1998]. Nannofossil assemblages offer insight into many aspects of past climates, such as surface and bottom-water temperatures, or productivity and nutrient levels.

Bralower [2002] used nannofossil assemblages to evaluate changes in sea surface temperatures and productivity at the beginning of the PETM. Levels of colder-water taxa such as *Biscutum* and *Chiasmolithus* were compared with those of warmer-water taxa such as *Discoaster*, *Ericsonic*, and *Fasciculithus* from ODP site 690 in the Weddell Sea. Based upon the turnover of groups at the onset of the PETM, *Bralower* [2002] concluded that sea surface temperatures increased.

Paleobiogeographic studies also indicate a shift to more oligotrophic surface and deep-water conditions in the open ocean. Despite this, in localized areas along continental margins and shelf regions eutrophic conditions persisted and even increased [e.g., *Kelly et al.*, 1996;

Thomas, 1998; *Bralower*, 2002; *Kelly*, 2002; *Tremolada and Bralower*, 2004; *Gibbs et al.*, 2006; *Zamagni et al.*, 2008].

During the PETM, there is considerable evidence that the calcite compensation depth (CCD) and therefore the lysocline shoaled significantly, caused by the rapid release of massive amounts of carbon [*Kelly et al.*, 2005; *Zachos et al.*, 2005]. ODP sites in the South Atlantic exhibit clay layers coincident with the PETM, which increase in thickness with depth [*Zachos et al.*, 2005]. Along with a decrease in bulk carbonate content, ODP site 690 also displayed a decrease in coarse (>63 μm) fraction and an increase in shell fragmentation of planktic foraminifers, indicative of fewer foraminiferal shells preserved and poorer shell preservation respectively [*Bains et al.*, 1999; *Farley and Eltgroth*, 2003; *Kelly et al.*, 2005]. These evidences indicate a shoaling of the CCD, possibly up to 2 kilometers [*Zachos et al.*, 2005].

1.4 Objectives

The goal of this study is to explore how potential changes in freshwater exchange between the Arctic and the Atlantic, Indian, and Pacific Oceans during the PETM affect climate, the carbon cycle, and deep-water circulation within the global oceans. For this purpose, sensitivity experiments will be carried out comparing an exchange between the Arctic and the Atlantic and Pacific Oceans and compared with a previous Eocene simulation prescribing the freshwater flux through the Turgay Strait (Arctic-Tethys Seaway). The results of this model will be analyzed against proxy data and previous model studies.

It is expected that varying the location where the Arctic is connected to the remainder of the global ocean will have significant effects upon circulation and thereby temperature and nutrient distribution. This study will investigate whether, as the largest ocean basin during the PETM, Arctic freshwater input into the Pacific Ocean would produce the strongest change in ocean circulation and temperature relative to the other two experiments. Ocean temperatures are most likely highest with Arctic freshwater input into the Pacific Ocean and circulation will be predominantly north to south within the global oceans. These temperature and circulation

changes would provide the necessary catalyst to release massive amounts of CO_2, by destabilizing methane hydrates along the slope and rise of continental margins (900-2000m depth), and thus serve as a contributing factor to the onset of the PETM [*Dickens et al.*, 1995] (Figure A.2).

Improvements in this study include using the fully coupled CCSM3 climate model, updated topography, and a carbon cycle model. Previous experiments concerning deep-water formation and circulation in relation to changing ocean passages do not include the carbon cycle. Changes in the land/sea distribution for the PETM have also been addressed.

CHAPTER 2

MODEL DESCRIPTION

2.1 Community Climate System Model - Overview

The Community Climate System Model 3 (CCSM3) is a coupled climate model containing four main components: atmosphere, ocean, land, and sea ice (Figure A.3). States and fluxes are exchanged between these components via the coupler. The CCSM3 is used for simulating past, present, and future climates and is described in detail by *Collins et al.* [2006]. The following are the model components: the Community Atmosphere Model version 3 (CAM3) [*Collins et al.*, 2004, 2006a], the Community Land Surface Model version 3 (CLM3) [*Oleson et al.*, 2004; Dickinson et al. 2006], the Community Sea Ice Model version 5 (CSIM5) [*Briegleb et al.*, 2004], and the Parallel Ocean Program version 1.4.3 (POP) [*Smith and Gent*, 2004]. The horizontal resolution in the CCSM3 is T31x3 in this study. The vertical resolution consists of 26 levels within CAM3 and 10 subsurface soil layers in CLM3 [*Collins et al.*, 2006]. For the ocean component POP, poles are located over Greenland and the true South Pole. The vertical resolution of the POP consists of 25 levels with a maximum depth of 5000m. The sea ice model is integrated on the same horizontal grid as the POP [*Collins et al.*, 2006]. The coupler exchanges basic state variables (e.g. heat, freshwater, and momentum) between the four components (atmosphere, ocean, land, and sea ice) of the model.

The ideal age tracer in the ocean component (POP) of the CCSM3 infers the age of water masses according to the time of water away from the surface in years [*Thiele and Sarmiento*, 1990; *England*, 1995]. The age is calculated according to the partial differential equation

$$\frac{\partial A}{\partial t} = L(A) + M(A) + 1$$

(2)

where *L* and *M* are advection and mixing operators acting on the potential temperature and salinity [*Bryan et al.*, 2006]. As is apparent, changes in ocean currents due to changes in freshwater flux, and thereby temperature and salinity, will greatly affect the age of water masses.

The coarse resolution of the CCSM3 T31x3 does not resolve narrow seaways, so freshwater flux exchange between the Arctic and the adjacent ocean is parameterized by the marginal sea parameterization. Excess freshwater is represented by

$$T_{ms} = \sum_{ms} \left(\left[MAX(0, QFLUX_{i,j}) c_q + (E_{i,j} + P_{i,j} + R_{i,j} + M_{i,j}) + F^S_{i,j} c_S \right] \Delta x_{i,j} \Delta y_{i,j} \right).$$

(3)

Here T_{ms} is the transport term from the marginal sea (ms) in kg s^{-1}, *QFLUX* is the frazil ice formation in W/m^2, and *E*, *P*, *R*, and *M* are evaporation, precipitation, river runoff, and ice melt in Kg/m^2s [*Smith and Gent*, 2004]. F^S is the salt flux due to ice melt, and Δx and Δy are the zonal and meridional grid spacings in m [*Smith and Gent*, 2004]. Finally, c_q and c_s are conversion factors used in order to change units of flux into transport;

$$c_q = -\frac{1}{L_f} \frac{S_o - S_i}{S_o}, c_s = -\frac{1}{S_o} \frac{\rho_{fw}}{\rho_{sw}}$$

(4)

where L_f is the latent heat of fusion, S_o is the ocean salinity, S_i is the sea ice salinity, and ρ_{fw} and ρ_{sw} are the densities of freshwater and saltwater respectively [*Smith and Gent*, 2004].

2.2 Ocean Carbon Cycle Model

2.2.1 The Carbon Pumps

The marine carbon component of the coupled climate-carbon cycle model is based upon the Ocean Carbon Model Intercomparison Project (OCMIP) [*Najjar and Orr*, 1998, http://www.ipsl.jussieu.fr/OCMIP/; *Doney et al.*, 2006] (Figure A.4). An ocean carbon pump is defined as a process that depletes the surface DIC relative to the deep-sea DIC. There are three pumps: a solubility pump, a soft tissue pump, and a carbonate pump [*Volk and Hoffert*, 1985]. At the surface organisms take carbon out of the water and utilize it for food and to build their tests or shells. This creates a drawdown in the level of carbon dioxide in the surface waters and allows more carbon to enter the ocean from the atmosphere (See Section 2.2.2). As the organisms die the carbon fixed in their bodies and shells then falls through the ocean layers. Most of this carbon dissolves or is incorporated into the shallow nutrient loop as organisms feed on the falling debris. What carbon does reach the bottom may be further depleted in the process of dissolving carbonate rocks. Any carbon remaining in the deep-ocean is eventually transported along currents back to the surface in areas of upwelling where organisms such as foraminifers or coccolithophores utilize it and the cycle begins anew.

2.2.2 CO_2 Air-Sea Gas Exchange

The model estimates air-sea fluxes of CO_2 using the equation

$$\Delta F_{ocn} = F_{ao} - F_{oa} = k_u \mathrm{B}_T \left(pCO_2^{atm} - pCO_2^{sw} \right) \left(1 - f_{ice} \right). \tag{5}$$

Here k_u is the wind-dependent gas exchange coefficient [*Wanninkhof*, 1992] across the air-sea interface, B_T is the temperature dependent solubility of CO_2, pCO_2^{atm} is the partial pressure of CO_2 in the lowest 2 layers of the atmosphere, pCO_2^{sw} the partial pressure in the uppermost layer of the ocean, and f_{ice} is the fraction of global ice coverage [*Doney et al.*, 2006]. The partial pressure of CO_2 in the upper layer of the ocean is calculated from model derived dissolved inorganic carbon (DIC), alkalinity (ALK), temperature, and salinity [*Doney et al.*, 2006].

An important concept within the air-sea gas exchange, fugacity is the tendency of a substance to prefer one phase over another, or for the substance to "escape" from one phase to another [*Lewis*, 1901; *Mackay and Paterson*, 1981]. For example, if the partial pressure of CO_2 in the atmosphere is greater than the partial pressure of dissolved CO_2 in the ocean, the CO_2 (gas) in the atmosphere will have the tendency to escape toward the dissolved phase in the ocean. In this instance, that would decrease the pH of the ocean (See Section 2.2.8).

$$\begin{aligned} &CO_2(gas) \rightarrow CO_2(dissolved) \\ &CO_2 + H_2O \Leftrightarrow H_2CO_3 \\ &H_2CO_3 \Leftrightarrow H^+ + HCO_3^- \\ &HCO_3^- \Leftrightarrow H^+ + CO_3^{2-} \end{aligned}$$

(13)

Concentration and fugacity can be related by the equation

$$C = K \cdot f$$

(14)

where C is the concentration of the substance in either the ocean or atmosphere, K is some coefficient (Henry's Law coefficient in the case of water), and f is the fugacity of the substance [*Millero*, 1995; *Emerson and Hedges*, 2008]. It can be seen then that as the concentration increases so to does the tendency to escape. Therefore, in areas of upwelling, where cold, CO_2 rich, deep waters rise, the fugacity should increase. The model reproduces this relationship well in areas where older water masses (higher age of water masses) have higher CO_2 fugacity (f_{CO_2}).

2.2.3 Productivity

Organism respiration and organic decay [*Chester*, 2000; *Burdige*, 2006]:

$$[CH_2O] + [O_2] \leftrightarrow [CO_2] + [H_2O]$$

(10)

and thereby productivity, are dependent upon oxygen concentrations and nutrient availability. Here CH_2O represents organic carbon (C_{org}) used in the process of aerobic respiration. Nutrients needed by organisms are brought to the surface by upwelling due to deep-water formation and ocean currents. Upwelling waters additionally are depleted in oxygen due to their long time away from the surface and we can see therefore that ocean currents have a significant affect upon productivity.

Nutrient uptake in this model occurs only in the production zone (z_c<75m, where z_c represents the compensation depth below which no net photosynthesis occurs) [*Lande and Yentsch*, 1988; *Doney et al.*, 2006]. The uptake of PO_4 is given by the following equation

$$J_{prod} = F_T \cdot F_N \cdot F_I \cdot B \cdot \max\left(1, z_{ml}/z_c\right)/\tau . \tag{6}$$

Here F_T is the temperature limitation function, F_N is the Michaelis-Menten limiting term for PO_4 and Fe, F_I is the irradiance limitation term, B is the biomass, and τ is the uptake time scale (15 days) [*Doney et al.*, 2006]. Iron in the model is represented by dissolved inorganic iron, the iron content of dissolved organic matter (DOFe, though this is not traced in the model), and the iron content of sinking particles (POFe) [*Doney et al.*, 2006]. The Redfield Ratio is held constant for our model.

2.2.4 Dissolved Inorganic Carbon

Dissolved inorganic carbon (DIC) is defined as [*Bolin et al.*, 1981]:

$$DIC = \left[CO_2\right] + \left[HCO_3^-\right] + \left[CO_3^{2-}\right] \tag{9}$$

The amount of CO_2 in the water column depends on many aspects like the air/sea gas exchange and the carbon rain rate. The air/sea gas exchange influences DIC concentrations in the surface via the amount of CO_2 transferred from the atmosphere to the ocean, i.e., a higher pCO_2 in the atmosphere would in turn increase the CO_2 in the surface ocean. Temperature also

affects the air/sea gas exchange because of the solubility of CO_2 within the water; warmer water has lower solubility. The carbon rain rate depends on the level of productivity in the surface water and that dependence in turn is regulated by the amount of nutrients and light availability in the water column, particularly nitrogen and phosphorous (in the form of phosphates), which supports biological productivity [*Bolin et al.*, 1981]. Nitrogen plays a role in many of the biogeochemical functions in the ocean; however, it is not included within this model experiment. Since there is high correlation between nitrogen and phosphorous [*Millero*, 1995], phosphorous may be used to calculate nitrogen concentrations.

2.2.5 Alkalinity

Alkalinity (ALK) is equal to the charges of all the weak ions in solution [*Stumm and Morgan*, 1981] and can be approximated by [*Dickson*, 1981]:

$$ALK = \left[HCO_3^-\right] + 2\left[CO_3^{2-}\right] + \left[B(OH)_4^-\right] + \left[OH^-\right] - \left[H^+\right] \tag{8}$$

Since bicarbonate and carbonate are the dominant anions of weak acids in seawater, alterations in their ratios are the major controlling factor in total alkalinity and thereby total alkalinity is approximated to carbonate alkalinity in seawater [*Chester*, 2000]. Decreasing either of the carbonate ions then will decrease the alkalinity of seawater. Decreasing carbonate ion concentrations can be accomplished by increasing precipitation, decreasing evaporation, increasing productivity and thereby increasing precipitation of calcium carbonate, or by influx of freshwater into seawater. As salinity is equivalent to the amount of dissolved solids in seawater (major anions contributing to salinity are listed in Table A.2), it too is directly affected by dilution of seawater by many of the same means [*Chester*, 2000].

2.2.6 Dissolved Oxygen

Dissolved O_2 levels are controlled via exchange across the air/sea interface, biological processes, and physical transport [*Chester*, 2000]. Within the mixed layer, oxygen levels are

primarily controlled by exchange between the atmosphere and ocean. Below the mixed layer depth in the intermediate waters, oxygen levels are controlled by organism respiration and organic decay [*Chester*, 2000; *Burdige*, 2006], which in turn is controlled by nutrient availability (See Section 2.2.2).

2.2.7 $\delta^{13}C$

The $\delta^{13}C$ is the ratio of Carbon-13 to Carbon-12 (See Section 1.3). Organisms preferentially use Carbon-12 to build their bodies and tests, which enriches the surface water dissolved inorganic carbon (DIC) in Carbon-13 while slightly depleting water below the euphotic zone in Carbon-13 as Carbon-12 rich bodies sink through the water column. As such, $\delta^{13}C$ depends on nutrient levels; an increase in nutrients will increase carbon consumption near the surface and induce afore mentioned effects. Therefore $\delta^{13}C$ is influenced by changes in ocean currents, which bring nutrient laden waters to the surface. Although the air-sea gas exchange affects $\delta^{13}C$ and is taken into account for data reconstructions, it is not taken into account in this model. Also, $\delta^{13}C$ is parameterized with a computer script, based upon the correlation between $\delta^{13}C$ and PO_4. $\delta^{13}C$ is first order inversely correlated to PO_4 concentration and can be approximated after *Broecker and Maier-Reimer* [1992] by the following expression:

$$\delta^{13}C = 2.9 - 1.1(PO_4) \tag{11}$$

2.2.8 pH

In general pH displays a negative relationship with the hydrogen ion concentration

$$pH = -\log_{10}\alpha_H \tag{12}$$

where α_H is the activity of the hydrogen ions [*Chester*, 2000]. Much research has shown however, that the carbonate system, and thereby pH, depends on many factors such as temperature, salinity, and pressure [i.e., *Millero*, 1995; *Lueker et al.*, 2000; *Emerson and*

Hedges, 2008]. For example, as CO_2 enters the ocean from the atmosphere via the air/sea gas exchange (See Section 2.2.2), the amount of H^+ ions in the ocean increases [*Chester*, 2000] and the pH decreases.

2.3 Boundary Conditions

2.3.1 Topography and Land-Sea Distribution

In this experiment the Eocene topography is based upon *Sewall et al.* [2000] and updated from *Shellito and Sloan* [2006] and Winguth et al. [in press]. The main modification, based upon data from the PALEOMAP Project [*www.scotese.com*], is that the Arctic Ocean is now closed and freshwater is exchanged per the surface freshwater flux balancing over marginal seas described in the Reference Manual for the Parallel Ocean Program (POP) [*Smith and Gent*, 2004] (see Section 2.1).

2.3.2 Landsurface Parameterizations

The land vegetation used in this experiment is that of *Sewall et al.* [2000] used in *Shellito et al.* [2003] and *Shellito and Sloan* [2006] (Fig. 1 therein). The twelve vegetation categories or types are those of *Dorman and Sellers* [1989].

2.3.3 Solar Forcing

The solar constant for the Paleocene/Eocene boundary is 1362 $W \cdot m^{-2}$ indicating a 0.44% decrease from modern values. This value is based upon the curve fit to model results of Boothroyd [*Caldeira and Kasting*, 1992; *Winguth et al.*, 2002]:

$$S(t) = (1 - 0.38t/\tau_o)^{-1} S_o \tag{15}$$

Here S(t) is the luminosity of the Sun at time t, years from the present, τ_o is 4.55 Gyr, and S_o is the present day value of luminosity (1368 W/m^2).

Eccentricity and a moving vernal equinox are set equal to zero, so that the earth's orbit around the sun is circular and the position of the Earth in its orbit does not change with each year. The use of this circular orbit ensures equal receipt of solar insolation for both

hemispheres [*Gibbs et al.*, 2002; *Winguth et al.*, 2002]. Earth's obliquity (axis tilt) is set to 23.5°, the same as the modern value.

2.3.4 Greenhouse Gas Forcing

CO_2 levels are set to observations. In this study the atmospheric partial pressure of CO_2 (pCO_2) is set to 2240 ppm, about 8x pre-industrial level. This level, although possibly low according to some estimates for the PETM, [*Hsieh and Yapp*, 1999; *Pearson and Palmer*, 2000; *Zachos et al.*, 2001] agrees with others [*Yapp*, 2004; *Zachos et al.*, 2008]. *Pagani et al.* [2006] suggests levels of CO_2 could be much higher in both the atmosphere and ocean if viewed as the only forcing mechanism for climate change. N_2O levels were set at 0.275 ppb and CH_4 levels at 0.700 ppb, both representative of pre-industrial values. The CH_4 level is not changed from its pre-industrial value because it's residence time in the atmosphere is so short, less than ten years, and it oxidizes into CO_2 [*Wallace and Hobbs*, 2006].

$$CH_4 + 2O_2 \rightarrow CO + 2H_2O \tag{16}$$

CHAPTER 3

EXPERIMENTAL DESIGN AND CLIMATE SIMULATIONS

3.1 Experimental Design and Initialization Conditions

In order to explore the impact of fresh water pulses from the Arctic on the climate and ocean circulation, and the carbon cycle's response to these changes, three simulations are conducted. The locations of possible Arctic shallow seaways are summarized in Table A.3 and shown in Figure A.1. Each experiment simulates exchange between the Eocene Arctic and different global ocean basins. All model simulations are integrated over 2000 years. Beginning global temperature and salinity profiles are from a previous 560-year Eocene Simulation with a pCO_2 of 2240 ppm [Shellito et al., 2009; *Winguth et al.*, in press]. The experiment that models exchange between the Arctic Ocean and the Indian Ocean is referred hereafter to as the Control experiment, and is more detailed in *Winguth et al.*, in press. The remaining two experiments are termed EOCPAC and EOCATL. In the EOCPAC experiment freshwater is exchanged between the Arctic and the Pacific whereas in the EOCATL experiment it is exchanged between the Arctic and the Atlantic.

It should be noted here that the freshwater exchange between the Arctic and the adjacent ocean is calculated with the use of the marginal sea parameterization (Section 2.1) to simulate shallow seaways. Initial conditions are based upon a previous 560-year Eocene simulation [*Winguth et al.*, in press] with boundary conditions from those of *Sewall et al.* [2000] and *Shellito et al.* [2003].

3.2 Sensitivity to Arctic Freshwater Pulses in the Indian/Tethys (Control Experiment)

The Control experiment, preformed by Winguth et al., in press, uses the initial and boundary conditions discussed above (Sections 2.3 and 3.1) and was integrated over 2000

years, simulating freshwater exchange between the Arctic and Indian Oceans through the Turgay Strait. Choosing the freshwater exchange between the Arctic and Indian Oceans as the Control experiment is based upon the paleogeographic reconstruction of the PALEOMAP Project [*Scotese*, 2008] as well as data, specifically microfossil data from the Turgay Strait region, from *Meulenkamp et al.* [2000], *Iakovleva et al.* [2001], and *Iakovleva and Heilmann-Clausen* [2007].

3.3 Sensitivity to Arctic Freshwater Pulses in the Pacific (EOCPAC Experiment)

The EOCPAC experiment uses the same initial and boundary conditions as the Control experiment (Section 3.2), and is also integrated for 2000 years, but simulates a freshwater exchange between the Arctic and the Pacific Oceans. The location of freshwater exchange is in the North Pacific, representing flow through the Bering Strait (Figure A.1).

3.3.1 Atmosphere

3.3.1.1 Surface Air Temperature (SAT)

Surface air temperature (SAT) here represents the temperature in °C of the lower few meters of the atmosphere above both terrestrial and ocean surfaces. The EOCPAC experiment exhibits noticeable differences in SAT relative to the Control experiment (Figure A.5). The experiment indicates a decrease in temperature relative to the Control experiment of 1.5-2°C over the North Pacific but illustrates an increase in ~2-2.5°C in the North Tethys Ocean. It also simulates a minor decrease, ~1°C, in the western Pacific Ocean along the coast of North America.

Changes in SAT between the EOCPAC and Control experiments correspond extremely well to changes in ocean surface temperatures (Figures A.5 and A.6). Even minor changes in sea surface temperatures (SSTs), like an increase of ~1°C near 45°N in the Eastern Pacific, correlates to similar changes, < 0.7°C, in the atmosphere. Note that the changes in atmospheric surface temperature over land are also directly connected to the changes in the

SSTs. For example, the ~0.3°C warming over the Asian continent in the EOCPAC experiment is seen to be an extension of the larger warming, ~2°C, in the North Tethys Ocean (Figure A.5).

3.3.1.2 Sea Level Pressure (SLP)

Sea level pressure (SLP) differences between the sensitivity experiments are most pronounced over the northern hemisphere (Figure A.7). For the EOCPAC experiment, pressure increases by ~1-1.5 hPa over the North Pacific and along the western coast of North America compared to the Control experiment. It decreases over the Arctic Ocean by ~1 hPa and over the North Indian Ocean and Southwest Asia by ~1.6 hPa.

Sea level pressure is controlled by temperature and moisture; as moisture decreases or temperature increases, the density of air decreases and thereby the pressure at that location. Differences in SLP between the EOCPAC and Control experiments correlate negatively to atmospheric and thereby to oceanic surface temperatures (Figures A.5-A.7). SLP is sensitive to minor changes in temperature, for example, the ~1°C decrease off of the western North American coast correlates highly to a 1 hPa increase in SLP. Changes between the EOCPAC and Control experiments for SLP, SSTs, and SAT are consistent with the change in location of Arctic freshwater flux between the two experiments (Figure A.1).

3.3.2 Ocean

3.3.2.1 Sea Surface Temperatures (SSTs)

Annually averaged sea surface temperatures in the North Pacific poleward of 45ºN are around 10-11°C, a decrease of ~1-2°C relative to the Control experiment (Figure A.6). SSTs in the EOCPAC experiment simulate a decrease of around 1-1.5°C along the western coasts of North America and Southwest Europe. Surface temperatures throughout the North Indian Ocean increase ~2°C and by around 1-1.5°C off the east coast of North America, compared to the Control experiment. The East-West temperature gradient across the Pacific is about ~1.5-2°C warmer than in the Control experiment. As discussed above, changes in SSTs affect both

SAT and surface pressure, and are primarily controlled by changes in ocean circulation (*see* Section 4.4).

3.3.2.2 Surface Salinity, Alkalinity, and pH

Annually averaged surface salinity levels for the EOCPAC experiment are highest around 35° North and South latitudes in both the Pacific and the Atlantic as well as the equatorial region in the Pacific. In these locations the salinity is ~36 psu. Salinity levels are lowest in the high north latitudes for both the Atlantic and Pacific, around 30 units. Relative to the Control experiment surface salinity levels simulate a decrease by ~3 psu in the North Pacific and increase by ~9 psu in the northern Indian Ocean (Figure A.8). The model produces lowest alkalinity (ALK) levels in the EOCPAC experiment in the far North Pacific (~1.8 μeq/L, above 60°N) and Atlantic Oceans (~1.6 μeq/L) (Figure A.9). Highest ALK levels are found along the mid-latitudes including the northern Tethys Ocean (~2.5 μeq/L). Compared to the Control experiment, the EOCPAC experiment simulates an increase of around 0.5 μeq/L in the North Tethys Ocean and a decrease of ~0.2 in the North Pacific.

Salinity and alkalinity correlate well in many parts of the ocean due to fact that the ratio of bicarbonate to salinity is nearly constant [*Millero*, 2006] and alkalinity levels depend mostly on carbonate ions, therefore, as CO_3 increases or decreases, so do both salinity and alkalinity. In areas of upwelling the surface alkalinity may increase more than the salinity due to the dissolution of $CaCO_3$ at depth producing CO_3, which increases alkalinity more than salinity. At the surface, both tracers decrease in the North Pacific and increase in the northern part of the Tethys Ocean in the EOCPAC experiment compared to the Control. These locations correlate to increased and decreased Arctic freshwater flux, respectively.

Lowest pH levels (~7.2) in the EOCPAC experiment are in the North Pacific and Atlantic Oceans above 60°N; highest levels (~7.4) are in the North Tethys Ocean and across the mid-latitudes. Relative to the Control experiment, the EOCPAC experiment simulates a decrease in pH (~0.03) in the North Pacific and an increase of about 0.1 in the North Indian Ocean (Figure

A.10). Surface pH correlates well with salinity and alkalinity and differences in pH between the Control and EOCPAC experiments display a positive relationship to differences in salinity, alkalinity, and DIC between the two experiments. As seawater temperatures decrease the disassociation of H^+ ions decreases, increasing overall pH [*Millero*, 2006]. Also at depth in the oceans the dissolution of $CaCO_3$ and the decrease in ρCO_2 increases the pH [*Chester*, 2000; *Emerson and Hedges*, 2008], so that one would expect higher pH levels in places where cold, nutrient rich waters come to the surface. Despite this information, it has been shown by measuring pH across surface waters that in areas of upwelling levels decrease in proportion to decreases in temperature [*Millero*, 2006]. The relationship can be seen in the EOCPAC experiment where cold, older waters flow up in the equatorial eastern Pacific Ocean and the pH is lower at the surface (Figures A.6, A.10).

3.3.2.3 Deep-Water Formation (Temperature, Salinity, Density and the Depth of the Mixed Layer)

Salinity and temperature primarily control density and the depth of the mixed layer is the primary control on formation of deep-water [*Bryan et al.*, 2006], and thereby the age of the water. By comparing the idealized age of the water mass along with temperature, salinity, density, and the maximum depth of the mixed layer, locations for deep-water formation may be reconstructed.

The EOCPAC experiment simulates stronger deep-water formation in the North Atlantic, North Tethys, and South Pacific, and weaker deep-water formation in the North Pacific. Although temperature and salinity are the major contributing factors to the calculation of the Idealized Age Tracer within the CCSM3 model (see Section 2.2.5), deep-water formation at each of these locations appears to be controlled by multiple factors. In the North Atlantic, despite the fact that both density and salinity are higher in the Control experiment, the EOCPAC experiment displays a younger water mass age and a deeper maximum mixed layer depth (Figure A.11). The younger water mass age and deeper maximum mixed layer depth indicate

that the lower temperature in the EOCPAC experiment relative to the Control experiment may possibly be the controlling factor of increased deep-water formation.

In the eastern North Pacific around 45°N lower temperatures, higher salinities, and greater density favor stronger deep-water formation in the Control experiment. In the North Tethys although temperature is lower and density higher in the Control experiment, salinity is higher, maximum mixed layer depth is deeper, and the age of the water mass is younger in the EOCPAC experiment. For both of these locations it appears that the change in location of freshwater input plays a predominant role in deep-water formation. In the South Pacific, temperature is lower, salinity higher, and density higher for the Control experiment. Despite this, the maximum mixed layer depth is deeper and the age of the water mass younger in the EOCPAC experiment, suggesting that the weakening of deep-water formation in the North Pacific due to increased freshwater input may allow for the strengthening of deep-water formation and overturning circulation in the South Pacific.

3.3.2.4 Change in Intermediate Water Masses

The most significant signal within the ocean layers occurs throughout intermediate waters (500-1500m). At ~1200m, the lowest temperatures in the EOCPAC experiment are in the South Pacific (~9°C), whereas the highest temperatures are in the North Pacific (~13°C). Temperatures in the EOCPAC experiment increase in the Northwest Pacific (~2°C), South Pacific (~0.1°C), and North Tethys Oceans (~1.5°C) relative to the Control experiment. They decrease compared to the Control experiment in the North Atlantic by around 1°C (Figures A.12 and A.13).

The ideal age tracer is a measure of the age of water masses throughout the ocean basins (see Section 2.2.5). In the EOCPAC experiment at around 1200m the youngest waters are in the South Pacific (~140 years) near the Eastern coast of Australia (Figure A.14). The oldest water masses occur in the eastern equatorial Pacific and throughout the mid-Atlantic Ocean (~1100 years). Relative to the Control experiment, the EOCPAC experiment displays

younger water masses, in the South Pacific (~+50 years), North Atlantic (~+200 years), and North Tethys Oceans (~+1000 years), and older water masses, ~400 years, in the North Pacific (Figure A.14 and A.15).

At 1200m, salinity increases in the EOCPAC experiment in the North Pacific near 30°N by ~0.5 psu; it decreases in the North Atlantic by ~0.2 psu (Figure A.16). In the EOCPAC experiment at depths around 1200m, ALK decreases by ~0.03 μeq/L in the North Tethys and increases by around 0.04 μeq/L in the northeastern part of the Pacific Ocean compared to the Control experiment (Figure A.17). Near 1200m in the EOCPAC experiment, the model simulates a stronger increase in alkalinity than in salinity in the North Pacific Ocean and a strong decrease in alkalinity compared with a weak increase in salinity in the North Tethys Ocean. The changes in alkalinity and salinity are due to a reduction in deep-water formation, and hence more stratification in the North Pacific, and a increase in deep-water formation and circulation in the North Indian Ocean, bringing down higher salinity concentrations from the surface.

The addition of freshwater input into the North Pacific changes the strength of intermediate water mass formation throughout the global oceans. It is stronger in the North Tethys, North Atlantic, and South Pacific and weaker in the North Pacific for the EOCPAC experiment compared to the Control experiment.

3.3.2.5 Ocean Heat Transport and Circulation

Maximum oceanic heat transport in the Northern Hemisphere is 1.5 PW at ~15°N latitude in the EOCPAC experiment, whereas maximum heat transport in the Southern Hemisphere is 1.2 PW at 15°S latitude (Figure A.18A). Also, oceanic heat transport at ~45°S latitude in the EOCPAC experiment actually flows toward the equator with a peak of 0.1 PW, most likely due to strong northward overturning circulation at that location. Global heat transport for the EOCPAC experiment is nearly identical to that for the Control experiment, with only a slight decrease, less than 0.1 PW, in the Northern Hemisphere. The stronger southward

flow of meridional overturning circulation at ~60°N in both the shallow and deep ocean in the EOCPAC experiment (Figure A.19A), in addition to weaker northward flow in intermediate waters near 30°N, supports the decreased northward heat transport in the EOCPAC experiment compared to the Control experiment.

Comparing meridional overturning circulation and northward heat transport for the Pacific basin only, the EOCPAC experiment simulates higher levels (0.2 PW) of northward heat transport than the Control experiment at latitudes poleward of 45°N and between 15°S and 45°S (Figure A.18B). The greater northward heat transport is concurrent with weaker southward overturning circulation in the Northern Hemisphere (~45°N) in intermediate waters and stronger southward circulation in intermediate waters in the Southern Hemisphere (15-45°S) (Figure A.19B).

Heat transport in the Atlantic basin is overall much weaker than that in the Pacific basin, with peak transport at ~0.6 PW compared to a Pacific basin peak of ~1.5 PW (Figure A.18C). Relative to the Control experiment, the EOCPAC experiment reproduces weaker northward heat transport around 30°N latitude, but stronger transport at higher latitudes, up to an increase of 0.15 PW greater. At 30°N, the EOCPAC experiment demonstrates weaker northward circulation in depths less than 500m and weaker southward circulation (2 Sv) at intermediate depths poleward of 35°N (Figure A.19C).

In the Indian basin around 15°S, northward (southward) heat transport for the EOCPAC experiment is weaker by 0.15 PW (Figure A.18D). Reduced southward heat transport correlates well with stronger northward overturning circulation in intermediate and deep-waters at ~15°S (Figure A.19D) .

Overall, though slight differences in global ocean circulation and heat transport are simulated, detailed changes are noted within the specific basins (Figures A.18 and A.19). The decrease in southward ocean circulation in the Pacific basin along with the increased northward heat transport in the Northern Hemisphere, correlates well with the increase in Arctic freshwater

flux entering the North Pacific and a reduction in deep-water formation. In the Atlantic basin, decreased southward flow in the EOCPAC experiment in intermediate waters is coincident with a (~100 yrs) younger water mass and increased northward heat transport compared to the Control experiment. In the Indian basin, decreases in southward heat transport and increased northward circulation coincide with a younger water mass, deep-water formation in the North Tethys, and decreased Arctic freshwater flux (Figures A.1, A.14, A.18, and A.19).

3.3.2.6 Dissolved Inorganic Carbon (DIC)

In the EOCPAC experiment DIC simulates highest values (~2.5 mmol/L) at the surface in the North Indian Ocean and at the mid-latitudes. Lowest values, around 2 mmol/L, are in the North Pacific and North Atlantic (above paleolatitude 60°N). Relative to the Control experiment, the EOCPAC displays an increase in DIC ~0.5 mmol/L in the northern part of the Tethys Ocean and a decrease of around 0.15 mmol/L in the North Pacific (Figure A.20). As with alkalinity, near 1200m DIC increases in the North Pacific (~0.3 mmol/L) and decreases in the North Atlantic (~0.05 mmol/L) and North Tethys Oceans (~0.02 mmol/L) (Figure A.21).

Decreases in the North Pacific and increases in the northern part of the Tethys Ocean in surface DIC between the EOCPAC experiment and the Control experiment correlate to increased and decreased Arctic freshwater flux respectively. As discussed above, at depth (~1200m) changes in DIC concentrations are connected to increased or decreased circulation. Therefore, as deep-water formation decreases in the North Pacific and waters become more stratified in the EOCPAC experiment compared to the Control experiment, the concentration of CO_3 and DIC increases.

3.3.2.7 Dissolved Oxygen concentration (O_2)

Highest surface dissolved oxygen concentrations for the EOCPAC experiment are simulated in the North Atlantic (0.33 mL/L) and North Pacific (0.29 mL/L). Lowest surface concentrations are across the equator and throughout the mid-latitudes (0.19 mL/L) (Figure A.22). Discernable differences between the EOCPAC and Control experiments in surface

concentrations include a decrease of ~0.025 mL/L in the North Tethys Ocean and an increase ~0.02 mL/L in the North Pacific. These differences correspond to a decrease and increase in freshwater input respectively.

Oxygen concentrations at a depth of ~1200m increase in the EOCPAC experiment compared to the Control experiment by ~0.1 mL/L in North Tethys Ocean and decreases over a substantial area of the North Pacific (~0.8 mL/L) (Figure A.23). The decrease in the North Pacific corresponds to decreased deep-water formation in the EOCPAC experiment compared to the Control experiment just as increased dissolved oxygen in the North Tethys corresponds to increased deep-water formation.

Oxygen concentrations at the surface increase pole-ward due to increasing O_2 solubility with decreasing temperature and vary negatively with evaporation levels. Differences in surface O_2 concentrations between the EOCPAC and Control experiments correlate not only to differences in freshwater input, but also to changes in exchange with the atmosphere. Colder fresher waters contain more oxygen, however, if oxygen levels are lower in the atmosphere, dissolved oxygen from the ocean will transfer to the gas phase in the atmosphere via the air-sea gas exchange. Transfer of oxygen between the atmosphere and ocean can be traced by observing f_{O_2}, oxygen fugacity, which represents the rate of O_2 transfer from the surface of the ocean to the lower atmosphere. Oxygen concentrations in the North Tethys Ocean, and off the southeast coast of North America, decrease with increased f_{O_2}, whereas concentrations in the North Pacific increase slightly with decreased fugacity relative to the Control experiment (Figure A.24).

3.3.2.8 $\delta^{13}C$

Deep-sea $\delta^{13}C$ is computed diagnostically using the relationship from equation (2). At ~1200m depth the EOCPAC experiment displays highest $\delta^{13}C$ levels, ~1.8‰, in the North Tethys Ocean and lowest levels ~-0.3‰ in the Southern Ocean. Compared to the Control experiment values in the North Pacific are around 0.5‰ lower than the EOCPAC experiment

and around 1.5‰ higher in the Tethys Ocean (Figure A.25). In the EOCPAC experiment, the increased levels of carbon 13 isotopes in the North Tethys Sea coincide with increased deep-water formation and a younger water mass. The decrease in the EOCPAC experiment compared to the Control experiment in $\delta^{13}C$ in the North Pacific correlates with decreased deep-water formation and an older water mass (see Section 1.3).

3.4 Sensitivity to Arctic Freshwater Pulses in the Atlantic (EOCATL)

The EOCATL experiment uses the same initial and boundary conditions as the Control experiment (Section 3.2), and is also integrated for 2000 years, simulating a freshwater exchange between the Arctic and the Atlantic Oceans. The location of freshwater exchange is in the North Atlantic, representing flow through a North Atlantic Seaway (Figure A.1).

3.4.1 Atmosphere

3.4.1.1 Surface Air Temperature (SAT)

The EOCATL experiment exhibits nominal differences in atmospheric surface temperature relative to the Control experiment (Figure A.5). It simulates an increase of ~1.2°C in the North Indian Ocean and a decrease in temperature relative to the Control experiment of about 1.2°C over the eastern Atlantic along the western coast of Europe. There is another minor decrease of around 1°C in the western part of the Pacific Ocean near 60°N.

As with the EOCPAC experiment, changes between the EOCATL and Control experiments in atmospheric surface temperatures correspond with changes in ocean surface temperatures (Figures A.5 and A.6). For example, off the southwest coast of Europe, the 2°C decrease in ocean surface temperature in the EOCATL experiment compared to the Control experiment correlates to about a 1.2°C drop in atmospheric surface temperature in the same area. Minor connections between differences in surface temperatures over the ocean and over land are simulated as well, such as the decrease in temperature over southwest Europe. Major differences between the EOCATL and Control experiments for ocean surface temperature and

surface air temperature are regionally consistent with the change in location of Arctic freshwater flux between the two experiments from the Atlantic to the Indian Oceans (Figures A.5 and A.6).

3.4.1.2 Sea Level Pressure (SLP)

Differences in the EOCATL experiment relative to the Control simulate pressure increases by ~1.3 hPa over the eastern North Pacific Ocean and by about 1 hPa over the eastern part of the Atlantic Ocean (Figure A.7). SLP decreases over the western Pacific Ocean near 60°N and in the North Tethys Ocean by ~0.5 hPa.

In the eastern Atlantic Ocean and North Tethys Oceans SLP correlates negatively to surface atmosphere and ocean temperatures. However, in the western Pacific Ocean SLP decreases above a decrease in surface ocean and atmosphere temperatures. Also, there is a significant anomaly (an increase >1.2 hPa) in SLP over the eastern Pacific Ocean with no corresponding anomaly in surface atmosphere or ocean temperature. Changes in SLP in both Pacific Ocean locations may be due to changes in moisture content in the air. Outside of the Pacific Ocean changes in SLP correlate well with changes in the location of freshwater flux between the EOCATL experiment and Control experiment (Figure A.7).

3.4.2 Ocean

3.4.2.1 Sea Surface Temperatures (SSTs)

For the EOCATL experiment, annually averaged sea surface temperatures in the western North Pacific around 30°N are about 12°C, a decrease of ~1°C relative to the Control experiment (Figure A.6). Sea surface temperatures also decrease by ~1°C in the North Atlantic near 30°N as well as by ~1.5-2°C along the southwest coast of Europe, spreading out into the eastern part of the central Atlantic Ocean. Surface temperatures in the EOCATL experiment increase along the coast of southwest Asia ~2°C compared to the Control experiment. Sea surface temperature changes between the EOCATL and Control experiments in the North Atlantic and Tethys Oceans correlate well to changes in the location of freshwater flux between the two experiments and the subsequent changes in ocean circulation. As freshwater enters

the North Atlantic it forms a lens in the upper ocean causing stagnation in the depths below and allowing for more robust southward circulation and less warm water brought up from the tropics.

3.4.2.2 Surface Salinity, Alkalinity, and pH

Annually averaged surface salinity levels for the EOCATL experiment are highest all through the mid-latitudes in the various oceans. The salinity level in these locations is ~36 psu. Low salinity is simulated in the high north latitudes (30 psu in the North Pacific and ~24 psu in the North Atlantic). Relative to the Control experiment, surface salinity is decreased by ~3-4 psu in the North Atlantic and increased by ~7 psu in the North Indian Ocean (Figure A.8). Lowest alkalinity (ALK) in the EOCATL experiment is in the high latitudes (~2.2-2.3 μeq/L) specifically in the North Atlantic (~1.6 μeq/L). Highest ALK is found along the mid-latitudes at values above 2.5 μeq/L. The EOCATL experiment indicates an increase, relative to the Control experiment, of around 0.5 μeq/L in the North Tethys Ocean and a decrease of ~0.25 μeq/L in the North Atlantic (Figure A.9). Surface concentrations for salinity and alkalinity in the EOCATL experiment compared to the Control experiment differ negatively with changes in freshwater input into either the North Atlantic or North Tethys Oceans.

Lowest pH levels (~7.32) in the EOCATL experiment are in the high latitudes whereas highest levels (~7.42) are near the mid-latitudes. Relative to the Control experiment, the EOCATL experiment displays a decrease in pH (~0.05) in the North Atlantic and an increase, 0.09, in the North Indian Ocean above 15°N (Figure A.10). pH correlates extremely well with salinity and alkalinity, and differences in pH between the Control and EOCATL experiment display a positive relationship to differences in salinity, alkalinity, and DIC between the two experiments. The decrease (0.02) in pH along the west coast of North American represents a location of upwelling (see Section 3.3.2.2).

3.4.2.3 Deep-Water Formation (Temperature, Salinity, Density and the Depth of the Mixed Layer)

Differences between the EOCATL and Control experiments are nominal in most cases and specific locations tend to show varying trends when comparing temperature, salinity, density, and the maximum mixed layer depth. The North Pacific and North Atlantic Oceans within the EOCATL experiment simulate warmer, less dense waters, with a shallower maximum mixed layer depth (Figure A.11). The salinity is increased in both of these locations suggesting that temperature is the dominant factor in regards to density. The locations appear to reproduce reduced deep-water formation in the EOCATL experiment compared to the Control experiment.

In the South Pacific and North Tethys the waters at ~1200m appear to be cooler and younger with deeper mixed layer depths in these regions compared to the Control experiment. Both locations simulate decreased salinity despite deeper mixed layer depths. Density is greater in the EOCATL experiment in the North Tethys suggesting again that temperature plays a greater role compared to salinity in controlling density. Increased deep-water formation is simulated for these locations in the EOCATL experiment compared to the Control experiment; however, density is lower in the EOCATL experiment in the South Pacific. Reduced deep-water formation in the North Pacific and thereby reduced overturning circulation there allows for an increase in deep-water formation in the South Pacific and increased northward circulation.

Intermediate water mass formation occurs in the same locations for the EOCATL and Control experiments. It is stronger in the North Tethys, North Atlantic, and South Pacific Oceans, and weaker in the North Pacific Ocean for the EOCPAC experiment compared to the Control experiment.

3.4.2.4 Changes in Intermediate Water Masses

Intermediate depth water (around 1200m) temperatures in the EOCATL experiment are warmest in the North Atlantic Ocean and part of the western Pacific Ocean near 30°N, around

12-13°C. Ocean temperatures are coolest in the South and North Pacific, ~9.5°C. With the exception of the central North Pacific Ocean all temperatures in the EOCATL experiment differ by less than 0.5°C compared to the Control experiment. North Pacific temperatures in the EOCATL experiment are around 0.7°C greater than in the Control experiment (Figures A.12 and A.13).

At around 1200m depth, the idealized age of the water masses is ~120-150 years in the North Pacific, ~200 years old in the South Pacific, ~600-650 years old in the North and South Atlantic, and ~1200 years old in the North Tethys. Again with the exception of the North Pacific Ocean all differences in the age of the water masses between the EOCATL and Control experiments are less than 50 years. In the EOCATL experiment the North Pacific has water masses at 1200m depth ~140-150 years older than the Control experiment (Figures A.14 and A.15).

Differences in salinity ~1200m are ~0.1 psu less than the Control experiment in the Tethys Ocean and ~0.1 psu greater in the North Pacific Ocean (Figure A.16). Near 1200m depths alkalinity increases by around 0.015 μeq/L in the Northeast Pacific near 45°N and decreases by ~ 0.01 μeq/L in the North Tethys Ocean compared to the Control experiment (Figure A.17). The increase in the EOCATL experiment in ALK in the North Pacific and decrease in the North Tethys at depths near 1200m compared to the Control experiment, support decreased deep-water formation in the Pacific Ocean and increased deep-water formation in the Tethys Ocean (see Section 3.3.2.5).

Freshwater input into the North Atlantic changes the location and strength of intermediate water mass formation very little in the EOCATL experiment compared to the Control experiment. Formation is strong in both the North and South Pacific for both experiments and weaker in the North Atlantic and North Tethys. The EOCATL does simulate a slight strengthening relative to the Control experiment in intermediate water mass formation in the North Tethys as salinity increases due to a reduction in freshwater input.

3.4.2.5 Ocean Heat Transport and Circulation

Global northward heat transport for the EOCATL experiment does not significantly differ from the Control experiment (< 0.05 Pw at any latitude (Figure A.26A). Overturning circulation is also similar to the Control experiment but shows stronger southward flow at ~20°S and weaker northward flow around 35°N in both the shallow and deep ocean (Figure A.27A).

In the Pacific Ocean basin, the EOCATL experiment simulates lower levels (~0.1 Pw) of northward heat transport than the Control experiment at latitudes northward of 15°N and stronger (~0.1 Pw) southward heat transport at latitudes between 15°S and 45°S (Figure A.26B). The EOCATL experiment simulates stronger southward circulation (2.5 Sv) around 15°S and 2500m, depths and weaker northward circulation near 45°N and 1000m depths (Figure A.27B).

Heat transport in the Atlantic basin is weaker than in the Pacific basin, with a maximum strength of 0.6 Sv in the northern hemisphere relative to a maximum in the Pacific basin of ~1.7 Sv. Relative to the Control experiment, the EOCATL experiment simulates stronger northward heat transport throughout most of the northern hemisphere with a maximum of ~0.1 Pw near 50°N (Figure A.26C). Overturning circulation produces stronger southward circulation in the EOCATL experiment compared to the Control experiment near 1000m, but noticeably stronger northward circulation ~50°N and depths of 2500m (Figure A.27C).

The EOCATL experiment simulates weaker southward heat transport in the Indian basin relative to the Control experiment south of the equator down to ~30°S (Figure A.26D) and weaker southward flow and stronger northward flow near 30°S and 3000m depths (A.27D).

The stronger southward flow globally near 20°S and weaker northward flow near 35°N correlate well to the changes in heat transport through the ocean. Within the Pacific basin, differences in the strength of overturning circulation again correspond well with changes in heat transport between the EOCATL and Control experiments. Within the simulation, the model shows that although meridional overturning circulation is stronger at intermediate depths in the

Atlantic basin, the reduction in northward overturning circulation in deep-water is the controlling factor on reducing heat transport to the north. In the Indian basin, although stronger northward circulation and weaker southward heat transport are simulated near 45°S, the major reduction in northward heat transport in the EOCATL experiment compared to the Control experiment is again due to the reduction in southward deep-water circulation changes near 15°S.

3.4.2.6 Dissolved Inorganic Carbon (DIC)

As with alkalinity, in the EOCATL experiment DIC simulates highest values (~2.5 mmol/L) throughout the mid-latitudes and the Arctic. Lowest values, around 2 mmol/L, are in the North Pacific above 60°N. Relative to the Control experiment the EOCATL displays an increase in DIC ~0.45 mmol/L in the northern Tethys and a decrease of around 0.35 mmol/L in the North Atlantic (Figure A.20). Also similar to ALK, near 1200m depths DIC increases in the North Pacific (~0.01 mmol/L) and decreases in the North Tethys (~0.01 mmol/L) (Figure A.21).

In the EOCATL experiment, an increase in surface DIC in the North Tethys and a decrease in the North Atlantic compared to the Control experiment are consistent with less freshwater input in the Tethys and more in the Atlantic Ocean. The increase in the North Pacific at 1200m depths supports decreased deep-water formation and the decrease in DIC concentration in the North Tethys Ocean supports an increase in deep-water formation and circulation compared to the Control experiment (see Section 3.3.2.5).

3.4.2.7 Dissolved Oxygen Concentration (O_2)

High surface oxygen concentrations in the EOCATL experiment are simulated in the North Atlantic (0.33 mL/L) and North Pacific Oceans (0.26 mL/L). Lowest surface concentrations are across the mid-latitudes (0.19 mL/L). Discernable differences between the EOCATL and Control experiments in surface concentrations include a decrease of ~0.02 mL/L in the North Tethys Ocean and increases ~0.015 mL/L in the North Atlantic near 55°N and along the southwestern coast of Europe (Figure A.22). Oxygen concentrations at a depth of

~1200m are lower in the North Pacific (0.02 mL/L) and higher in the North Tethys Ocean (0.01 mL/L) (Figure A.23).

Surface oxygen concentrations increase with temperature decrease poleward (see Section 3.3.2.8). Changes in surface O_2 levels between the EOCATL and Control experiments, as in the EOCPAC experiment, are predominantly controlled by fluctuations in the air-sea gas exchange. With increased oxygen fugacity, ocean dissolved oxygen concentrations decrease (Figures A.22 and A.24). As oxygen concentrations decrease and fugacity increases for the EOCATL experiment compared to the Control in the North Tethys Ocean, while dissolved oxygen concentrations increase off the Southwest coast of Europe and f_{O_2} decreases. Within the intermediate waters, decreases in oxygen concentrations correlate to increases in the age of the water mass (Figures A.14 and A.23).

3.4.2.8 $\delta^{13}C$

$\delta^{13}C$ levels in intermediate waters (~1200m) in the EOCATL experiment are highest, around 1.5‰, in the North Pacific Ocean and lowest (~-0.3‰) in the Southern Ocean and up into the South Atlantic. Relative to the Control experiment these values are around 0.08‰ lower in the North Pacific and around 0.08‰ higher in the Southern Ocean and South Atlantic (Figure A.25). One location in the Eastern Pacific decreases by ~0.3‰ compared to the Control experiment. The decreases in the North Pacific and North Atlantic correspond to decreased deep-water formation as the increase in the North Tethys and South Pacific correspond to increased deep-water formation (see Section 1.3). $\delta^{13}C$ and PO_4 display a precise correlation throughout the simulation based upon equation 11 (see Section 2.2.5).

CHAPTER 4

DISCUSSION

4.1 Physics

4.1.1 Water Mass Age (Ideal Age Tracer) and Temperature

Ocean deep-water formation is sensitive to changes in surface buoyancy and momentum fluxes. Changes such as temperature decrease or salinity increase lead to an increase in density relative to underlying waters and causes the water mass to sink [*Pond and Pickard*, 1983]. In the South Pacific for all three experiments, relative to surrounding waters, density increases due to decreased temperature. In the North Pacific density increases due to decreased temperature for the EOCATL and Control experiments. However, in the EOCPAC experiment, temperature in the North Tethys is higher than the surrounding waters but salinity is also noticeably higher. The EOCPAC experiment simulates younger intermediate water masses in the North Tethys and older in the North Pacific relative to the Control experiment indicating increased and decreased deep-water formation respectively.

Temperature change between the sensitivity experiments is largest between the EOCPAC experiment and Control experiment. Potential temperatures of intermediate waters are higher throughout most of the global ocean and specifically in the Pacific basin in the EOCPAC experiment compared to the Control experiment. Increased temperatures in intermediate waters in the EOCPAC experiment suggest that an increase in freshwater input into the North Pacific through the Bering Strait during the late Paleocene might have led to initial warming across the globe which in turn could induce the release of methane hydrates [i.e. *Pagani et al.*, 2006] and be a contributing factor to the onset of the PETM. The simulated

increase in temperatures for the EOCPAC experiment then supports the initial hypothesis that freshwater flux through the Bering Strait might have contributed as a precursor for the PETM.

Teleconnections refer to events where changes occur in one location due to affects at a totally different location. There are multiple examples throughout the simulations, specifically with temperature and intermediate water mass formation. In the EOCPAC experiment, increased temperatures in the western Pacific and North Atlantic Oceans near 45°N coincide with increased freshwater input into the North Pacific Ocean (Figures A.5 and A.6). In the EOCATL experiment decreased temperature in the North Pacific near 30°N coincides with increased freshwater input into the North Atlantic Ocean. Teleconnections in intermediate water masses are apparent in the EOCPAC experiment where freshwater input into the North Pacific decreases the age of the water mass at ~1200m in the North Atlantic Ocean (Figure A.14).

The *Tripati and Elderfield* [2005] reconstruction of deep-sea temperatures and circulation changes based respectively upon $\delta^{18}O$ and $\delta^{13}C$ ratios and Mg/Ca ratios from benthic foraminifers differ significantly from our model results. The Foraminifera data suggests bottom water temperatures in the North Pacific (Shatsky Rise) and South Atlantic (Walvis Ridge) of around 17°C, whereas changes in oxygen and carbon isotope levels are presented as evidence that convection and deep-water formation increased in the North Pacific and decreased in the Southern Ocean [*Tripati and Elderfield*, 2005]. The Control and EOCATL experiments simulate temperatures around 9°C throughout the deeper oceans; they also display the strongest deep-water formation in the North Pacific and Southern Ocean (Figure A.19). Changes in ocean temperatures at depths greater than 1000m in the EOCATL and EOCPAC experiments are minimal, less than 1°C (Figure A.13). However, of the three experiments, the EOCPAC simulates the highest intermediate and deep-water temperatures. The EOCPAC experiment reproduces little deep-water formation in the North Pacific, but does simulate stronger southward circulation at depths greater than ~1500m, as well as the weakest deep-water formation and circulation between the three experiments in the Southern Ocean. Overall, the

experiments are around 6°C cooler than data presented in *Tripati and Elderfield* [2005]. The EOCATL and Control experiments reproduce stronger deep-water formation in the North Pacific Ocean but weaker southward circulation than the EOCPAC experiment, and the EOCPAC experiment simulates the highest deep-sea temperatures, strongest southward circulation in the Pacific Ocean, and weakest deep-water formation and circulation in the Southern Ocean. Increased temperature with a decrease in deep-water formation in the North Pacific Ocean is in disagreement with the conclusion of *Tripati and Elderfield* [2005] that increased deep-water formation in the North Pacific would cause warming of intermediate waters. Potential causes for model-data discrepancies are discussed elsewhere (see *Winguth et al.*, in press). The EOCPAC experiment results of increased southward circulation in the North Pacific Ocean and deep-water formation in the North Atlantic Ocean, as well as reduced circulation in the Southern Ocean, do support the modeling results of *Bice and Marotzke* [2002] though.

Unlike past experiments [*Manabe and Stouffer*, 1995; *Schiller et al.*, 1997] the response of the Atlantic Ocean to massive surface fresh water flux from the Arctic increases the strength of the thermohaline circulation. The EOCATL experiment simulates stronger southward overturning circulation for the Atlantic basin than either the EOCPAC or Control experiments. Changes in sea surface temperatures and air surface temperatures are sensitive to perturbations in freshwater flux in both the EOCPAC and EOCATL experiments (Figure A.6) as shown in the *Manabe and Stouffer* [1995].

Compared to proxy temperature reconstructions for the Arctic [*Tripati et al.*, 2001; *Brinkhuis et al.*, 2006; *Eberle et al.*, 2006; *Moran et al.*, 2006; *Sluijs et al.*, 2006], which suggest temperatures ranging as high as 23°C during the PETM; none of the three experiments simulate similarly high values. However of the three, the highest Arctic surface ocean annual temperatures are produced in the Control and EOCATL experiments with peak annual average temperatures ~10°C. Although still significantly lower than proxy reconstructions, the change in Arctic surface temperatures associated with changes in fresh water flux to the global ocean

lends credence to the conclusions of *Shellito et al.* [2009] that changes in size or depth of Arctic passageways may have played a role in the high Arctic temperatures of the PETM.

4.1.2 Destabilization of Methane Hydrates and the Onset of the PETM

Destabilization of methane hydrates, clathrate hydrates, within the oceans depends on temperature and pressure. These hydrates are crystal ice structures that contain molecules of CH_4 within. As temperature increases or pressure decreases, the ice structures will melt and release the methane, which contains large amounts of carbon. The critical pressure (or depth) of the methane hydrate release depends on the temperature; the higher the temperature the deeper the critical depth of the release (see *Dickens et al.*, 1995 and Figure 1 therein). Most hydrates are formed and are stable on the continental margins, specifically the slope and rise that are between 900-2000m [*Dickens*, 2001].

Bice and Marotzke [2002] propose a positive feedback loop responsible for the onset of the PETM due to the release of these hydrates (see Figure 9 therein). They conclude from their ocean model study that an initial increase in CO_2 in the atmosphere, caused possibly by volcanic outgassing, would increase the strength of the hydrological cycle. These increases could cause a warming at intermediate depths within the ocean on a regional scale that could induce limited methane hydrate destabilization. They argue that this release of CH_4 would then oxidize to CO_2 in either the ocean or atmosphere and further exacerbate extremes in the hydrological cycle and eventually switch high southern latitude deep-water formation to high northern latitude deep-water formation. This switch would bring sudden warm water to the ocean bottoms and incite methane release on a global scale. Figure 10 therein illustrates possible areas of methane hydrates and depths below which the hydrates would be stable given this switch from southern to northern deep-water formation. Based upon their results, this switch in overturning circulation would destabilize methane hydrates throughout all of the Atlantic and Indian Oceans as well as most of the Pacific down to a depth of 1900m, and even further through the North Pacific, down do 2400m. They conclude that this circulation switch

and the subsequent methane release would serve as the catalyst necessary to drive the start of the PETM event.

The EOCPAC experiment illustrates a similar feedback loop (Figure A.2). Increased freshwater flux through the Bering Strait would decrease surface salinity and thereby surface density, reducing deepwater formation and deep overturning circulation from the North Pacific. Increased intermediate water circulation and advection of warm waters from the western and South Pacific could then serve to destabilize methane hydrates first in the North Pacific and then throughout the global ocean. The release of these hydrates and their subsequent dissolution to carbon dioxide entering both the ocean and atmosphere would further increase temperatures and serve as a possible catalyst for the PETM.

4.2 Carbon Cycle and Climate Feedbacks

4.2.1 Salinity and Alkalinity

As discussed in Section 2.2.2, many factors affect salinity and alkalinity levels within the ocean. In the case of this study, dilution by freshwater influx is the obvious process of interest and changes in alkalinity between the EOCPAC or EOCATL experiments and the Control experiment correlate well to changes in freshwater flux. As expected the model simulates decreased alkalinity and salinity in the North Pacific and North Atlantic for the EOCPAC and EOCATL experiments respectively, and increased salinity and alkalinity in the North Tethys Ocean relative to the Control experiment.

4.2.2 Dissolved Inorganic Carbon (DIC)

Changes in surface DIC are controlled by the dilution of bicarbonates, carbonates, and CO_2 in the ocean due to freshwater influx, which affects ocean circulation and biological production. In the North Tethys there is a minor decrease in dissolved oxygen along with the increase in DIC for both the EOCPAC and EOCATL experiments. Relative to the Control experiment, the increase in DIC in the North Tethys compared to decreases in the North Pacific and North Atlantic in the EOCPAC and EOCATL experiments is about five times greater. The

greater increase in the North Tethys Ocean may indicate enough of an increase in productivity to reduce dissolved oxygen levels at the surface due to consumption and oxidation.

4.2.3 Phosphate (PO_4), dissolved oxygen (O_2), and stable carbon isotopes ($\delta^{13}C$)

Relative to the Control experiment in intermediate depths (~1200m) in the EOCPAC experiment the age of the water mass is older, the PO_4 level increases, and dissolved oxygen decreases in the North Pacific. These changes in water mass, PO_4, and dissolved oxygen occur for the EOCATL experiment compared to the Control experiment in the North Atlantic as well. The EOCPAC and EOCATL experiments simulate a younger water mass age, lower PO_4 levels, and increased oxygen in the North Tethys compared to the Control experiment. This indicates that freshwater influx from the Arctic causes stratification in the oceans and reduces the amount of nutrients in the upper layers due to reduced overturning circulation. Furthermore $\delta^{13}C$, which as stated above is simulated based upon a linear relationship with PO_4, will then be affected by these changes in ocean currents.

Nunes and Norris [2006] records average $\delta^{13}C$ for ODP sites throughout the ocean basins. At depths near 1200m both the EOCATL and the EOCPAC experiment show an average $\delta^{13}C$ gradient in the Atlantic Ocean of ~0.7, decreasing from North to South and in agreement with the results of *Nunes and Norris* [2006]. Combining the $\delta^{13}C$ gradient along with a younger water mass age and deeper mixed layer depth in the North Atlantic, all three experiments simulate ocean circulation patterns from North to South in the Atlantic Ocean, similar to the results of *Nunes and Norris* [2006] during the PETM [*see* Figure 3, *Nunes and Norris*, 2006]. All three experiments reproduce some level of flow from the North Atlantic and/or North Tethys and Western Pacific into to the Southern Ocean, in agreement with the conclusions of *Nunes and Norris* [2006] for circulation during the PETM and contrary to the proposed flow paths of *Thomas et al.* [2003]. Also, looking at the depth of the mixed layer and the age of the water masses, each of the experiments reproduces the East to West flow proposed by *Nunes and Norris* [2006] in the Pacific Ocean during the PETM, with $\delta^{13}C$

gradients in the same direction. Of the three sensitivity experiments, the EOCPAC experiment simulates the strongest $\delta^{13}C$ gradients from the North to South Atlantic Ocean, and from the North Tethys and West Pacific Oceans into the Southern Ocean. The model reproduces $\delta^{13}C$ gradients in the Pacific Ocean similar to the data of *Nunes and Norris* [2006].

Zachos et al. [2005] records $CaCO_3$ content of ODP sites 1262, 1263, 1265, 1266, and 1267 on Walvis Ridge in the South Atlantic. From their data they produce the $\delta^{13}C$ at times surrounding the PETM, ~55Ma, (see Figure 3 therein). For three of the sites they provide paleodepths as well: 1263 (1500m), 1266 (2600m), and 1262 (3600m). The $\delta^{13}C$ values recorded at these sites during the PETM range from 1 to -1‰ [*Zachos et al.*, 2005]. All three model experiments simulate the $\delta^{13}C$ values within this range for those depths in the South Atlantic Ocean with the EOCPAC experiment reproducing highest values and the Control experiment simulating lowest values. Similarly, in *John et al.* [2008] a reconstruction of changes in the $\delta^{13}C$ throughout the PETM is produced from the Bass River, ODP 174 site in the North Atlantic. Values there range from 3 to -3‰ for most of the PETM [*John et al.*, 2008]. Carbon isotope values for the Control, EOCPAC, and EOCATL experiments fall within this range with the Control experiment having the highest values, ~2.7‰, and the EOCPAC simulating the lowest values, ~2.6‰.

CHAPTER 5

CONCLUSIONS AND SUMMARY

The use of climate models continues to improve our knowledge of the past, present, and future states of our world. They allow us to interpret the effects of change from a variety of sources on different environments and their impact on the global system. In this study two sensitivity experiments were conducted and compared against the Control experiment discussed in *Winguth et al.* (in press). These experiments examined the affect that Arctic fresh water pulses would have on global ocean circulation, climate, and thereby the carbon cycle during the PETM. The experiments compared Arctic thru flow into the Pacific (EOCPAC) and Atlantic Oceans (EOCATL) against thru flow into the Indian/Tethys Ocean (Control). By analyzing the results and comparing them to proxy data and recent models we may gain insight into the climatic conditions of the PETM, specifically the role Arctic seaways played.

Overall, both the EOCPAC and EOCATL experiments display noticeable changes in ocean and atmospheric properties relative to the Control experiment. Within the ocean, the location of freshwater flux affects both physical and biogeochemical aspects from temperature and salinity to dissolved oxygen levels. Temperature, salinity, and levels of dissolved gases in turn affect atmospheric properties such as pressure, temperature, and gas concentrations. All three experiments reproduce limited deep-water formation in the Southern Ocean and prominent North-South circulation in the Atlantic Ocean, in contrast to the conclusions of *Thomas et al.* [2003] and *Panchuk et al.* [2008] and in agreement with other such as *Nunes and Norris* [2006]. The EOCPAC experiment, however, simulates more dramatic differences to the Control experiment, seemingly more in line with data and modeling results. The increased southern circulation in the Pacific and Atlantic Oceans in the EOCPAC experiment appears to

agree well with previous modeling results such as *Bice and Marotzke* [2002]. The EOCPAC experiment matches the overturning circulation patterns of *Nunes and Norris* [2006] (see Figure 3B therein) during their PETM time slice. Despite neglecting the air-sea gas exchange in our equations, which the computation of carbon isotope ratios depends on, the EOCPAC experiment simulates $\delta^{13}C$ values in agreement with multiple data from ODP cores such as from Walvis Ridge [*Zachos et al.*, 2005] and ODP site 690, the Weddell Sea, [*Kelly et al.*, 2005] in the South Atlantic as well as others [*Nunes and Norris*, 2006; *John et al.*, 2008]. It also reproduces the warmest deep-sea temperatures between the three model simulations. However, among the three experiments the Control experiment most closely simulates sea surface salinity [*Pagani et al.*, 2006] and temperature levels in the Arctic. It also reproduces the closest overall matches to global surface sea and atmosphere temperatures from the data (Figure A.1 and Table A.4). Furthermore, there is significant data that there may have been an open Turgay Strait during the PETM [i.e., *Meulenkamp et al.*, 2000; *Iakovleva et al.*, 2001; *Aleksandrova and Radionova*, 2006; *Iakovleva and Heilmann-Clausen*, 2007].

In conclusion, the model results of these sensitivity experiments indicate that freshwater flux through the Bering Strait may have produced similar circulation patterns to what data indicate for the PETM as well as warming throughout the intermediate and deep ocean layers. Flow through the Turgay Strait also may have produced circulation patterns similar to what data suggests for the PETM, and contributed to increased surface temperatures during that time period. Perhaps flow through the Bering Strait produced a circulation patter that triggered the release of methane hydrates and a secondary or later flow through the Turgay Strait increased temperatures to PETM levels, or vice versa. The fact that warmest ocean temperatures were simulated by the EOCPAC experiment supports the hypothesis that freshwater flow through the Bering Strait could lead to an increase in intermediate water mass temperatures. From the results of this study we conclude that this increase in temperature in intermediate waters could cause a local destabilization of methane hydrates, releasing carbon dioxide into the ocean and

then atmosphere, causing further warming of the atmosphere and then ocean, thereby inducing destabilization on a global scale. The EOCPAC simulation indicates, however, that freshwater input into the North Pacific would already cause a significant shift from northward overturning circulation at intermediate depths to southward overturning circulation and might in itself induce enough widespread warming of ocean waters to release CH_4 on a global scale. The change in circulation pattern along with warmer ocean temperatures in the EOCPAC experiment lends support to the hypothesis that flow through the Bering Strait may have served to trigger the release of methane hydrates and thereby the PETM. Physical and biogeochemical changes in the EOCPAC, EOCATL, and Control experiments, indicate not only that Arctic fresh water pulses may have played a significant role in the global climate and ocean circulation, and thus the carbon cycle during the PETM, but also that the location of Arctic Seaways was an important factor.

Future work may include incorporating the ability to track the depth of the lysocline and/or CCD. Simulating the lysocline depth would allow more detailed comparison to data recovered from ODP sites, specifically the carbonate saturation profile produced by foraminifers and calcareous nannofossils [*Kelly et al.*, 2005; *Zachos et al.*, 2005; *Petrizzo*, 2007]. This capability within a fully coupled general circulation model would present an improvement over some previous models [i.e. *Dickens et al.*, 1997] and allow comparison to others [i.e. *Ridgwell*, 2007; *Ridgwell and Hargreaves*, 2007]. Another future improvement, especially for observing regional changes or detailing the discrepancies between model results and data, is using a higher resolution version of the CCSM3. Other reasons for discrepancies between the model and data could include having incorrect greenhouse gas levels or incorrect paleogeography to include land/sea distribution and orography. The model still inaccurately simulates the high temperatures of the greenhouse world in the early Cenozoic Period as well as the reduced gradient between the polar and tropical regions. Improved knowledge of clouds, for example the abundance of cloud condensation nuclei (CCN), which affects droplet formation and the

albedo level of clouds [*Kump and Pollard*, 2008], might improve these temperature discrepancies within the model. Incorrect orbital parameterization in the model, which could affect solar radiation distribution across the earth, might serve as an explanation for discrepancies between model and data. Also, improved descriptions of plant functional types could reduce discrepancies between model results and data.

APPENDIX A

TABLES AND FIGURES

Table A.1. Partial list of paleoproxies and the data they provide.

Paleoproxy	Data
$\delta^{13}C$	$ppCO_2$
$\delta^{18}O$	Ice Volume
δD	Source Water
Mg/Ca	Temperature
TEX_{86}	Sea Surface Temperature

Table A.2. Major Ions contributing to salinity, from *Wilson*, 1975.

Ion	Concentration (g/kg, S=35‰)
Cl^-	19.354
SO_4^{2-}	2.712
Br^-	0.0673
F^-	0.0013
B	0.0045
Na^+	10.77
Mg^{2+}	1.29
Ca^{2+}	0.4121
K^+	0.399
Sr^{2+}	0.0079

Table A.3. Paleolocation and number of model years integrated for each experiment. Again the marginal sea parameterization is used to model freshwater exchange between the Arctic and Global Oceans.

Experiment Name	Freshwater Exchange	Paleolatitude	Paleolongitude	Years Integrated
Control	Arctic -> Indian/Tethys	40°N	55°	2000
EOCPAC	Arctic -> Pacific	60°N	180°	2000
EOCATL	Arctic -> Atlantic	50°N	355°	2000

Table A.4. Surface, intermediate, and deep-water data-model temperature comparison (annual average years 1950-2000) for locations shown in Figure 1.1 (see also for references). Table after *Winguth et al.*, in press. Paleolocations have been calculated using the PointTracker software by C. Scotese.

Name	Paleo-location	Data Avg.	Age	Depth (m)	Data (°C)	Control avg. (°C)	Pacific avg. (°C)	Atlantic avg. (°C)
DSDP 277	60.6°S, 170.7°W	20.0	~51 Ma	Surface	20	11.7	11.6	11.6
Waipara River	52.1°S, 160.8°W	33.5	~51 Ma	Surface	30-37	14.3	14.1	14.3
Seymour Island	63.4°S, 64.1°W	12.0	~54-53 Ma	Surface	6-18	10.9	11.6	11.5
ODP 690	65.7°S, 7.2°W	18.5	PETM	Surface	17-20	11.9	11.9	11.8
DSDP 74	34.8°S, 10.5°W	N.A.	PETM	Surface	N.A.	23.7	23.5	23.4
Wilson Lake	39.7°N, 57.3°W	33.0	PETM	Surface	33	25.1	16.8	16.8
IODP 302	81.5°N, 42.6°E	23.0	PETM	Surface	23	3.2	2.4	2.8
ODP 865	8.3°N, 151.4°W	33.5	PETM	Surface	32-35	31.6	31.3	31.5
ODP 1209	23.6°N, 171.1°W	34.0	PETM	Surface	33-35	28.1	28	28
Tanzania	19.2°S, 30.9°E	32.0	PETM	Surface	30-34	30.9	30.9	30.8
Bighorn Basin	49.0°N, 89.5°W	23.0	PETM	Surface	20-26	9.5	9	9
Cerrejon Formation	8.4°N, 60.0°W	32.0	~58 Ma	Surface	30-34	31.2	30.3	30.1

Name	Paleo-location		Age	Depth (m)	Data (°C)	Control avg. (°C)	Pacific avg. (°C)	Atlantic avg. (°C)
DSDP 277	60.6°S, 170.7°W	15.0	~51 Ma	Seafloor	15	8.7	8.6	8.6
Waipara River	52.1°S, 160.8°W	21.5	~51 Ma	Interme diate	19-24	9.1-9.5	8.8-9.2	8.7-9.1
ODP 690	65.7°S, 7.2°W	16.0	PETM	~2100	14-18	9.3	9.1	9.1
DSDP 74	34.8°S, 10.5°W	14.5	PETM	~3100-3400	14-15	9.2	6.9	6.9
ODP 865	8.3°N, 151.4°W	15.0	PETM	~1300	13-17	10.4	10.7	10.3
ODP 1209	23.6°N, 171.1°W	17.0	PETM	~2400	13-21	9.4	9.9	9.4

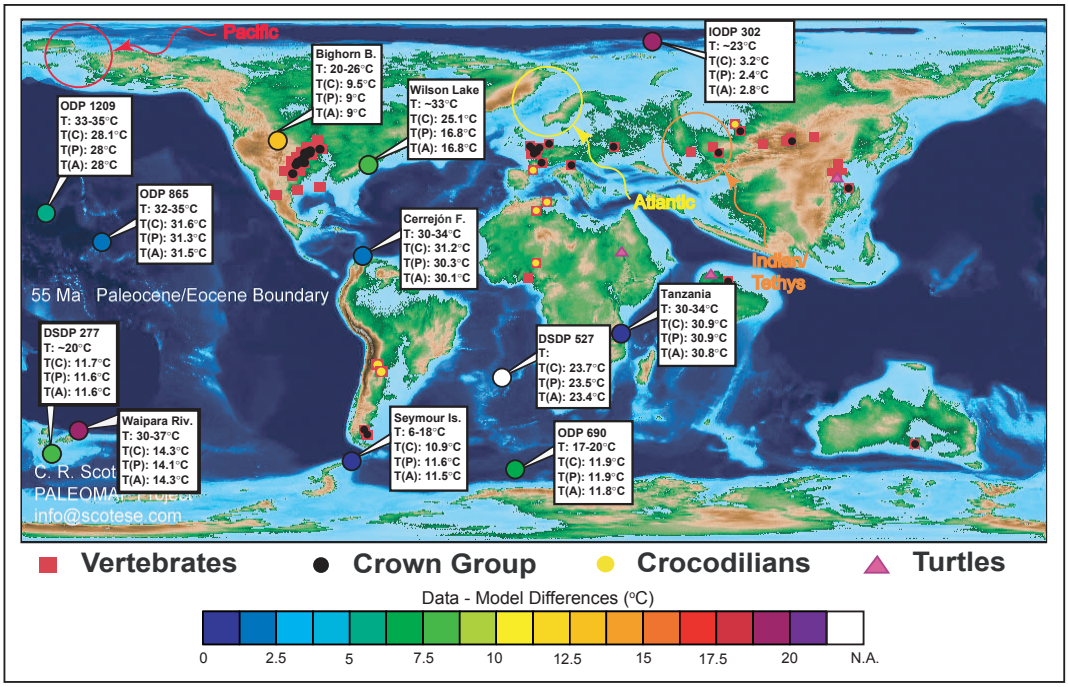

Figure A.1. Geographical reconstruction for the PETM with possible freshwater exchange locations between the Arctic and the remainder of the global ocean; from the PALEOMAP Project (www.scotese.com). Boxes indicate reconstructed surface temperatures across the Paleocene-Eocene boundary for the Control, EOCPAC, and EOCATL experiments (Shackleton and Kennett 1975; Thmas et al. 1999; Wing et al. 2005; Tripatie and Elderfield 2005; Bralower et al. 2006; Zachos et al. 2004, 2006; Sluijs et al. 2006, 2007b, and 2008a; Pearson et al. 2007; Ivany et al. 2008 Hollis et al. 2009). Fossil locations taken from Markwick (1997). Figure after Winguth et al., in press.

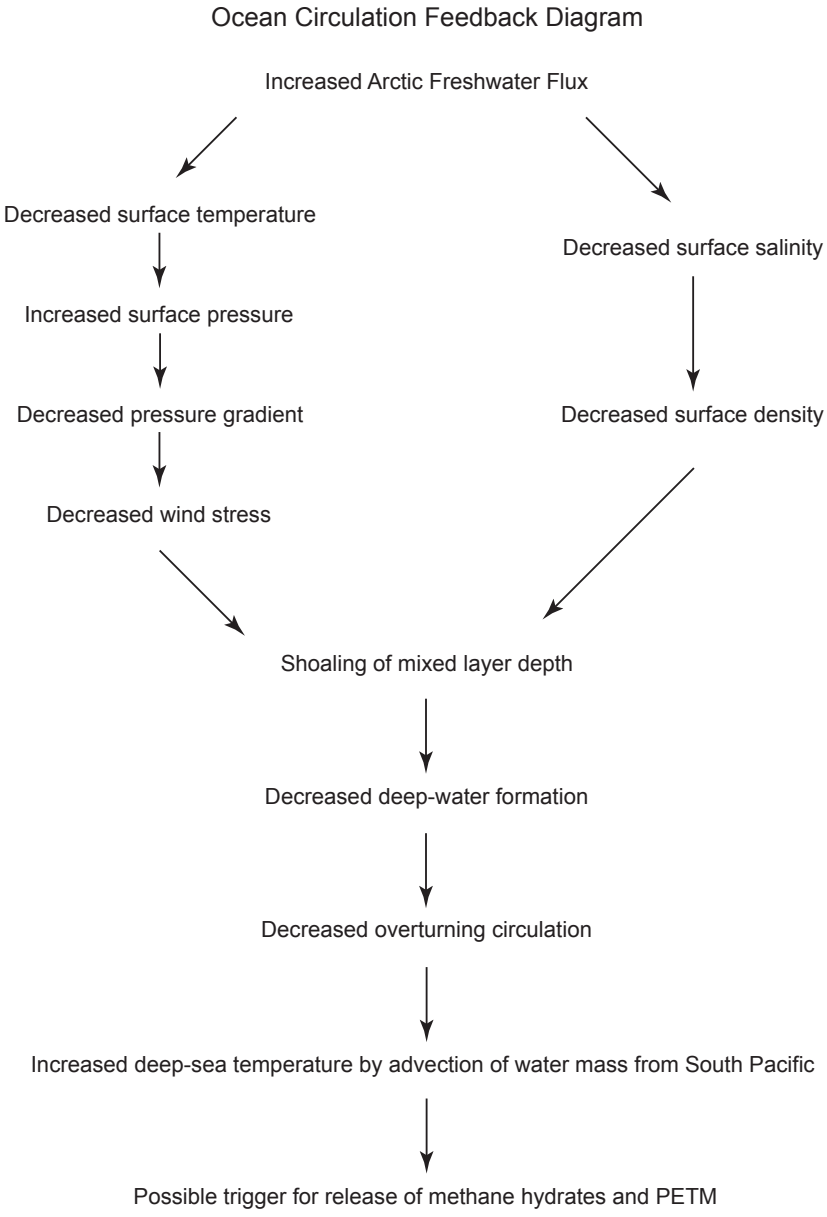

Figure A.2. Feedback diagram of ocean circulation; details possible means for changes in freshwater input from the Arctic to serve as a contributing factor to the onset of the PETM.

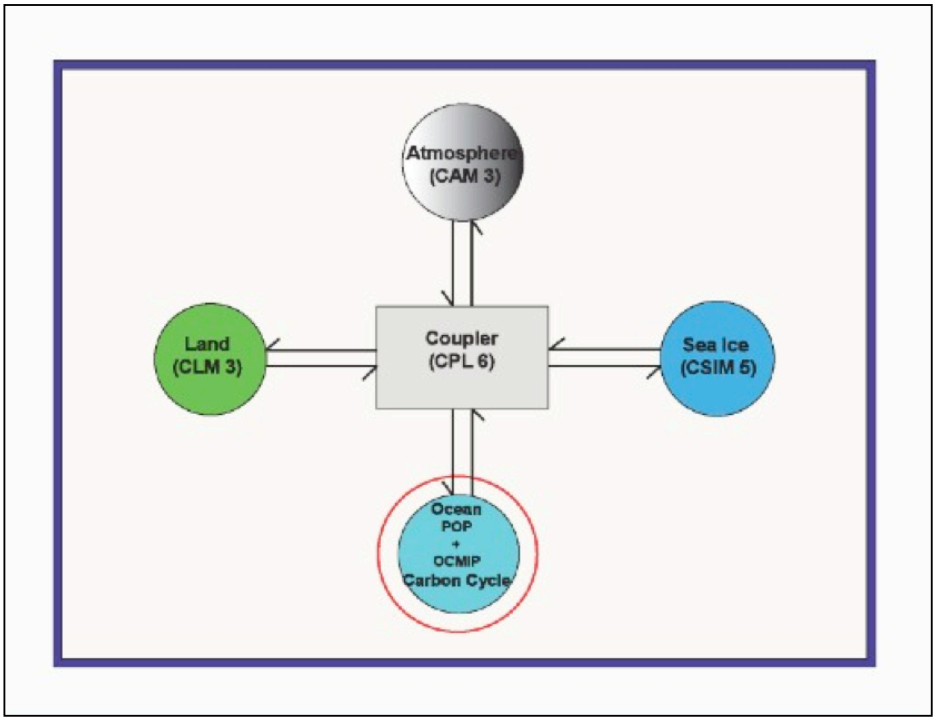

Figure A.3. CCSM3 model component diagram, including the carbon cycle.

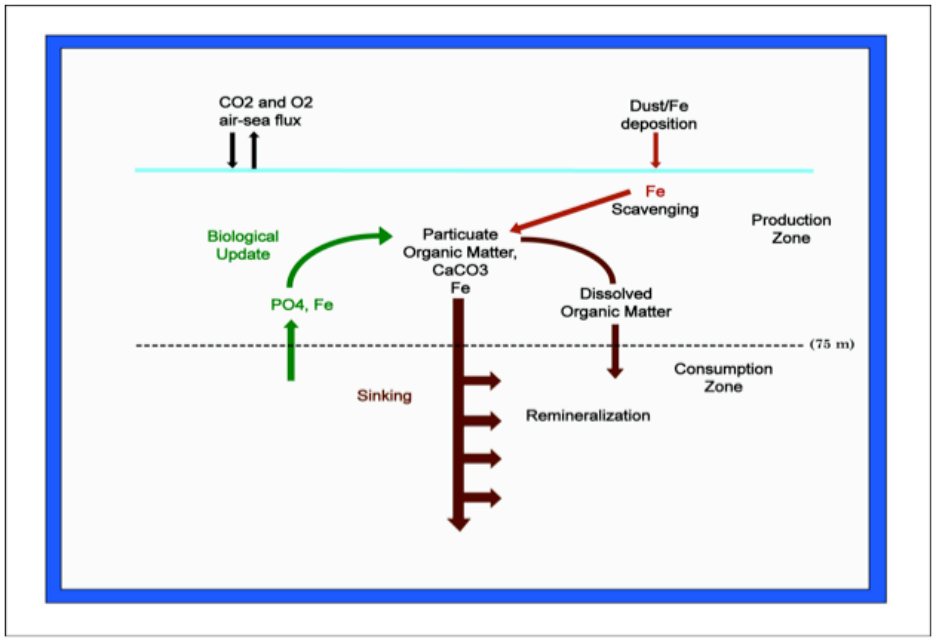

Figure A.4. Carbon Cycle after Doney et al., 2006.

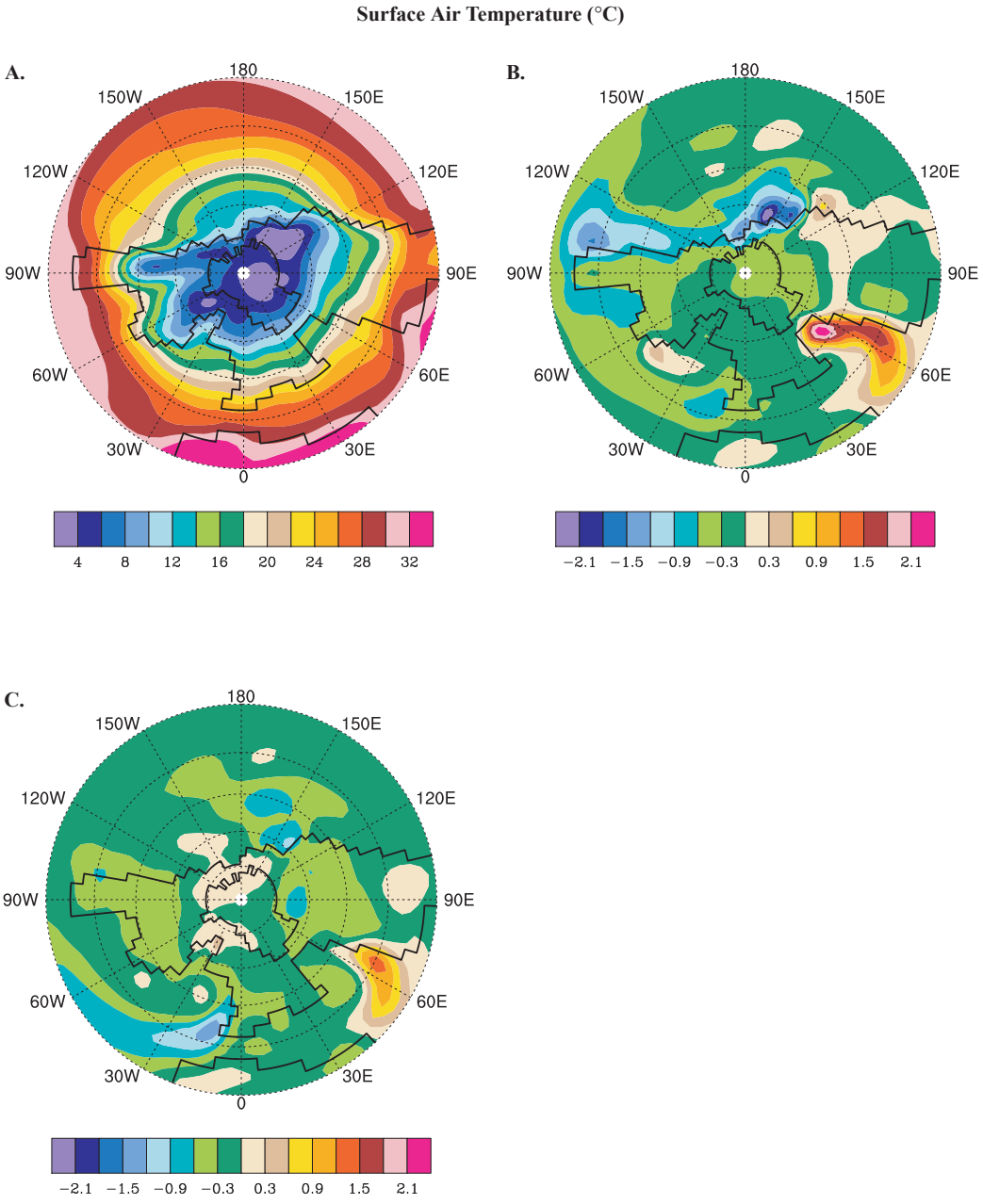

Figure A.5. Surface air temperature (°C, annual average years 1950-2000), northern hemisphere polar projection from 15°N to 90°N; A) Control experiment, B) EOCPAC – Control experiment, C) EOCATL – Control experiment.

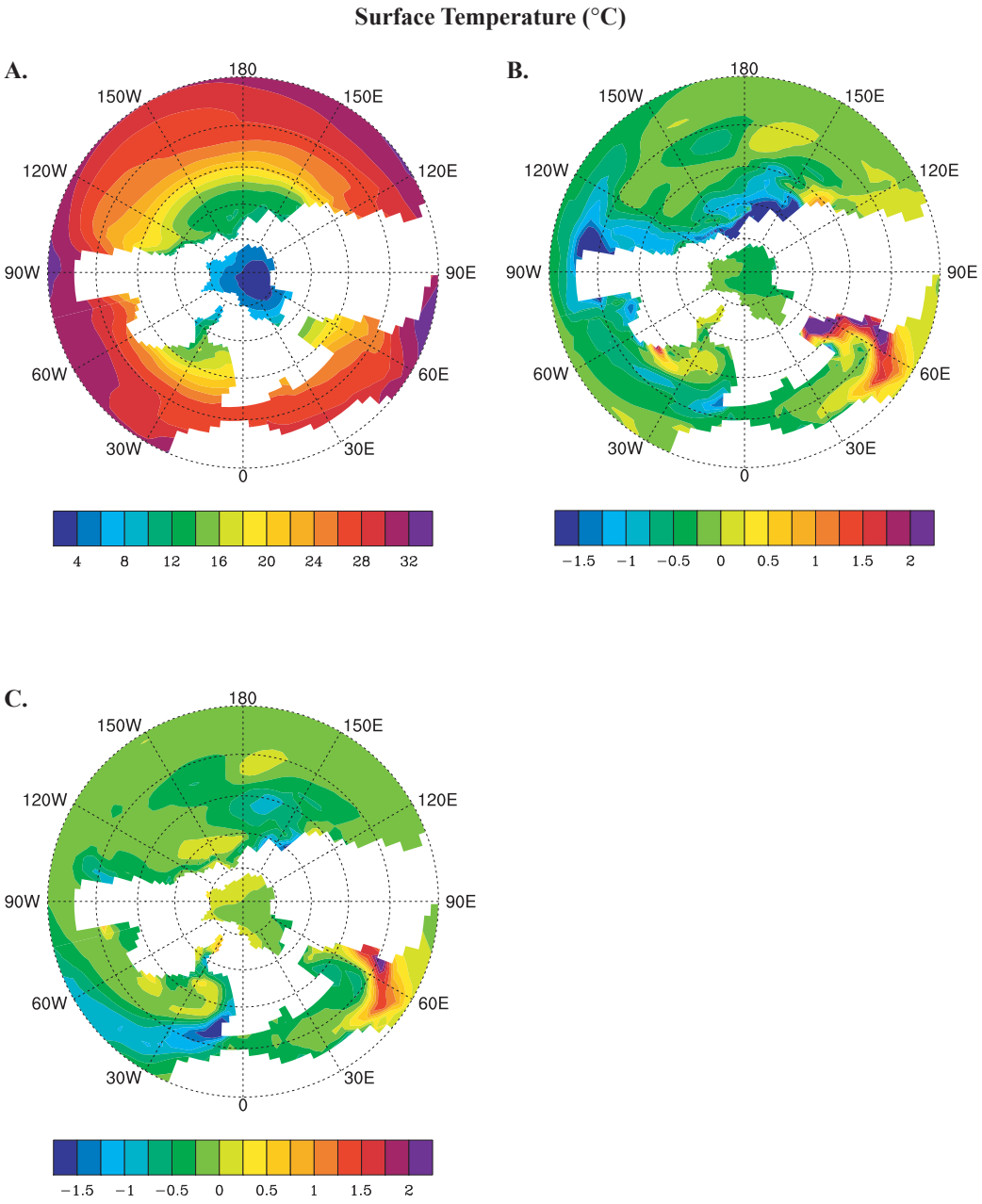

Figure A.6. **Sea** surface temperature (°C, **annual average years 1950-2000), northern hemisphere polar projection from 15°N to 90°N; A) Control experiment, B) EOCPAC – Control experiment, C) EOCATL – Control experiment.**

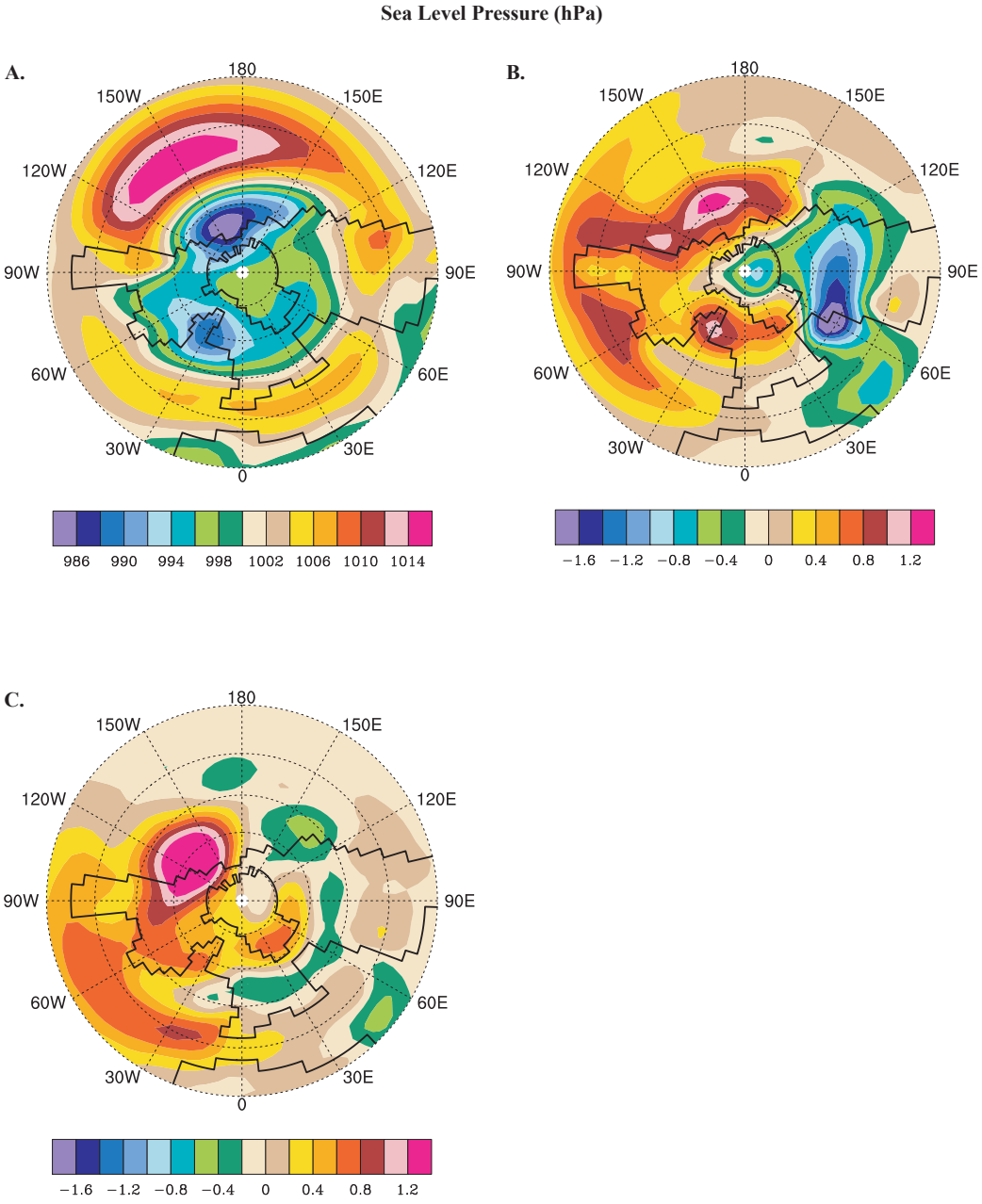

Figure A.7. Sea level pressure (hPa, annual average years 1950-2000), northern hemisphere polar projection from 15°N to 90°N; A) Control experiment, B) EOCPAC – Control experiment, C) EOCATL – Control experiment.

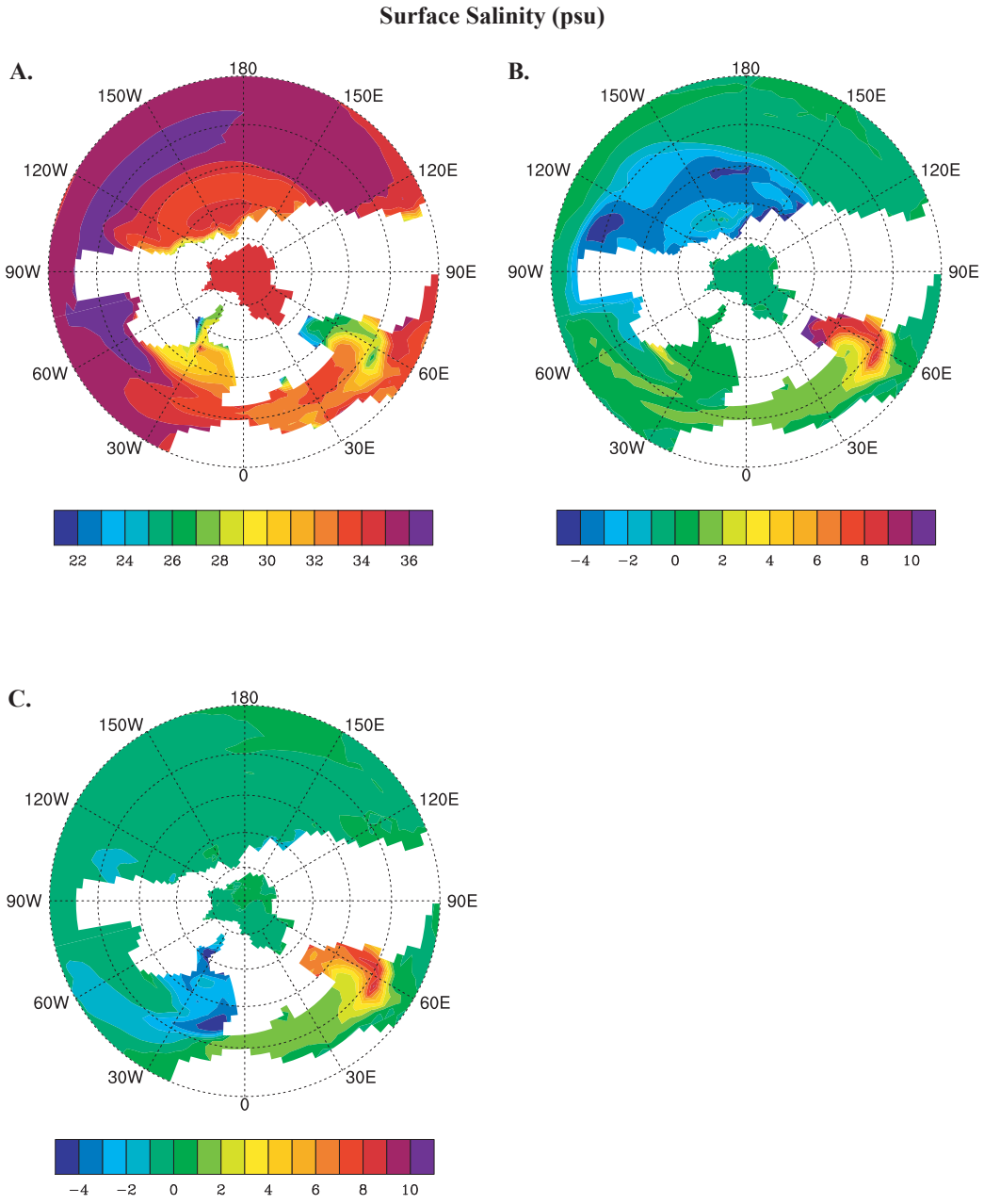

Figure A.8. Surface salinity (psu, annual average years 1950-2000), northern hemisphere polar projection from 15°N to 90°N; A) Control experiment, B) EOCPAC – Control experiment, C) EOCATL – Control experiment.

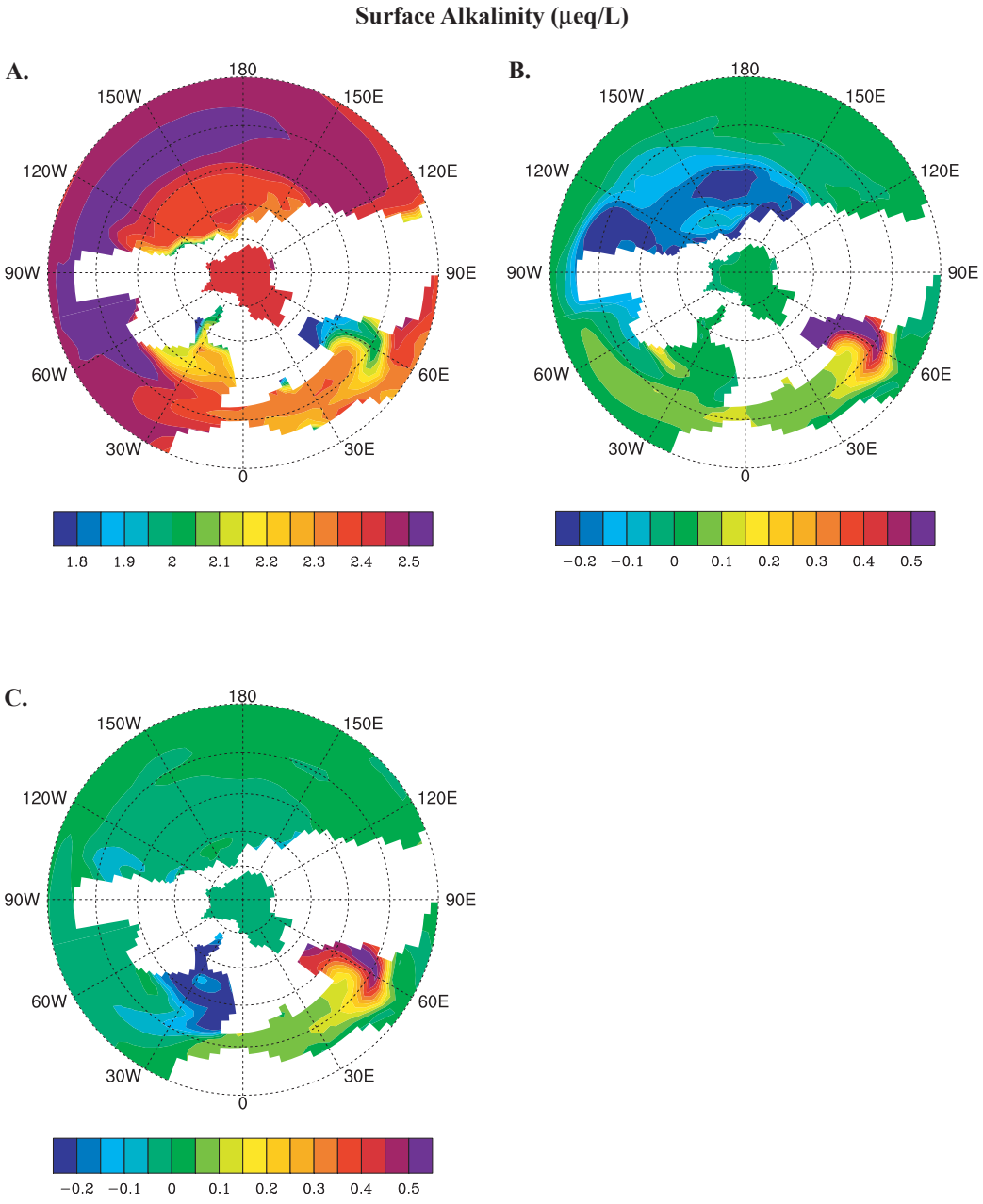

Figure A.9. Surface alkalinity (μeq/L, annual average years 1950-2000), northern hemisphere polar projection from 15°N to 90°N; A) Control experiment, B) EOCPAC – Control experiment, C) EOCATL – Control experiment.

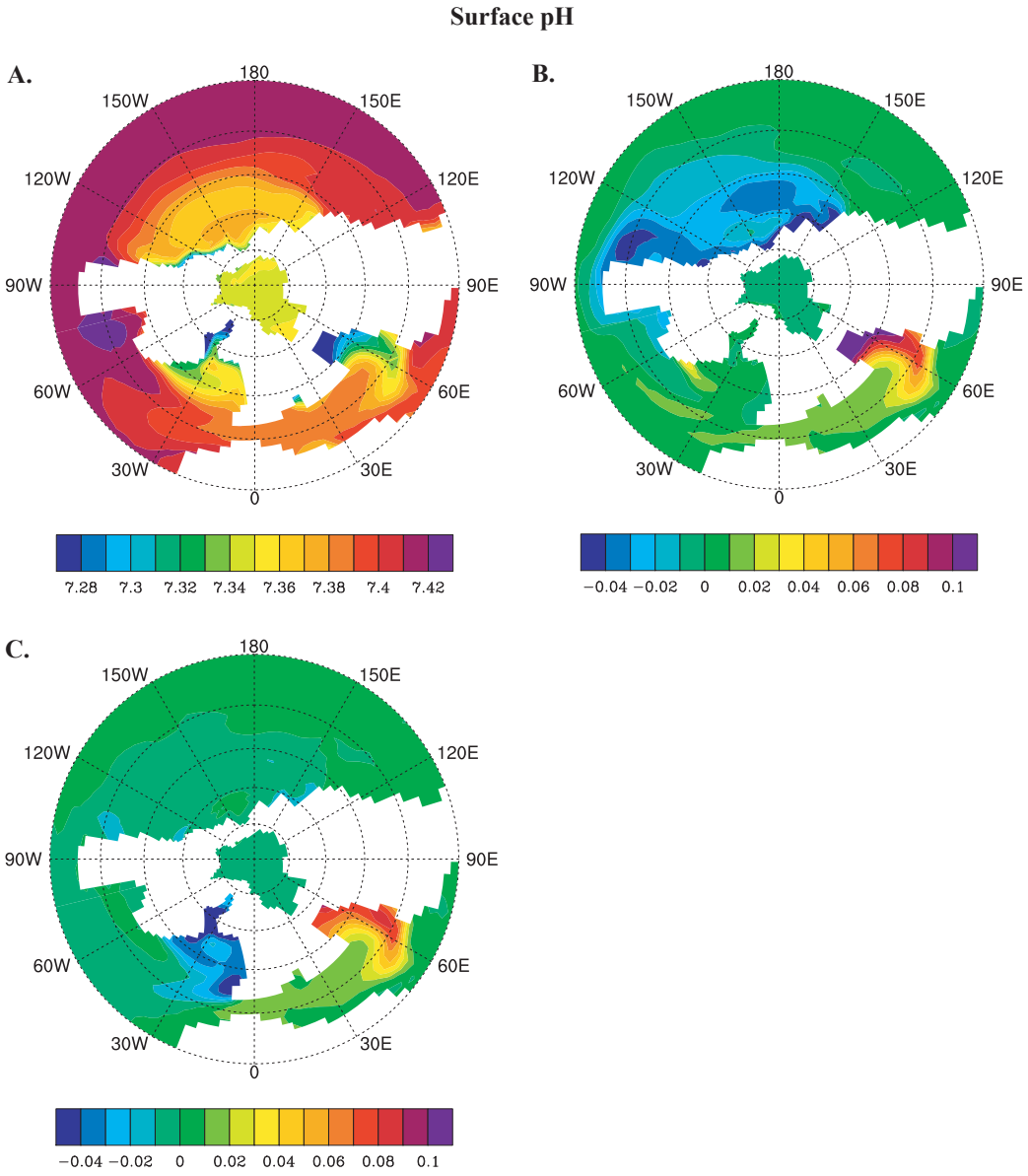

Figure A.10. Surface pH (annual average years 1950-2000), northern hemisphere polar projection from 15°N to 90°N; A) Control experiment, B) EOCPAC – Control experiment, C) EOCATL – Control experiment.

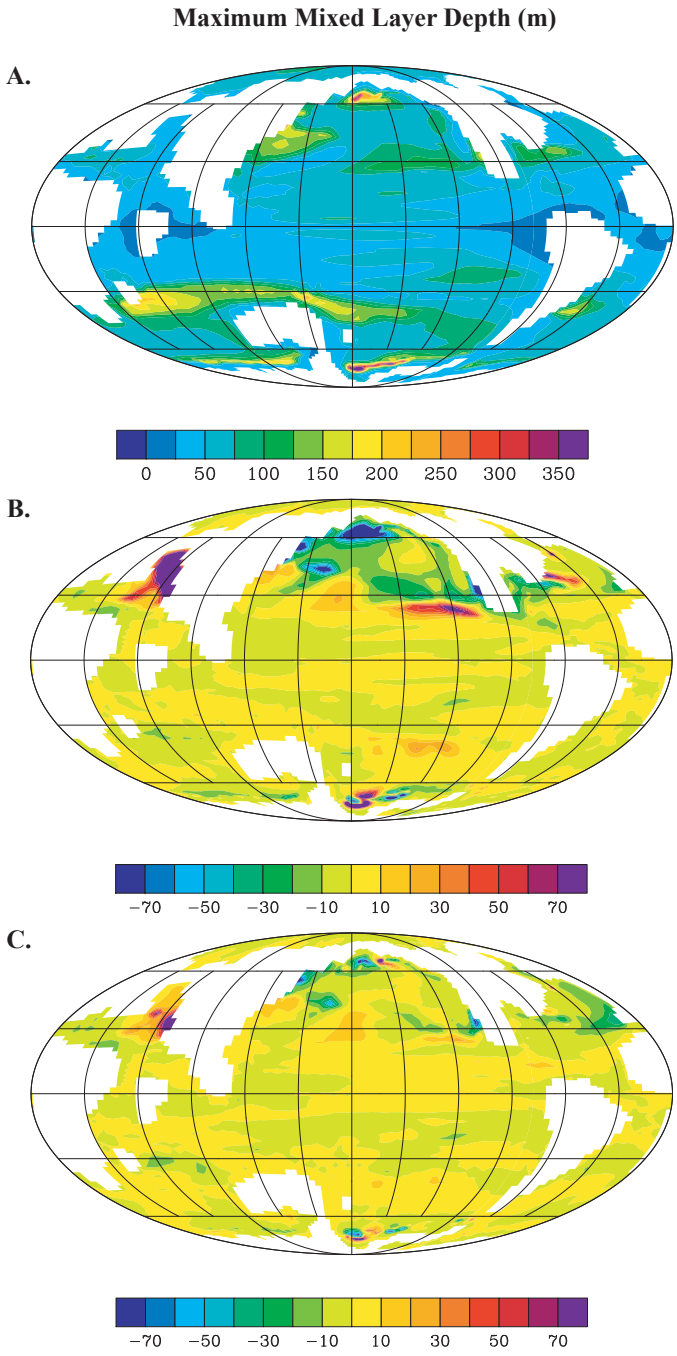

Figure A.11. Maximum mixed layer depth, (annual average years 1950-2000), projection centered on 180°; A) Control experiment, B) EOCPAC – Control experiment, C) EOCATL – Control experiment.

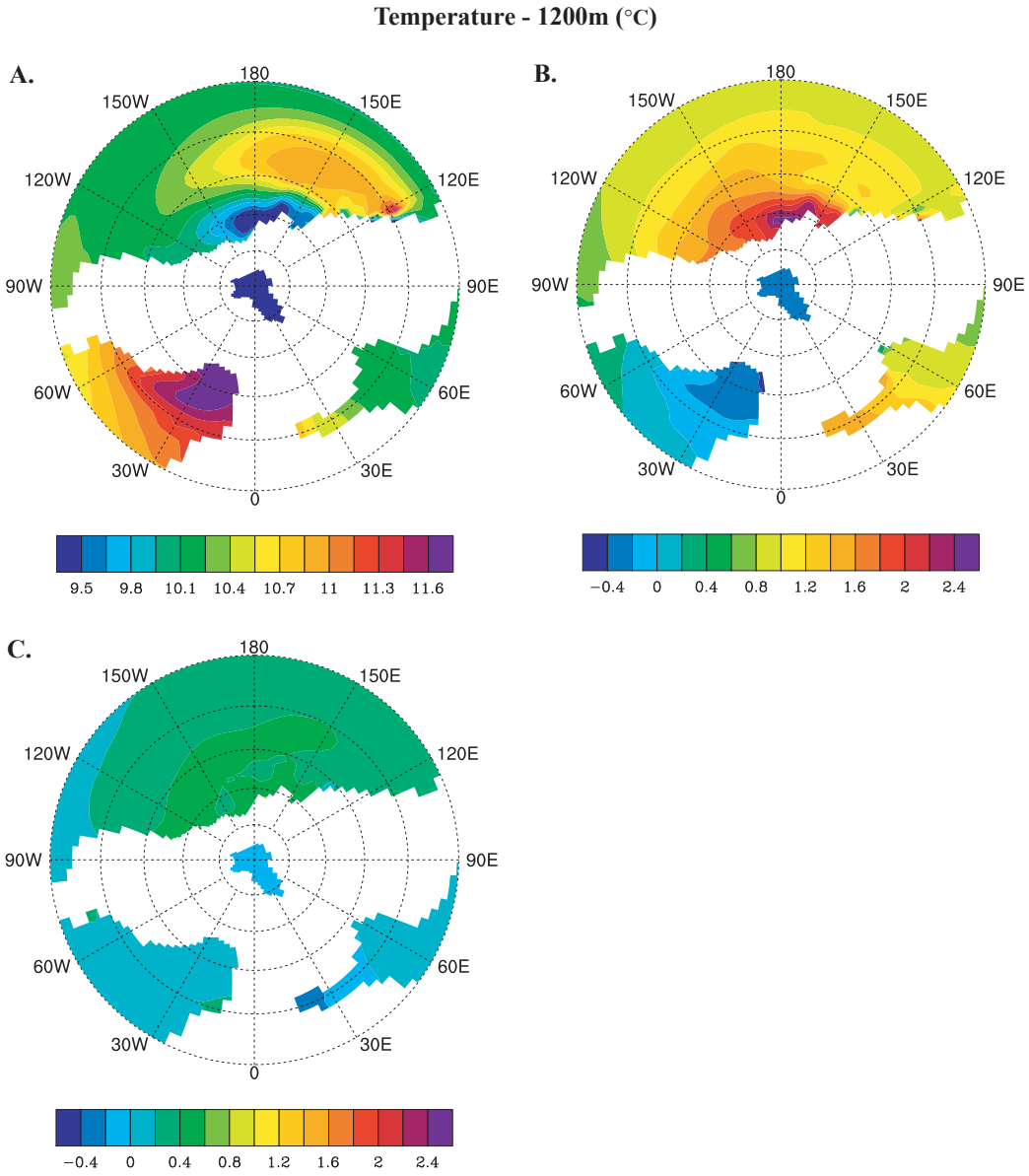

Figure A.12. Temperature, (°C, 1200m, annual average years 1950-2000), northern hemisphere polar projection from 15°N to 90°N; A) Control experiment, B) EOCPAC – Control experiment, C) EOCATL – Control experiment.

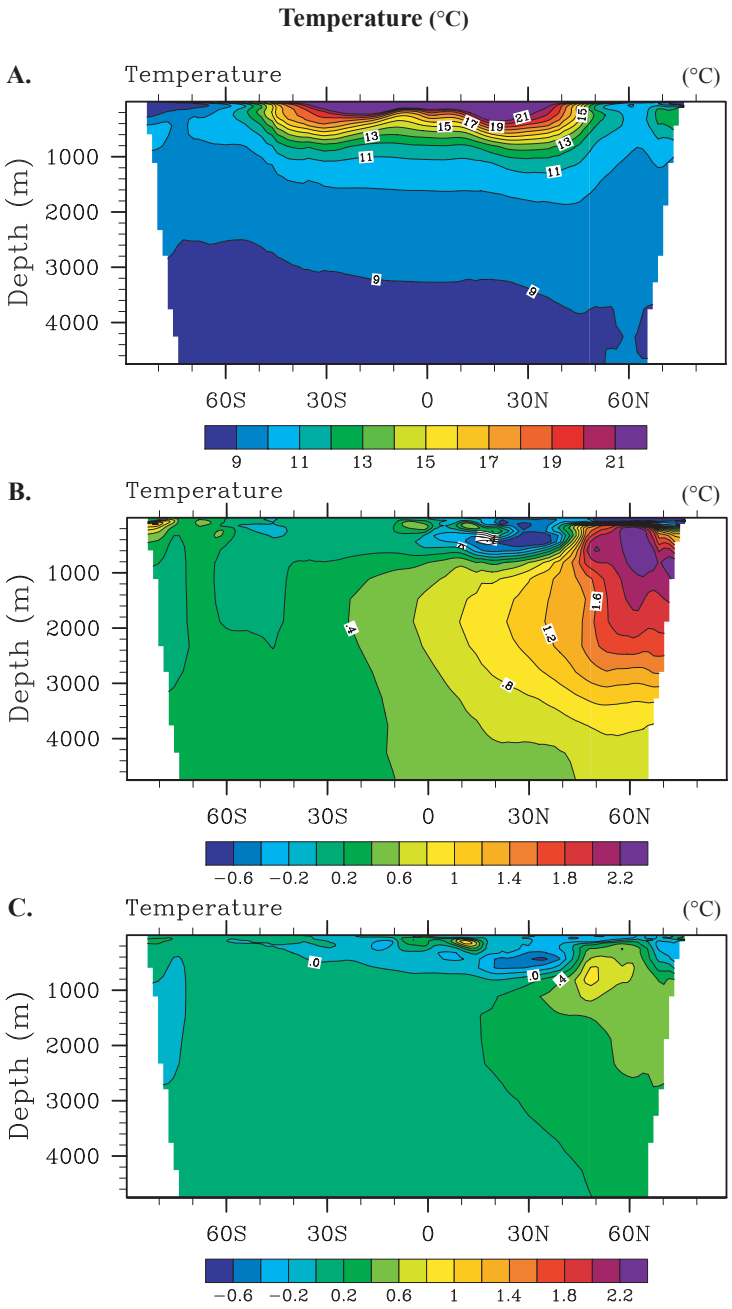

Figure A.13. Temperature, (°C, annual average years 1950-2000), Zonal meridional projection, Pacific Ocean basin, depth in meters; A) Control experiment, B) EOCPAC – Control experiment, C) EOCATL – Control Experiment.

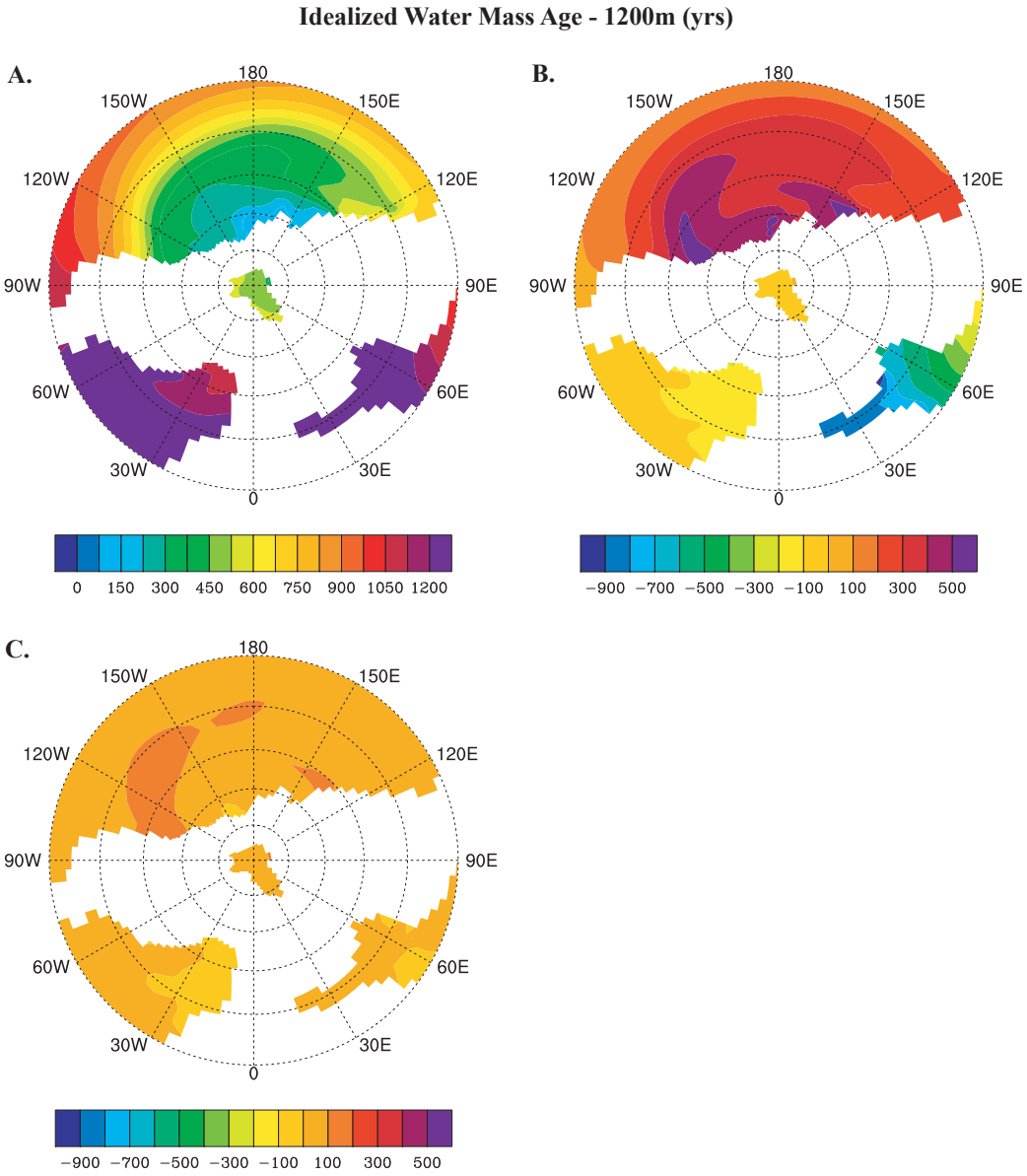

Figure A.14. Idealized water mass age, (years, 1200m, annual average years 1950-2000), northern hemisphere polar projection from 15°N to 90°N; A) Control experiment, B) EOCPAC – Control experiment, C) EOCATL – Control experiment.

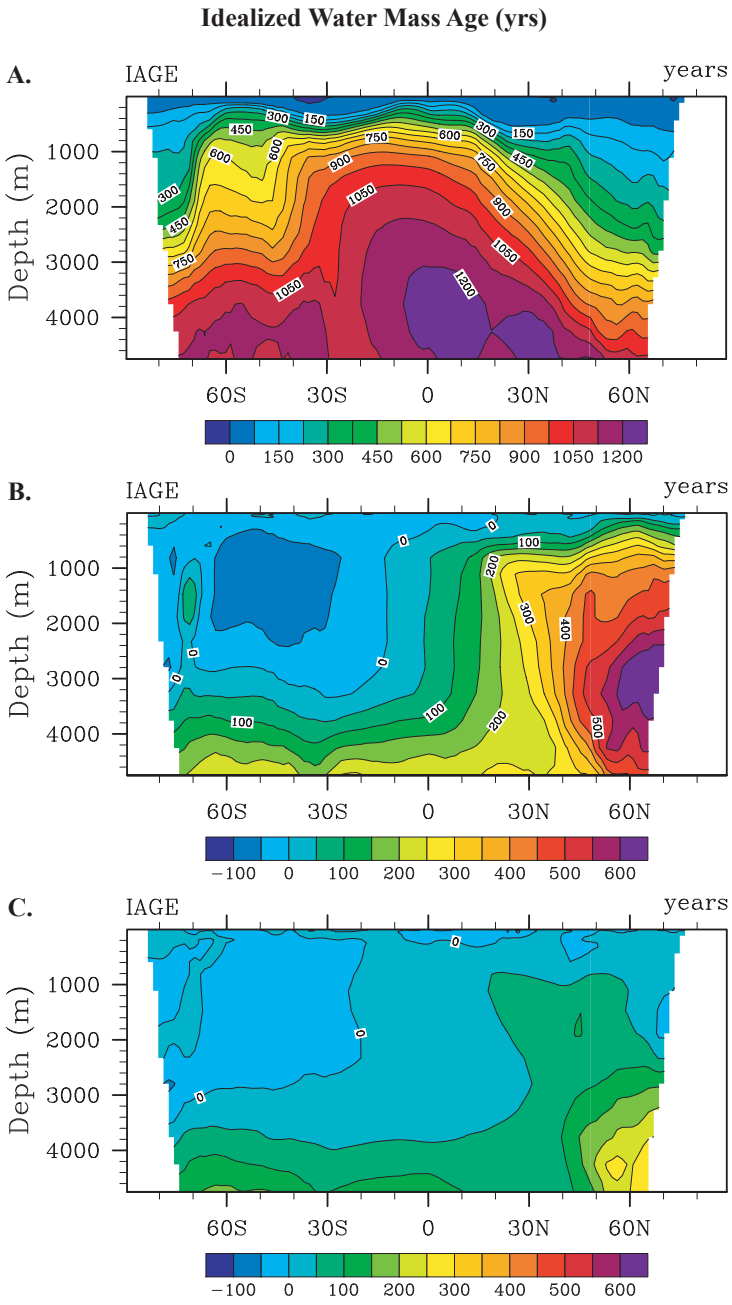

Figure A.15. Idealized water mass age, (years, annual average years 1950-2000), Zonal meridional projection, Pacific Ocean basin, depth in meters; A) Control experiment, B) EOCPAC – Control experiment, C) EOCATL – Control Experiment.

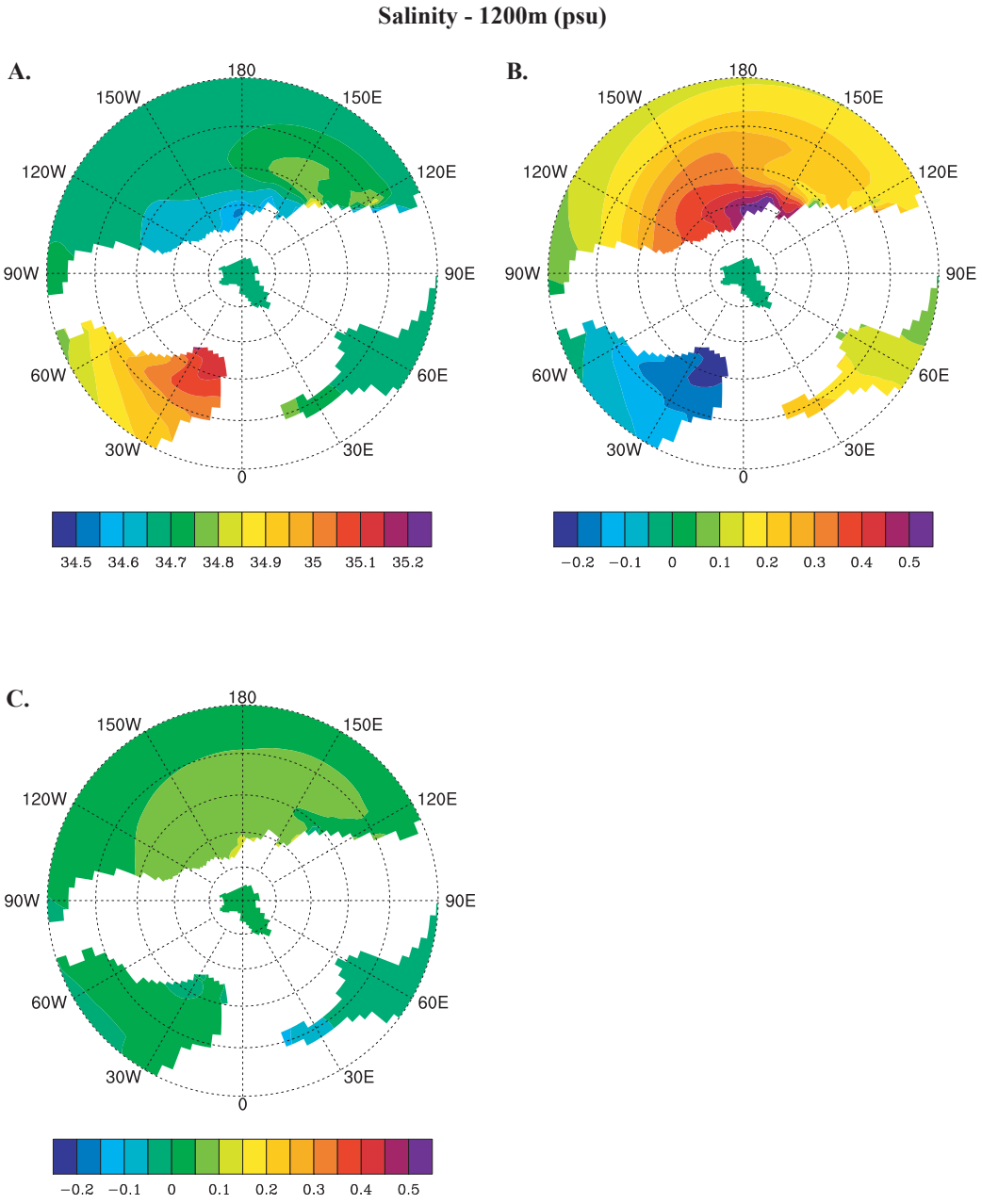

Figure A.16. Salinity (psu, 1200m, annual average years 1950-2000), northern hemisphere polar projection from 15°N to 90°N; A) Control experiment, B) EOCPAC – Control experiment, C) EOCATL – Control experiment.

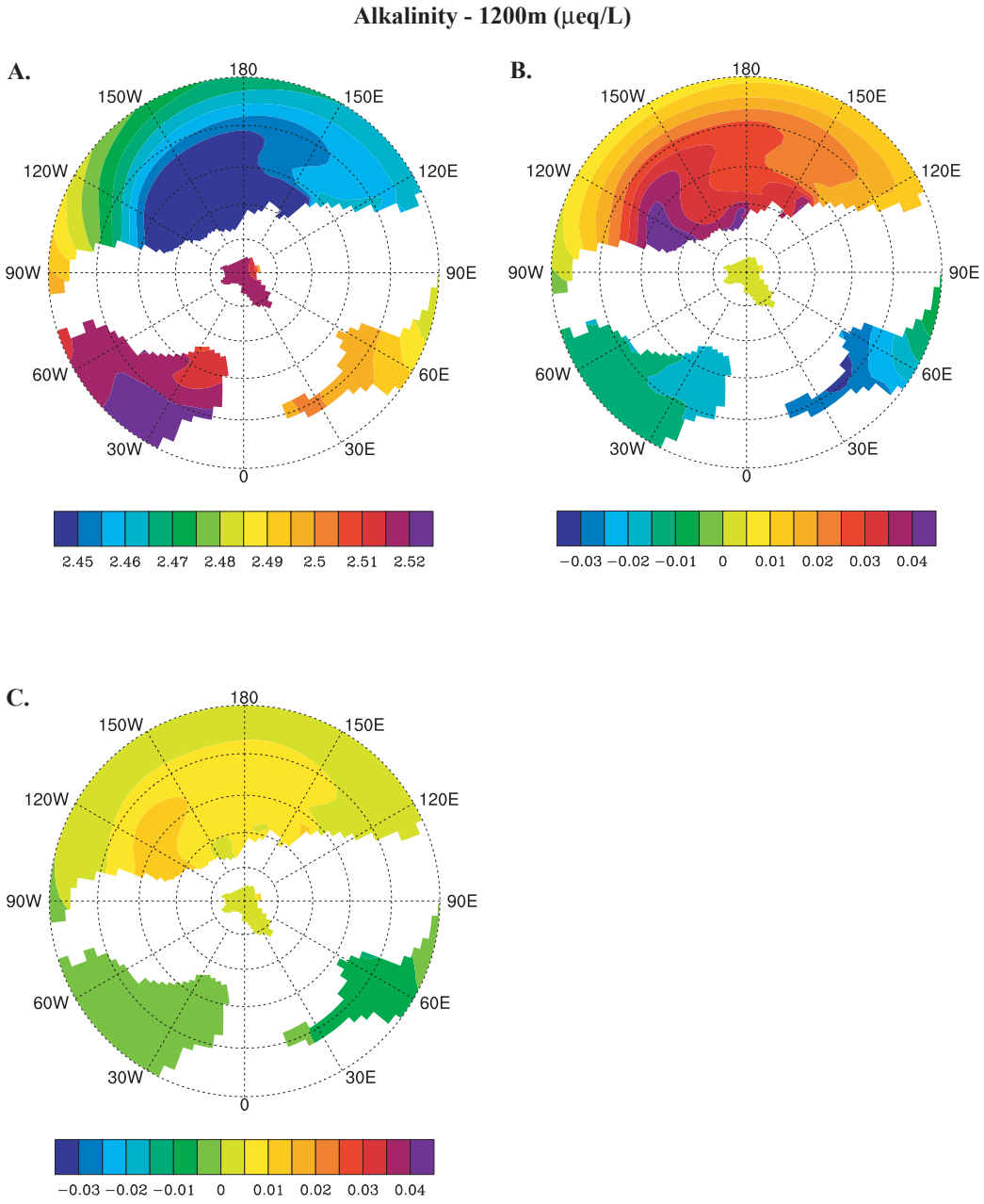

Figure A.17. Alkalinity (μeq/L, 1200m, annual average years 1950-2000), northern hemisphere polar projection from 15°N to 90°N; A) Control experiment, B) EOCPAC – Control experiment, C) EOCATL – Control experiment.

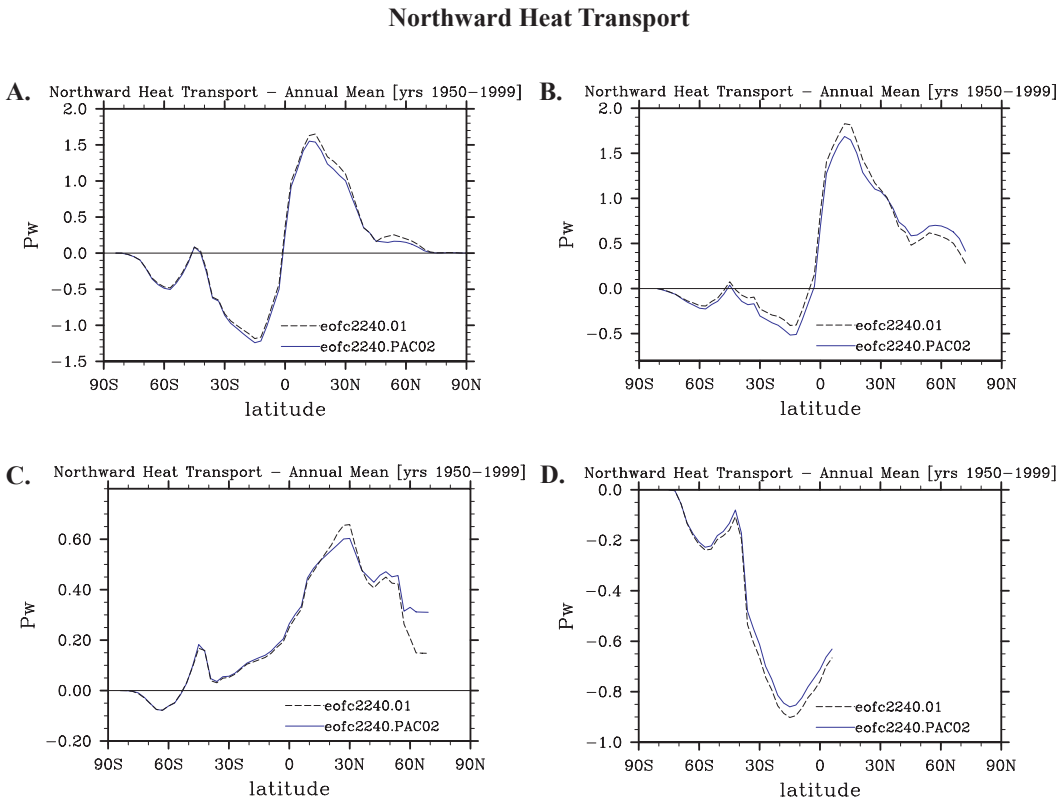

Figure A.18. Northward heat transport (heat transport in PW, annual average years 1950-2000), EOCPAC (solid) compared to Control (dashed); A) Global average, B) Pacific basin average, C) Atlantic basin average, D) Indian basin average.

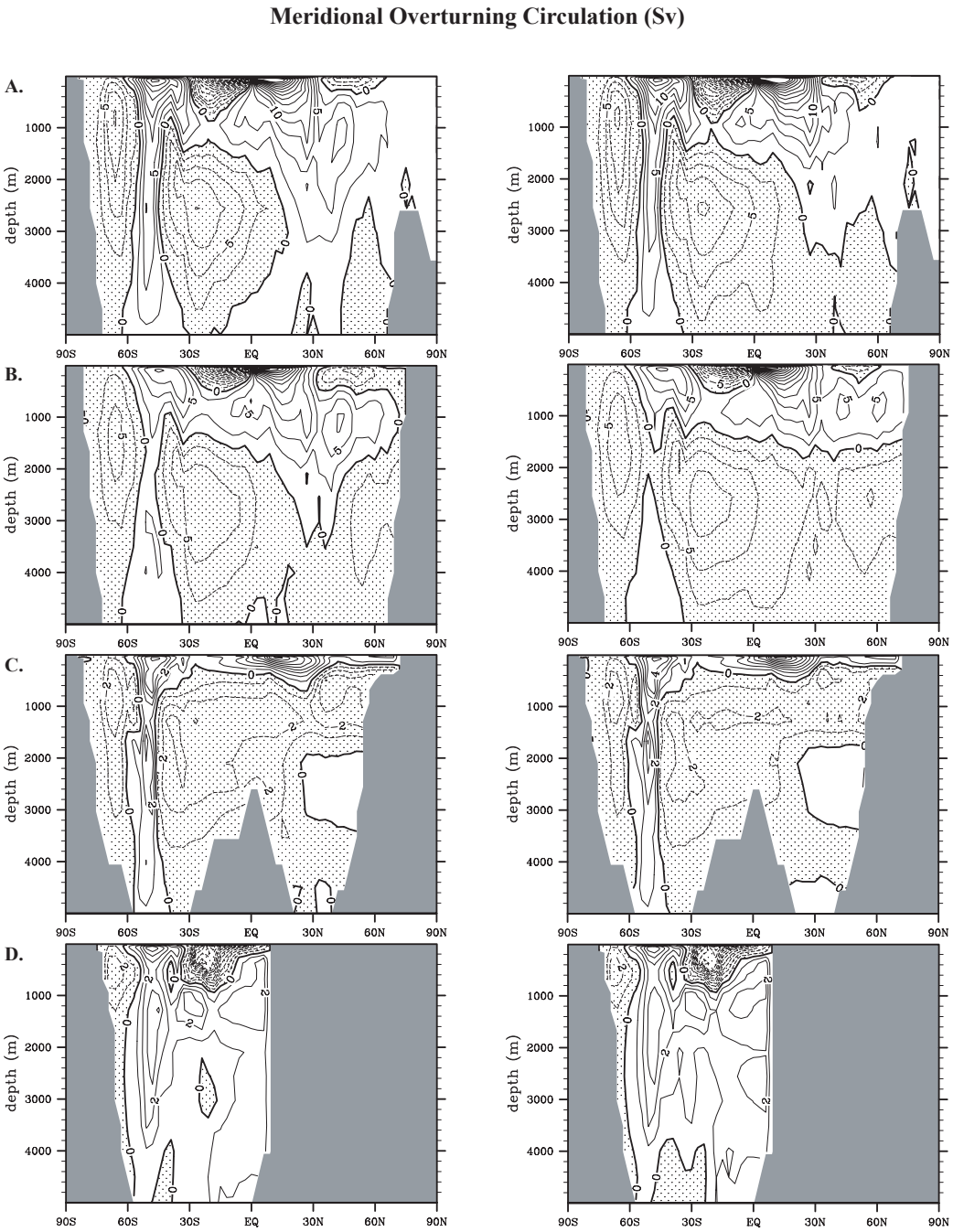

Figure A.19. Meridional overturning circulation (flow strength in Sv, annual average years 1950-2000), Control (left), EOCPAC (right); A) Global average, B) Pacific basin average, C) Atlantic basin average, D) Indian basin average.

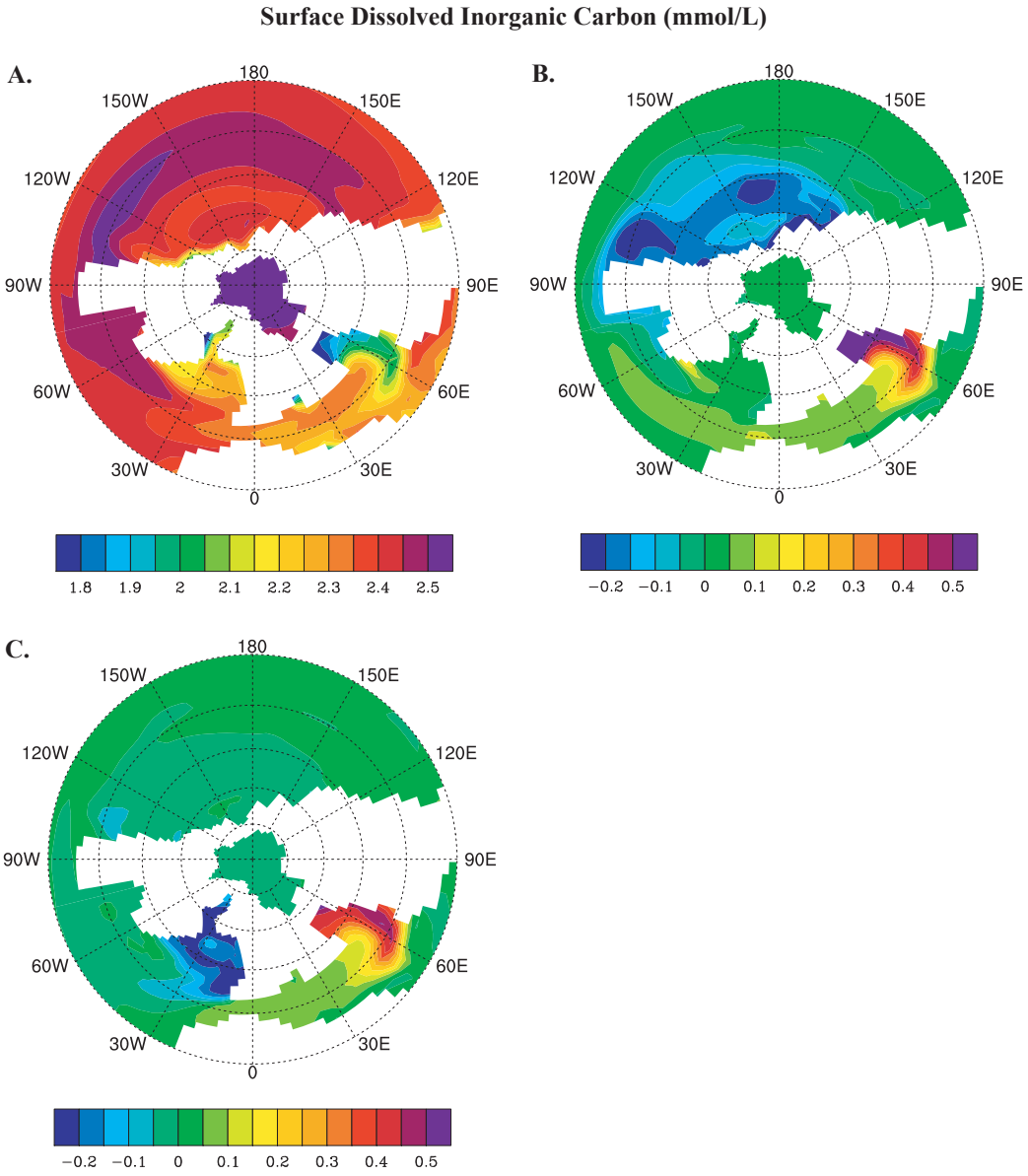

Figure A.20. Dissolved Inorganic Carbon (mmol/L, annual average years 1950-2000), northern hemisphere polar projection from 15°N to 90°N; A) Control experiment, B) EOCPAC – Control experiment, C) EOCATL – Control experiment.

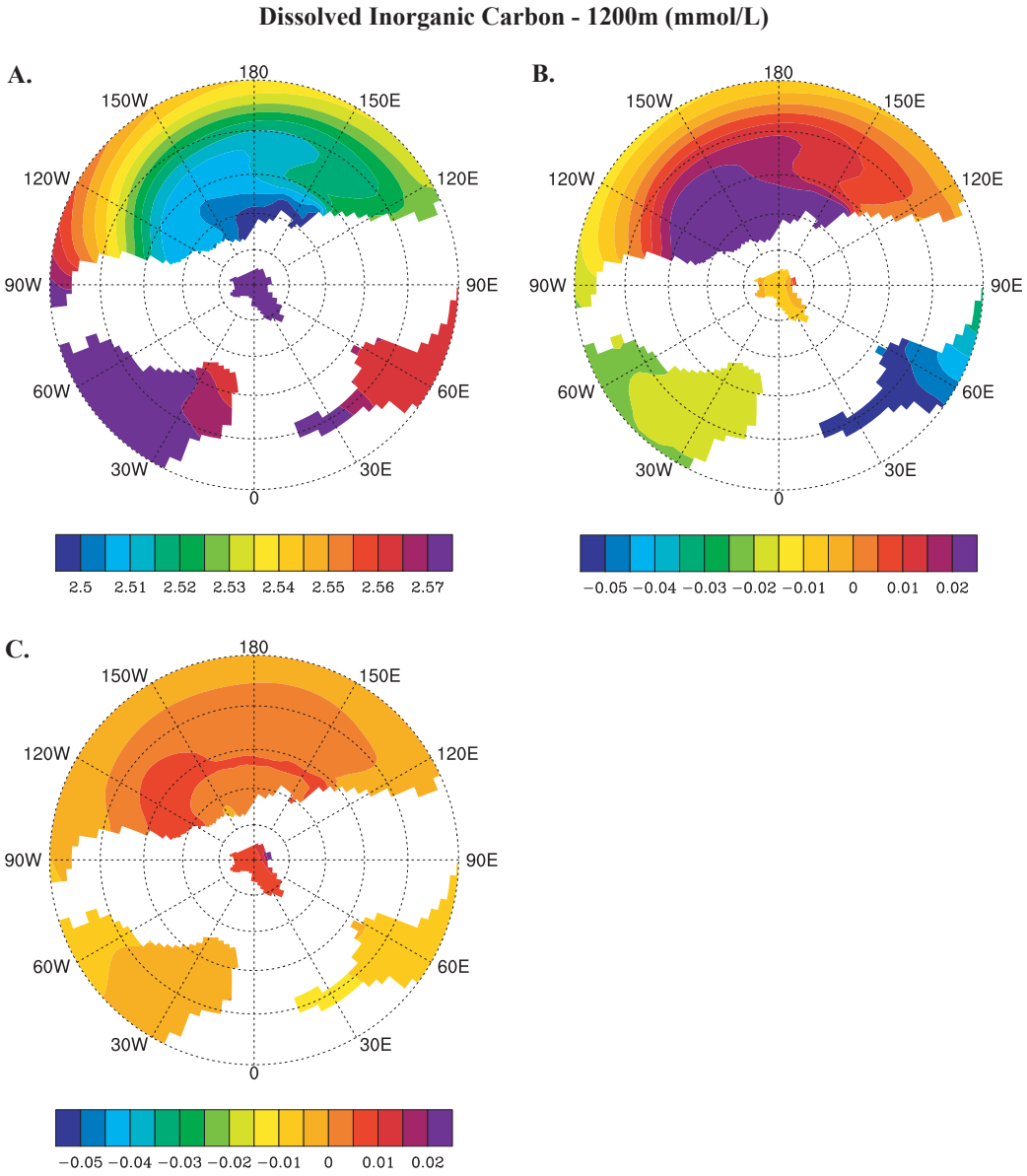

Figure A.21. Dissolved Inorganic Carbon (mmol/L, 1200m, annual average years 1950-2000), northern hemisphere polar projection from 15°N to 90°N; A) Control experiment, B) EOCPAC – Control experiment, C) EOCATL – Control experiment.

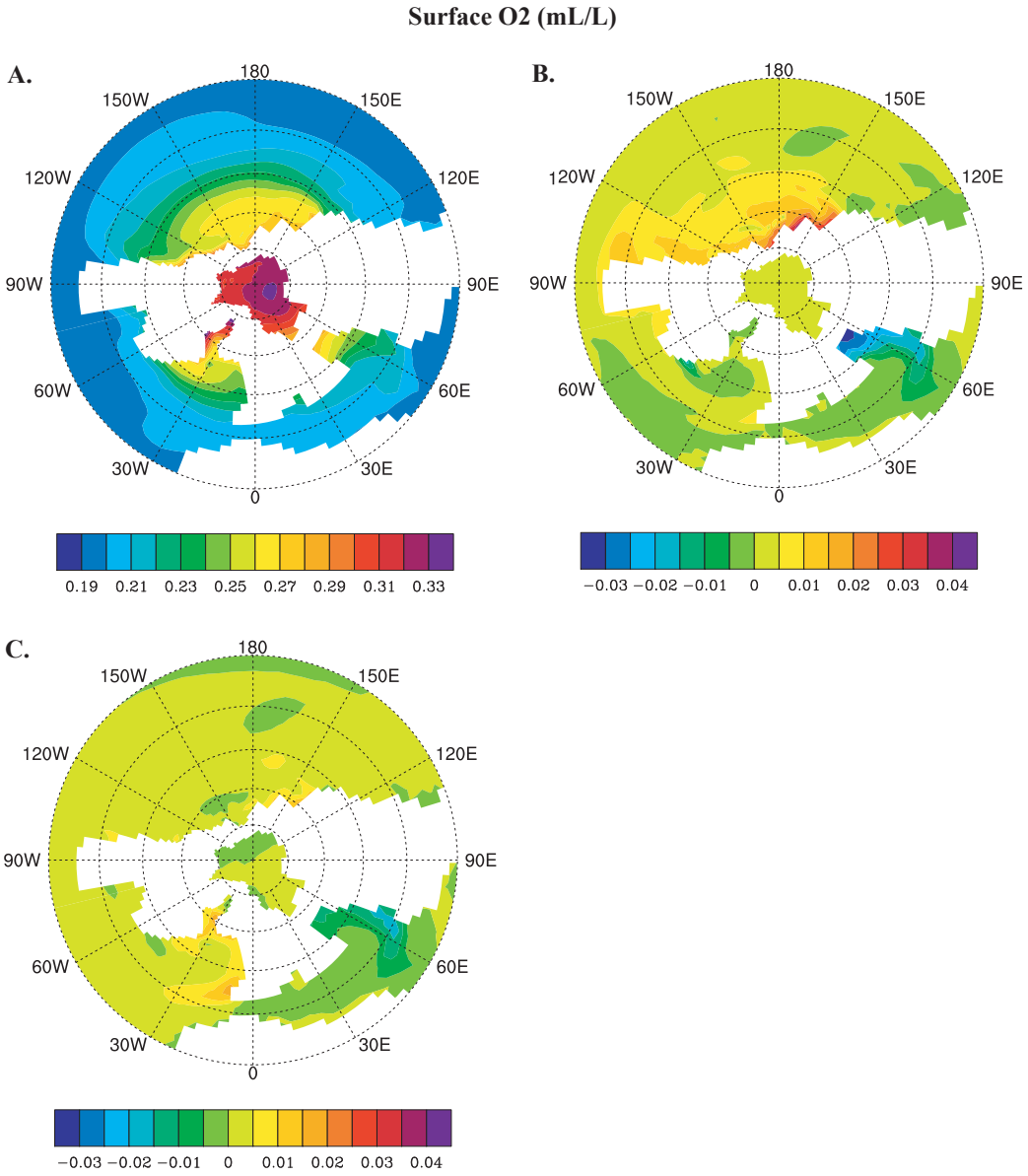

Figure A.22. Surface dissolved oxygen (mL/L, annual average years 1950-2000), northern hemisphere polar projection from 15°N to 90°N; A) Control experiment, B) EOCPAC – Control experiment, C) EOCATL – Control experiment.

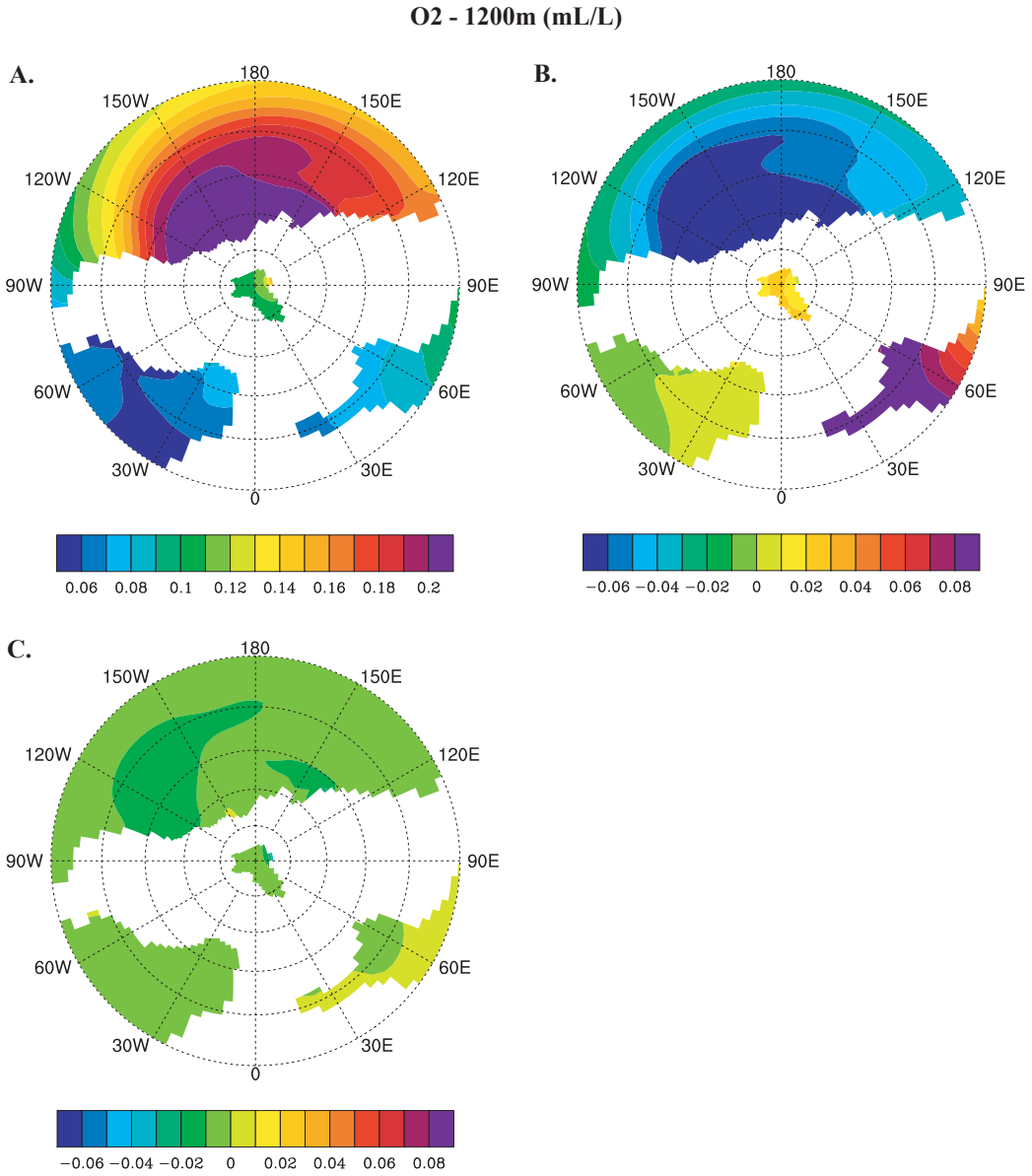

Figure A.23. Dissolved oxygen (mL/L, 1200m, annual average years 1950-2000), northern hemisphere polar projection from 15°N to 90°N; A) Control experiment, B) EOCPAC – Control experiment, C) EOCATL – Control experiment.

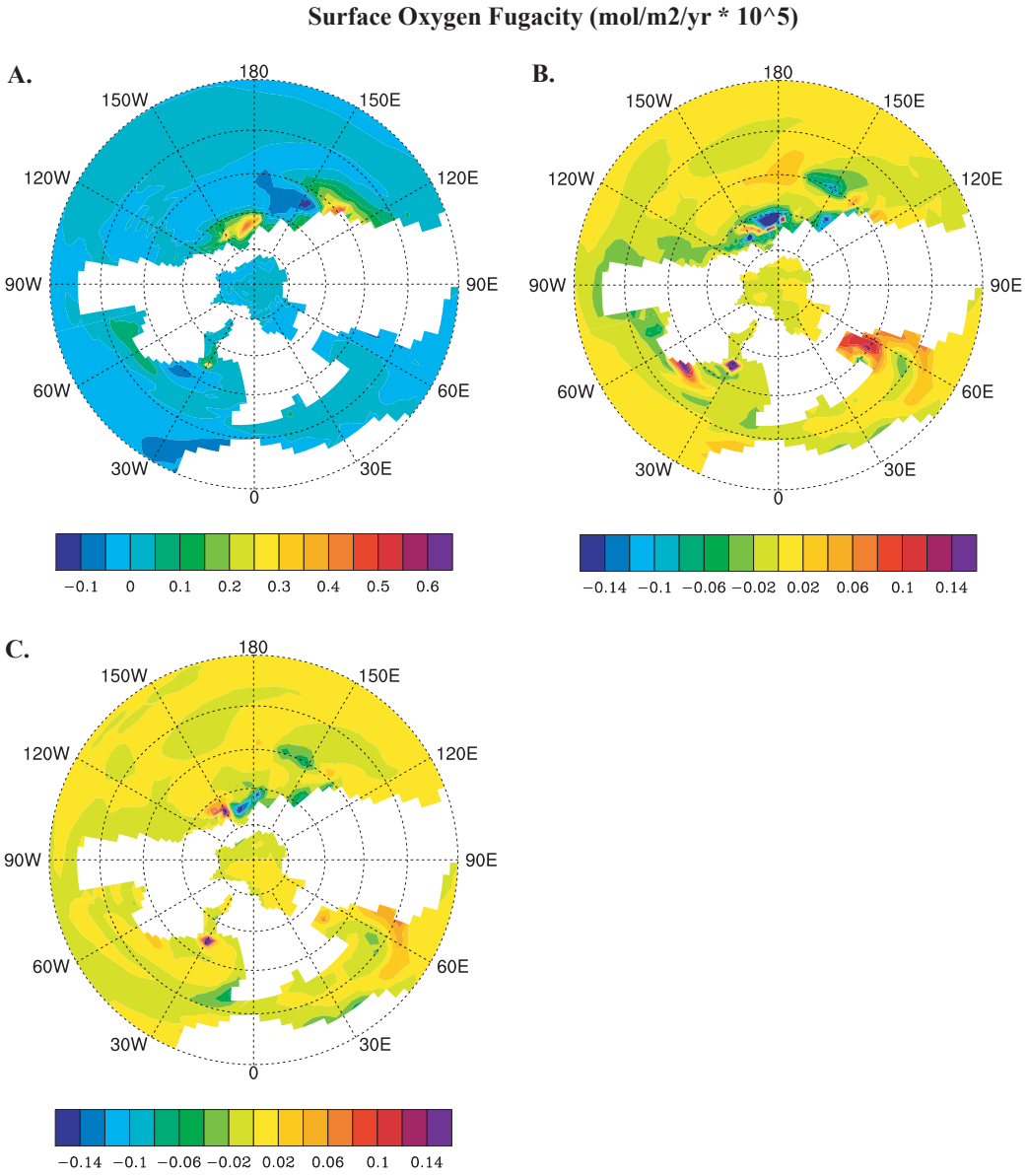

Figure A.24. Oxygen Fugacity (mol/m^2/yr * 10^5, annual average years 1950-2000), northern hemisphere polar projection from 15°N to 90°N; A) Control experiment, B) EOCPAC – Control experiment, C) EOCATL – Control experiment.

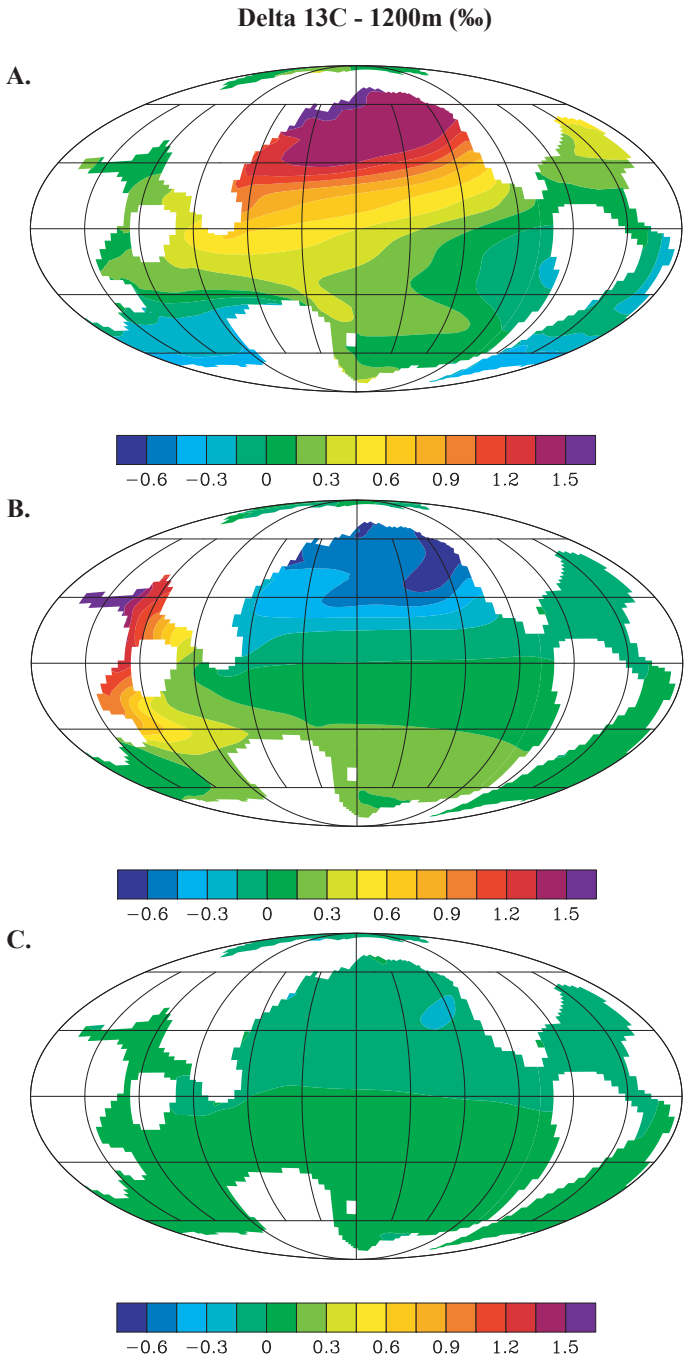

Figure A.25. $\delta^{13}C$ (‰, 1200m, annual average years 1950-2000), A) Control experiment, B) EOCPAC – Control experiment, C) EOCATL – Control experiment.

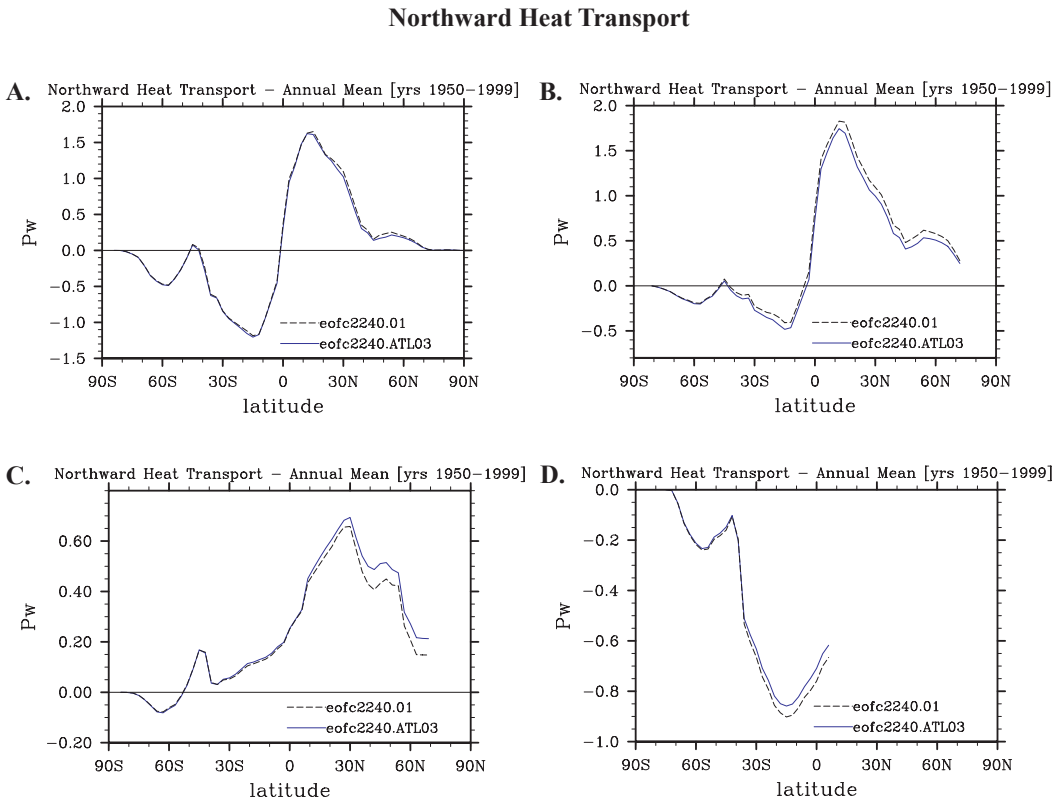

Figure A.26. Northward heat transport (heat transport in PW, annual average years 1950-2000), EOCATL (solid) compared to Control (dashed); A) Global average, B) Pacific basin average, C) Atlantic basin average, D) Indian basin average.

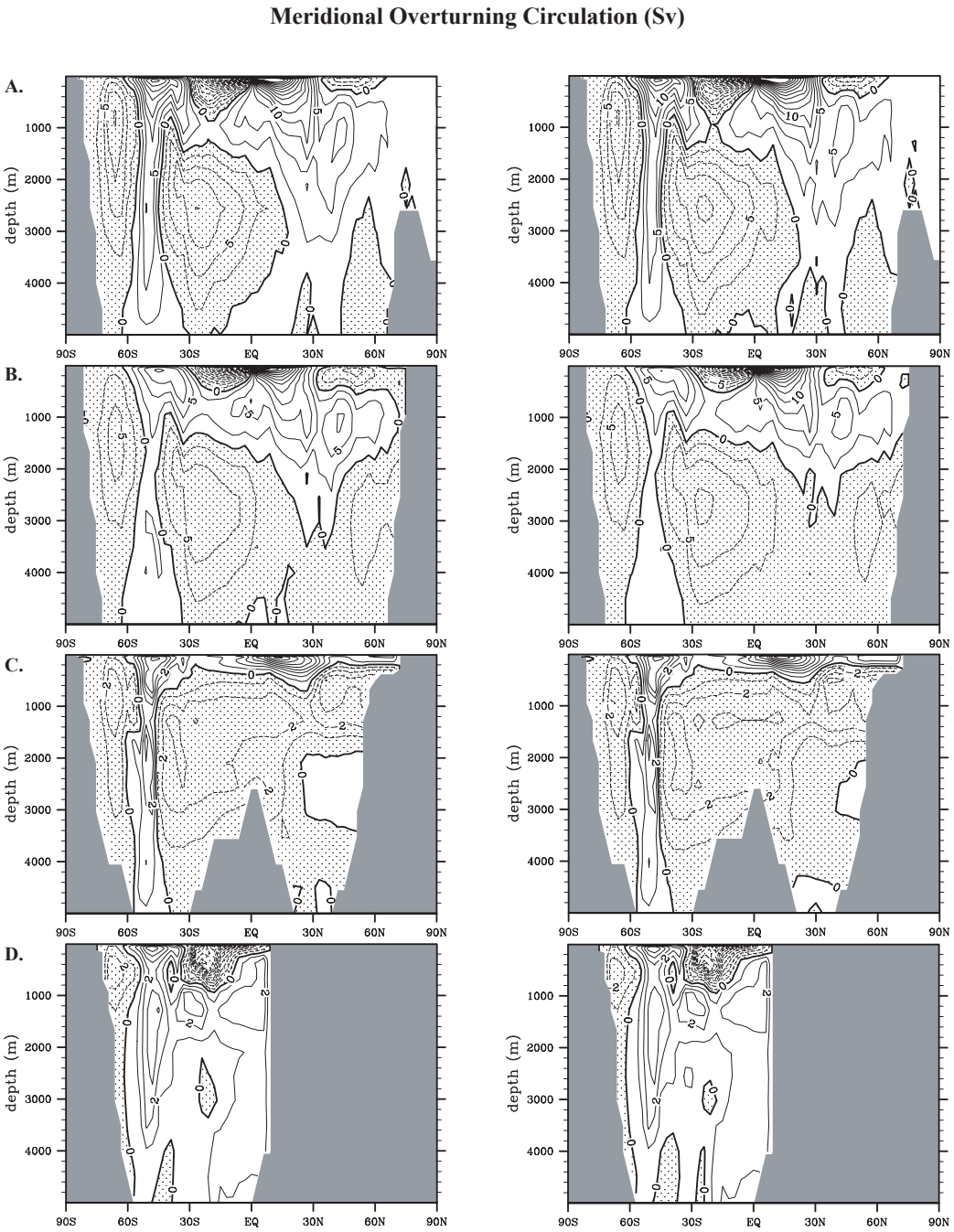

Figure A.27. Meridional overturning circulation (flow strength in Sv, annual average years 1950-2000), Control (left), EOCATL (right); A) Global average, B) Pacific basin average, C) Atlantic basin average, D) Indian basin average.

REFERENCES

Aleksandrova, G. N., and E. P. Radionova, 2006, On the Late Paleocene Stratigraphy of the Saratov Volga Region: Micropaleontological Characteristics of the Kamyshin Formation, Dyupa Gully Section, *Paleontological Journal*, 40, S543-S557.

Antonov, J. I., S. Levitus, and T. P. Boyer, 2005, Thermosteric Sea Level Rise, 1955-2003, *Geophysical Research Letters*, 32, L12602, doi:10.1029/2005GL023112.

Aubry, M.–P., 1998, Early Paleogene Calcareous Nannoplankton Evolution: A Tale of Climatic Amelioration, in *Late Paleocene and Early Eocene Climatic and Biotic Evolution*, edited by M.-P. Aubry, S. Lucas, and W. A. Berggren, 158-203, Columbia University Press, New York.

Bains, S., R. M. Corfield, and R. D. Norris, 1999, Mechanisms of Climate Warming at the End of the Paleocene, *Science*, 285, 724-727.

Bice, K. L., and J. Marotzke, 2002, Could Changing Ocean Circulation Have Destabilized Methane Hydrate at the Paleocene/Eocene Boundary?, *Paleoceanography*, 17, 1018, doi:10.1029/2001PA000678.

Boeckel, B., and K.-H. Baumann, 2004, Distribution of Coccoliths in Surface Sediments of the South-Eastern South Atlantic Ocean: Ecology, Preservation and Carbonate Contribution, *Marine Micropaleontology*, 51, 301-320.

Bolin, B., A. Bjorkstrom, C. D. Keeling, R. Bacastow, and U. Siegenthaler, 1981, Carbon Cycle Modeling, in *SCOPE 16: Carbon Cycle Modeling*, edited by B. Bolin, John Wiley and Sons, New York, pp. 1-28.

Bowen, G. J., D. J. Beerling, P. L. Koch, J. C. Zachos, and T. Quattlebaum, 2004, A Humid Climate State During the Palaeocene/Eocene Thermal Maximum, *Nature*, 432, 495-499.

Bralower, T. J., 2002, Evidence of Surface Water Oligotrophy During the Paleocene-Eocene Thermal Maximum: Nannofossil Assemblage Data From Ocean Drilling Program Site 690, Maud Rise, Weddell Sea, *Paleoceanography*, 17, 1-13, doi:10.1029/2001PA000662.

Briegleb, B. P., C. M. Bitz, E. C. Hunke, W. H. Lipscomb, and M. M. Holland, 2004, Scientific Description of the Sea Ice Component in the Community Climate System Model, Version Three, Tech. Rep., NCAR/TN-463+STR, *National Center for Atmospheric Research*, Boulder, CO, 78 pp.

Brinkhuis, H., S. Schouten, M. C. Collinson, A. Sluijs, J. S. S. Damsté, G. R. Dickens, M. Huber, T. M. Cronin, J. Onodera, K. Takahashi, J. P. Bujak, R. Stein, J. Burgh, J. S. Eldrett, I. C. Harding, A. F. Lotter, F. Sangiorgi, H. K. Cittert, J. W. Leeuw, J. Matthiessen, J. Backman, K. Moran, and the Expedition 302 Scientists, 2006, Episodic fresh surface waters in the Eocene Arctic Ocean, *Nature*, 441, 606-609.

Broecker, W. S., and T. H. Peng, 1982, *Tracers in the sea*, Eldigio Press, 679 pp.

Broecker, W. S., and E. Maier-Reimer, 1992, The Influence of Air and Sea Exchange on the Carbon Isotope Distribution in the Sea, *Global Biogeochemical Cycles*, 6, 315-320.

Bryan, F. O., G. Danbasoglu, N. Nakashiki, Y. Yoshida, D-H. Kim, J. Tsutsui, S. C. Doney, 2006, Response of the North Atlantic Thermohaline Circulation and Ventilation to Increasing Carbon Dioxide in CCSM3, *Journal of Climate*, 19, 2382-2397.

Burdige, D. J., 2006, *Geochemistry of Marine Sediments*, Princeton University Press, 609 pp.

Calderia, K., and J. F. Kasting, 1992, The life span of the biosphere revised, *Nature*, 360, 721-723.
Case, J. A., 1988, Paleogene Floras from Seymour Island, Antarctic Peninsula, *Geological Society of America Memoir*, 169, 523-530.
Chester, R., 2000, *Marine Geochemistry*, 2nd ed., Blackwell Science, 506 pp.
Collins, W. D., P. H. Rasch, B. A. Boville, J. J. Hack, J. R. McCaa, D. L. Williamson, J. T. Kiehl, B. Briegleb, C. Bitz, S-J. Lin, M. Zhang, and Y. Dai, 2004, Description of the NCAR Community Atmosphere Model (CAM3), Tech. Rep., NCAR/TN-464+STR, *National Center for Atmospheric Research*, Boulder, CO, 226 pp.
Collins, W. D., C. M. Bitz, M. L. Blackmon, G. B. Bonan, C. S. Bretherton, J. A. Carton, P. Chang, S. C. Boney, J. J. Hack , T. B. Henderson, J. T. Diehl, W. G. Large, D. S. McKenna, B. D. Santer, and R. D. Smith, 2006, The Community Climate System Model Version 3 (CCSM3), *Journal of Climate*, 19, 2122-2143.
Collins, W. D., P. J. Rasch, B. A. Boville, J. J. Hack, J. R. McCaa, D. L. Williamson, B. P. Briegleb, C. M. Bitz, S-J. Lin, and M. Zhang, 2006a, The Formulation and Atmospheric Simulation of the Community Atmosphere Model Version 3 (CAM3), *Journal of Climate*, 19, 2144-2161.
Dickens, G. R., J. R. O'Neil, D. K. Rea, and R. M. Owen, 1995, Dissociation of oceanic methane hydrate as a cause of the carbon isotope excursion at the end of the Paleocene, *Paleoceanography*, 10, 965-971.
Dickens, G. R., M. M. Castillo, and J. C. G. Walker, 1997, A blast of gas in the latest Paleocene: Simulating First-Order Effects of Massive Dissociation of Oceanic Methane Hydrate, *Geology*, 25, 259-262.
Dickens, G. R., 2001, The Potential Volume of Oceanic Methane Hydrates with Variable External Conditions, *Organic Geochemistry*, 32, 1179-1193.
Dickens, G. R., 2003, Rethinking the Global Carbon Cycle with a Large Dynamic and Microbially Mediated Gas Hydrate Capacitor, *Earth and Planetary Science Letters*, 213, 169-183.
Dickens, G. R., 2004, Hydrocarbon-driven warming, *Nature*, 429, 513-515.
Dickinson, R. E., K. W. Oleson, G. Bonan, F. Hoffman, P. Thornton, M. Vertenstein, Z-L. Yang, And X. Zeng, 2006, The Community Land Model and its Climate Statistics as a Component of the Community Climate System Model, *Journal of Climate*, 19, 2302-2324.
Dickson, A. G., 1981, An Exact Definition of Total Alkalinity and a Procedure for the Estimation of Alkalinity and Total Inorganic Carbon from Titration Data, *Deep Sea Research Part A. Oceanographic Research Papers*, 28, 609-623.
Doney, S. C., K. Lindsay, I. Fung, and J. John, 2006, Natural Variability in a Stable, 1000-Yr Global Coupled Climate-Carbon Cycle Simulation, *Journal of Climate*, 19, 3033-3054.
Dorman, J. L., and P. J. Sellers, 1989, A Global Climatology of Albedo, Roughness Length and Stomatal Resistance for Atmospheric General Circulation Models as Represented by the Simple Biosphere Model (SiB), *Journal of Applied Meteorology*, 28, 833-855.
Eberle, J. J., 2006, Early Eocene Brontotheriidae (Perissodactyla) from the Eureka Sound Group, Ellesmere Island, Canadian High Arctic-Implications for Brontothere Origins and High-Latitude Dispersal, *Journal of Vertebrate Paleontology*, 26, 381-386.
Emerson, S. R., and J. I. Hedges, 2008, *Chemical Oceanography and the Marine Carbon Cycle*, Cambridge University Press, 453 pp.
England, M. H., 1995, The Age of Water and Ventilation Timescales in a Global Ocean Model, *Journal of Physical Oceanography*, 25, 2756-2777.
Estes, R., and J. H. Hutchison, 1980, Eocene Lower Vertebrates from Ellesmere Island, Canadian Arctic Archipelago, *Paleogeography, Paleoclimatology, Paleoecology*, 30, 325-347.

Farley, K. A., and S. F. Eltgroth, 2003, An Alternative Age Model for the Paleocene-Eocene Thermal Maximum Using Extraterrestrial ^{3}He, *Earth Planetary Science Letters*, 208, 135-148.

Fincham, M. J., and A. Winter, 1989, Paleoceanographic Interpretations of Coccoliths and Oxygen-isotopes from the Sediment Surface of the Southwest Indian Ocean, *Marine Micropaleontology*, 13, 325-351.

Gale, A. S., J. Hardenbol, B. Hathway, W. J. Kennedy, J. R. Young, and V. Phansalkar, 2002, Global Correlation of Cenomanian (Upper Cretaceous) Sequences: Evidence for Milankovitch Control on Sea Level, *Geology*, 30, 291-294.

Gibbs, M. T., P. M. Rees, J. E. Kutzbach, A. M. Ziegler, P. J. Behling, and D. B. Rowley, 2002, Simulation of Permian climate and comparison with climate-sensitive sediments, *Journal of Geophysical Research*, 93, 9341-9364.

Gibbs, S. J., T. J. Bralower, P. R. Bown, J. C. Zachos, and L. M. Bybell, 2006, Shelf and Open-ocean Calcareous Phytoplankton Assemblages Across the Paleocene-Eocene Thermal Maximum: Implications for Global Productivity Gradients, *Geology*, 34, 233-236.

Heinze, C., and E. Maier-Reimer, 1992, The Hamburg Oceanic Carbon Cycle Circulation Model (Cycle 1), Tech. Rep. 5, 32 pp., *Deutsches Klimarechenzentrum*, Germany.

Heinze, C., and T. J. Crowley, 1997, Sedimentary Response to Ocean Gateway Circulation Changes, *Paleoceanography*, 12, 742-754.

Hsieh, J. C. C., and C. J. Yapp, 1999, Stable Carbon Isotope Budget of CO_2 in a Wet, Modern Soil as Inferred From $Fe(CO_3)OH$ in Pedogenic Goethite: Possible Role of Calcite Dissolution, *Geochimica et Cosmochimica Acta*, 63, 767-783.

Huber, M., and L. C. Sloan, 2001, Heat Transport, Deep Waters, and Thermal Gradients: Coupled Simulation of an Eocene Greenhouse Climate, *Geophysical Research Letters*, 28, 3481-3484.

Huber, M., and R. Caballero, 2003, Eocene El Niño: Evidence for Robust Tropical Dynamics in the "Hothouse", *Science*, 299, 877-881.

Huber, M., and D. Nof, 2006, The Ocean Circulation in the Southern Hemisphere and its Climatic Impacts in the Eocene, *Palaeogeography, Palaeoclimatology, Palaeoecology*, 231, 9-28.

Iakovleva, A. I., H. Brinkhuis, and C. Cavagnetto, 2001, Late Palaeocene-Early Eocene Dinoflagellate Cysts From the Turgay Strait, Kazakhstan; Correlations Across Ancient Seaways, *Palaeogeography, Palaeoclimatology, Palaeoecology*, 172, 243-268.

Iakovleva, A. I., and C. Heilmann-Clausen, 2007, Wilsonidium Pechoricum New Species – A New Dinoflagellate Species with Unusual Asymmetry From the Paleocene/Eocene Transition, *Journal of Paleontology*, 81, 1020-1030.

Kelly, D. C., T. J. Bralower, J. C. Zachos, I. P. Silva, and E. Thomas, 1996, Rapid Diversification of Planktonic Foraminifera in the Tropical Pacific (ODP Site 865) During the Late Paleocene Thermal Maximum, *Geology*, 24, 423-426.

Kelly, D. C., 2002, Response of Antarctic (ODP Site 690) planktonic foraminifera to Paleocene-Eocene thermal maximum: Faunal evidence for ocean/climate change, Paleoceanography, 17, 1071, doi:10.1029/2002PA000761.

Kelly, D. C., J. C. Zachos, T. J. Bralower, and S. A. Schellenberg, 2005, Enhanced terrestrial weathering/runoff and surface ocean carbonate production during the recovery stages of the Paleocene-Eocene thermal maximum, *Paleoceanography*, 20, PA4023, doi:10.1029/2005PA001163.

Kennett, J. P., and L. D. Stott, 1991, Abrupt Deep-sea Warming, Palaeoceanographic Changes and Benthic Extinctions at the End of the Palaeocene, *Nature*, 353, 225-229.

Kump, L. R., and D. Pollard, 2008, Amplification of Cretaceous Warmth by Biological Cloud Feedbacks, *Science*, 320, 195.

Lande, R., and C. S. Yentsch, 1988, Internal Waves, Primary Production, and the Compensation Depth of Marine Phytoplankton, *Journal of Plankton Research*, 10, 565-571.

Larson, K. M., A. R. Lowry, V. Kostoglodov, W. Hutton, O. Sánchez, K. Hadnut, and G. Suárez, 2004, Crustal Deformation Measurements in Guerrero, México, *Journal of Geophysical Research*, 109, B04409, doi:10.1029/2003JB002843.

Lewis, G. N., 1901, The Law of Physico-Chemical Change, *Proceedings of the American Academy of Arts and Sciences*, 37, 49-69.

Long A. J., and I. Shennan, 1994, Sea-Level Changes in Washington and Oregon and the "Earthquake Deformation Cycle", *Journal of Coastal Research*, 10, 825-838.

Lueker, T. J., A. G. Dickson, and C. D. Keeling, 2000, Ocean pCO_2 Calculated from Dissolved Inorganic Carbon, Alkalinity, and Equations for K_1 and K_2: Validation Based on Laboratory Measurements of CO_2 in Gas and Seawater at Equilibrium, *Marine Chemistry*, 70, 105-119.

Mackay, D., S. Paterson, 1981, Calculating Fugacity, *Environmental Science and Technology*, 15, 1006-1012.

Manabe, S., and R. J. Stouffer, 1995, Simulation of Abrupt Climate Change Induced by Freshwater Input to the North Atlantic Ocean, *Nature*, 378, 165-167.

Markwick, P. J., 1998, Fossil crocodilians as indicators of Late Cretaceous and Cenozoic climates: implications for using paleontological data in reconstructing paleoclimate, *Paleogeography, Paleoclimatology, Paleoecology*, 137, 205-271.

McIntyre, A., and A. W. H. Bé, 1967, Modern Cocolithophoridae of the Atlantic Ocean, I, Placoliths and Cyrtoliths, *Deep-Sea Research*, 14, 561-597.

Meulenkamp, J. E., W. Sissingh, and V. N. Beniamovskii, 2000, Map 17. Early/Middle Ypresian, in *Atlas Peri-Tethys, Palaeogeographic Maps*, edited by J. Dercourt, M. Gaetani, B. Vrielynck, E. Barrier, B. Biju-Duval, M. F. Brunet, J. P. Cadet, S. Crasquin, and M. Sandulescu, Comission de la Carte Géologique du Monde, Paris.

Mikolajewicz, U., and T. J. Crowley, 1997, Response of a Coupled Ocean/Energy Balance Model to Restricted Flow Through the Central American Isthmus, *Paleoceanography*, 12, 429-441.

Miller, K. G., G. S. Mountain, J. V. Browning, M. Kominz, P. J. Sugarman, M. Christie-Blick, M. E. Katz, and J. D. Wright, 1998, Cenozoic Global Sea Level, Sequences, and the New Jersey Transect: Results from Coastal Plain and Continental Slope Drilling, *Reviews of Geophysics*, 36, 569-601.

Miller, K. G., M. A. Kominz, J. V. Browning, J. D. Wright, G. S. Mountain, M. E. Katz, P. J. Sugarman, B. S. Cramer, N. Christie-Blick, and S. G. Pekar, 2005, The Phanerozoic Record of Global Sea-Level, *Science*, 310, 1293-1298.

Millero, F. J., 1995, Thermodynamics of the Carbon Dioxide System in the Oceans, *Geochimica et Cosmochimica Acta*, 59, 661-667.

Moran, K., J. Backman, H. Brinkhuis, S. C. Clemens, T. Cronin, G. R. Dickens, F. Eynaud, J. Gattacceca, M. Jakobsson, R. W. Jordan, M. Kaminski, J. King, N. Koc, A. Krylov, N. Martinez, J. Matthiessen, D. McInroy, T. C. Moore, J. Onodera, M. O'Regan, H. Pälike, B. Rea, D. Rio, T. Sakamoto, D. C. Smith, R. Stein, K. St John, I. Suto, N. Suzuki, K. Takahashi, M. Watanabe, M. Yamamoto, J. Garrell, M. Frank, P. Kubik, W. Jokat, and Y. Kristoffersen, 2006, The Cenozoic Palaeoenvironment of the Arctic Ocean, *Nature*, 441, 601-605.

Najjar, R. G., and J. C. Orr, 1999, Ocean Carbon-cycle Model Intercomparison Project OCMIP-2 Biotic HOWTO, unpublished manuscript, http://www.ipsl.jussieu.fr/OCMIP/.

Nunes, F., and R. D. Norris, 2006, Abrupt reversal in ocean overturning during the Palaeocene/Eocene warm period, *Nature*, 439, 60-63.

Oleson, K. W., G. B. Bonan, C. Schaff, F. Gao, and Y. Jin, 2004, Technical description of the Community Land Model (CLM), Tech. Rep., NCAR/TN-461+STR, *National Center for Atmospheric Research*, Boulder, CO, 174 pp.
Pagani, M., K. Caldeira, D. Archer, and J. C. Zachos, 2006, An Ancient Carbon Mystery, *Science*, 314, 1556-1557.
Pagani, M., N. Pedentchouk, M. Huber, A. Sluijs, S. Schouten, H. Brinkhuis, J. S. S. Damsté, G. R. Dickens, and the Expedition 302 Scientists, 2006, Arctic Hydrology During Global Warming at the Palaeocene/Eocene Thermal Maximum, *Nature*, 442, 671-675.
Panchuk, K., A. Ridgwell, and L. R. Kump, 2008, Sedimentary response to Paleocene-Eocene Thermal Maximum carbon release: A model-data comparison, *Geology*, 36, 315-318.
Pearson, P. N., and M. R. Palmer, 2000, Atmospheric Carbon Dioxide Concentrations Over the Past 60 Million Years, *Nature*, 406, 695-699.
Petrizzo, M. R., 2007, The Onset of the Paleocene-Eocene Thermal Maximum (PETM) at Sites 1209 and 1210 (Shatsky Rise, Pacific Ocean) as Recorded by Planktonic Foraminifera, *Marine Micropaleontology*, 63, 187-200.
Pond, S., and G. L. Pickard, 1983, *Introductory Dynamical Oceanography*, Butterworth-Heinemann, 329.
Ridgwell, A., 2007, Interpreting Transient Carbonate Compensation Depth Changes by Marine Sediment Core Modeling, *Paleoceanography*, 22, PA4102, doi:10.1029/2006PA001372.
Ridgwell, A., and J. C. Hargreaves, 2007, Regulation of Atmospheric CO_2 by Deep-sea Sediments in an Earth System Model, *Global Biogeochemical Cycles*, 21, GB2008, doi:10.1029/2006GB002764.
Sauer, P. E., T. I. Eglinton, J. M. Hayes, A. Schimmelmann, and A. L. Sessions, 2001, Compound-specific D/H Ratios of Lipid Biomarkers From Sediments as a Proxy for Environmental and Climatic Conditions, *Geochimica et Cosmochimica Acta*, 65, 213-222.
Schiller, A., U. Mikolajewicz, and R. Voss, 1997, The stability of the North Atlantic Thermohaline Circulation in a Coupled Ocean-Atmosphere General Circulation Model, *Climate Dynamics*, 13, 325-347.
Schmitz, B., and V. Pujalte, 2003, Sea-Level, humidity, and land-erosion records across the initial Eocene thermal maximum from a continental-marine transect in northern Spain, *Geology*, 31, 689-692.
Schouten, S., E. C. Hopmans, E. Schefuß, and J. S. S. Damsté, 2002, Distributional Variations in Marine Crenarchaeotal Membrane Lipids: A New Tool for Reconstructing Ancient Sea Water Temperatures?, *Earth and Planetary Science Letters*, 204, 265-274.
Scotese, C. R., 2008, PALEOMAP Project, www.scotese.com.
Sewall, J. O., L. C. Sloan, M. Huber, S. Wing, 2000, Climate Sensitivity to Changes in Land Surface Characteristics, *Global and Planetary Change*, 26, 445-465.
Shellito, C. J., L. C. Sloan, and M. Huber, 2003, Climate Model Sensitivity to Atmospheric CO_2 Levels in the Early-Middle Paleogene, *Palaeogeography, Palaeoclimatology, Palaeoecology*, 193, 113-123.
Shellito, C. J., and L. C. Sloan, 2006, Reconstructing a Lost Eocene Paradise, Part II: On the Utility of Dynamic Global Vegetation Models in pre-Quaternary Climate Studies, *Global and Planetary Change*, 50, 18-32.
Shellito, C. J., J.-F. Lamarquie, and L. C. Sloan, 2009, Early Eocene Arctic Climate Sensitivity to pCO_2 and Basin Geography, *Geophysical Research Letters*, 36, L09707, doi:10.1029/2009GL037248.
Sluijs, A., S. Schouten, M. Pagani, M. Woltering, H. Brinkhuis, J. S. S. Damsté, G. R. Dickens, M. Huber, G. Reichart, R. Stein, J. Matthiessen, L. J. Lourens, N. Pedentchouk, J. Backman, K. Moran, and the Expedition 302 Scientists, 2006, Subtropical Arctic Ocean

Temperatures During the Palaeocene/Eocene Thermal Maximum, *Nature*, 441, 610-613.
Sluijs, A., H. Brinkhuis, S. Schouten, S. M. Bohaty, C. M. John, J. C. Zachos, G. Reichart, J. S. S. Damsté, E. M. Crouch, and G. R. Dickens, 2007, Environmental precursors to rapid light carbon injection at the Palaeocene/Eocene boundary, *Nature*, 450, 1218-1221.
Smith, R. D., and P. R. Gent, 2004, Reference Manual for the Parallel Ocean Program (POP), Ocean Component of the Community Climate System Model (CCSM2.0 and 3.0), Tech. Rep. LAUR-02-2484, *Los Alamos National Laboratory*, [Available online at http://www.ccsm.ucar.edu/models/ccsm3.0/pop].
Speijer, R. P., and A. M. Morsi, 2002, Ostracode turnover and sea-level changes associated with the Paleocene-Eocene thermal maximum, *Geology*, 30, 23-26.
Sternberg, L. D. L., 1988, D/H Ratios of Environmental Water Recorded by D/H ratios of Plant Lipids, *Nature*, 333, 59-61.
Storey, M., R. A. Duncan, and C. C. Swisher III, 2007, Paleocene-Eocene Thermal Maximum and the Opening of the Northeast Atlantic, *Science*, 316, 587-589.
Stumm, W., and J. J. Morgan, 1981, Aquatic Chemistry, an Introduction emphasizing Chemical Equilibria in Natural Waters, 2nd ed. John Wiley, New York.
Svensen, H., S. Planke, A. Malthe-Sorenssen, B. Jamtvelt, R. Myklebust, T. R. Eidem, and S. S. Rey, 2004, Release of Methane from a Volcanic Basin as a Mechanism for Initial Eocene Global Warming, *Nature*, 429, 542-545.
Thiele, G., and J. L. Sarmiento, 1990, Tracer Dating and Ocean Ventilation, *Journal of Geophysical Research*, 95, 9377-9391.
Thomas, D. J., T. J. Bralower, and C. E. Jones, 2003, Neodymium Isotopic Reconstruction of Late Paleocene-Early Eocene Thermohaline Circulation, *Earth and Planeteary Science Letters*, 209, 309-322.
Thomas, E., 1998, Biogeography of the Later Paleocene Benthic Foraminiferal Extinction, in *Late Paleocene-Early Eocene Climatic and Biotic Events in the Marine and Terrestrial Records*, edited by M.-P. Aubry, S. G. Lucas, and W. A. Berggen, 214-235, Columbia University Press, New York.
Tremolada, F., and T. J. Bralower, 2004, Nannofossil Assemblage Fluctuations During the Paleocene-Eocene Thermal Maximum at Sites 213 (Indian Ocean) and 401 (North Atlantic Ocean): Palaeoceanographic Implications, *Marine Micropaleontology*, 52, 107-116.
Tripati, A., J. Zachos, L. Marincovich Jr., and K. Bice, 2001, Late Paleocene Arctic Coastal Climate Inferred from Molluscan Stable and Radiogenic Isotope Ratios, *Palaeogeography, Palaeoclimatology, Palaeoecology*, 170, 101-113.
Tripati, A., and H. Elderfield, 2005, Deep-Sea Temperature and Circulation Changes at the Paleocene-Eocene Thermal Maximum, *Science*, 308, 1894-1898.
Volk, T., and M. I. Hoffert, 1985, Ocean Carbon Pumps: Analysis of Relative Strengths and Efficiencies in Ocean-driven Atmospheric CO_2 Changes, in *The Carbon Cycle and Atmospheric CO_2: Natural Variations Archean to Present*, edited by E. T. Sundquist, and W. S. Broecker, 99-109, American Geophysical Union, Washington, D. C.
Wanninkhof, R., 1992, Relationship Between Wind Speed and Gas Exchange Over the Ocean, *Journal of Geophysical Research*, 97, 7373-7382.
Wallace, J. M., and P. V. Hobbs, 2006, *Atmospheric Science: An Introductory Survey*, Academic Press Publications, 483 pp.
Watts, A. B., and J. Thorne, 1984, Tectonics, global changes in sea level and their relationship to stratigraphical sequences at the US Atlantic continental margin, *Marine and Petroleum Geology*, 1, 319-339.
Weijers, J. W. H., S. Schouten, A. Sluijs, H. Brinkhuis, J. S. S. Damsté, 2007, Warm Arctic Continents During the Palaeocene-Eocene Thermal Maximum, *Earth and Planetary Science Letters*, 261, 230-238.

Wilson, T. R. S., 1975, Salinity and the Major Elements of Sea Water, in *Chemical Oceanography*, vol. 1, 2nd ed., edited by Riley, J. P., and Skirrow, G., pp. 365-413, Academic Press.

Winguth, A. M. E., C. Heinze, J.E. Kutzbach, E. Maier-Reimer, U. Mikolajewicz, D. Rowley, A. Rees, and A. M. Ziegler, 2002, Simulated warm polar currents during the middle Permian, *Paleoceanography*, 17, doi:10.1029/2001PA000646.

Winguth, A. M. E., C. Shellito, C. Shields, and C. Winguth, *in press*, Climate Response at the Paleocene-Eocene Thermal Maximum to Greenhouse Gas Forcing – A Model Study with CCSM3.

Yakir, D., 1998, in *Stable Isotopes* (ed. Griffiths, H.), 147-168, BIOS Scientific Publishers, Oxford.

Yapp, C. J., 2004, $Fe(CO_3)OH$ in Goethite from a Mid-latitude North America Oxisol: Estimate of Atmospheric CO_2 Concentration in the Early Eocene "Climatic Optimum", *Geochimica et Cosmochimica Acta*, 68, 935-947.

Zachos, J. C., M. Pagani, L. Sloan, E. Thomas, and K. Billups, 2001, Trends, Rhythms, and Aberrations in Global Climate 65 Ma to Present, *Science*, 292, 686-693.

Zachos, J. C., U. Röhl, S. A. Schellenberg, A. Sluijs, D. A. Hodell, D. C. Kelly, E. Thomas, M. Nicolo, I. Raffi, L. J. Lourens, H. McCarren, and D. Kroon, 2005, Rapid Acidification of the Ocean During the Paleocene-Eocene Thermal Maximum, *Science*, 308, 1611-1615.

Zachos, J. C., S. M. Bohaty, C. M. John, H. McCarren, D. C. Kelly, and T. Nielsen, 2007, The Palaeocene-Eocene Carbon Isotope Excursion: Constraints From Individual Shell Planktonic Foraminifer Records, *Philosophical Transactions of the Royal Society A*, 365, 1829-1842.

Zachos, J. C., G. R. Dickens, and R. E. Zeebe, 2008, An Early Cenozoic Perspective on Greenhouse Warming and Carbon-cycle Dynamics, *Nature*, 451, 279-283.

Zamagni, J., M. Mutti, and A. Kosir, 2008, Evolution of Shallow Benthic Communities During the Late Paleocene-Earliest Eocene Transitions in the Northern Tethys (SW Slovenia), *Facies*, 54, 25-43.

BIOGRAPHICAL INFORMATION

Jesse Tiner Cope IV was born on December 5, 1979 in Bryan, Texas to Jesse and Anita Cope. He grew up in Wheelock, Texas and graduated from Franklin High School in 1998. He attended Centenary College of Louisiana in Shreveport, Louisiana where he obtained a Bachelor's of Science in Physics in 2002. After graduating, he worked as a tennis instructor at Southern Trace Country Club in Shreveport, Louisiana. He married Katherine Elizabeth Meinen after her graduation from Centenary College in July of 2003. In the summer of 2002 Jesse Cope joined the United States Marine Corps as a Logistics Officer and was on active duty, stationed on Marine Corps Base Hawaii, in Kaneohe Bay, Hawaii from 2003 through 2006. In the spring of 2007 he enrolled at the University of Texas at Arlington (UTA) and was accepted as a graduate student in the spring of 2008. He is scheduled to graduate with a Masters in Geology from UTA in the fall of 2009.